UNIVERSITY OF OKLAHOMA

GRADUATE COLLEGE

DEVELOPMENT AND EVALUATION OF AN ADVANCED REGIONAL AND GLOBAL HYDROLOGICAL PREDICTION SYSTEM ENABLED BY SATELLITE REMOTE SENSING, NUMERICAL WEATHER FORECASTING, AND ENSEMBLE DATA ASSIMILATION

A DISSERTATION

SUBMITTED TO THE GRADUATE FACULTY

in partial fulfillment of the requirements for the

Degree of

DOCTOR OF PHILOSOPHY

By

YU ZHANG
Norman, Oklahoma
2013

DEVELOPMENT AND EVALUATION OF AN ADVANCED REGIONAL AND GLOBAL HYDROLOGICAL PREDICTION SYSTEM ENABLED BY SATELLITE REMOTE SENSING, NUMERICAL WEATHER FORECASTING, AND ENSEMBLE DATA ASSIMILATION

A DISSERTATION APPROVED FOR THE
SCHOOL OF CIVIL ENGINEERING AND ENVIRONMENTAL SICENCE

BY

_____
Dr. Yang Hong, Chair

_____
Dr. Xuguang Wang, Co-Chair

_____
Dr. Jonathan J. Gourley

_____
Dr. David A. Sabatini

_____
Dr. Randall L. Kolar

Table of Contents

List of Figures

List of Tables

Abstract

This dissertation advanced the traditional hydrological prediction via multi-sensor satellite remote sensing products, numerical weather forecasts and advanced data assimilation approach in sparsely gauged or even ungauged regions and then extend this approach to global scale with enhanced efficiency for prototyping a flood early warning system on a global basis.

This dissertation consists of six chapters: the first chapter is the introductive chapter which describes the problem and raises the hypotheses, Chapters 2 to 5 are the four main Chapters followed by Chapter 6 which is an overall summary of this dissertation.

For regional hydrological prediction in Chapter 2 and 3, two rainfall – runoff hydrological models: the HyMOD (Hydrological MODel) and the simplified version of CREST (Coupled Routing and Excess Storage) Model were set up and tested in Cubango River basin, Africa. In Chapter 2, first, the AMSR-E (Advanced Microwave Scanning Radiometer for Earth observing system) signal/TMI (TRMM Microwave Imager) passive microwave streamflow signals are converted into actual streamflow domain with the unit of m^3/s by adopting the algorithm from Brakenridge et al. (2007); then the HyMOD was coupled with Ensemble Square Root Filter (EnSRF) to account for uncertainty in both forcing data and model initial conditions and thus improve the flood prediction accuracy by assimilating the signal converted streamflow, in comparison to the benchmark assimilation of in-situ streamflow observations in actual streamflow domain with the unit of m^3/s. In Chapter 3, the remote-sensing streamflow signals, without conventional in-situ hydrological measurements, was applied to force, calibrate and update the hydrologic model coupled with EnSRF data assimilation

approach in the same research region, but resulting in exceedance probability-based flood prediction.

For global hydrological predictions in Chapter 4 and 5, a physical based distributed hydrological model CREST is set up at 1/8 degree from 50°N to 50°S and forms the Real Time Hydrological Prediction System (http://eos.ou.edu) which was co-developed by HyDROS (Hydrometeorology and Remote Sensing Laboratory) lab at the University of Oklahoma and NASA Goddard center. In Chapter 4, the CREST model is described with details and then the Real Time Global Hydrological Monitoring System will be comprehensively evaluated on basis of gauge based streamflow observation and gridded global runoff data from GRDC (Global Runoff Data Center, http://www.bafg.de/GRDC/EN/Home/homepage_node.html). In order to extend the hydrological forecast horizon for the Real Time Global Hydrological Prediction System, the deterministic precipitation forecast fields from a numerical meteorological model GFS (Global Forecasting System) as well as the ensemble precipitation forecast fields are introduced as the forcing data to be coupled into the global CREST model in order to generate the global hydrological forecasting up to around 7 days lead time in Chapter 5. The July 21, 2012 Beijing extreme flooding event is selected to evaluate the hydrological prediction skills for extremes of both the deterministic and the ensemble GFS products.

Keywords: Remote Sensing; Numerical weather forecasts; Data assimilation; Hydrological model

Chapter 1. Introduction

1.1 Statement of Problems

Flooding, which is considered as one of the most hazardous disasters in both rural and urban areas, accounts for around one-third of all global geophysical hazards (Adhikari et al. 2010; Smith and Ward 1998). Looking back at the past year 2012, which was a moderate year, there were 905 natural disasters worldwide, of which 36% were floods (http://en.wikipedia.org/wiki/Natural_disaster). In the first half of 2013 alone, flooding occurred in Europe, Canada, Asia and Australia causing a total economic loss of around 45 billion dollars. (Munich Re; http://go.nature.com/ku2qff). Wake recently pointed out that "the number, extent and global impact of the flood events this year (2013) is extraordinary and accounts for about 47% of global economic losses from nature disasters" (Wake 2013).

Every year there are hundreds and thousands of flood events around the world that cause significant human suffering, loss of life and property damage (Adhikari et al. 2010; Hong et al. 2007a). As mentioned by Adhikari et al., "The International Flood Network indicates that from 1995 to 2004, natural disasters caused 471,000 fatalities worldwide and economic losses totaling approximately $49 billion USD, out of which approximately 94,000 (20%) of the fatalities and $16 billion USD (33%) of the economic damages were attributed to floods alone" (Adhikari et al. 2010). Throughout the history, severe floods occurred frequently: In 1931, China experienced the ever recorded deadliest "Central China floods" of the 20th century over Yellow River, Yangtze River and Huai River basins, which caused an estimated 2.5 to 3.7 million fatalities (http://en.wikipedia.org/wiki/1931_China_floods); in 1887 and 1938, Yellow

River was inundated and caused around 0.9-2 million and 0.5-0.7 million deaths, respectively, making them the second and third most devastating floods in Chinese history. The 1975 Ru River flood in China (0.231 million fatalities), the 2004 Indian Ocean tsunami in Indonesia (0.23 million fatalities) and the 1530 St. Felix's flood in Netherlands are ranked No. 4, 5 and 6, respectively, in terms of death toll.

In the future, which will be strongly impacted by human activities and changing climate, it is reasonably anticipated that the flood risk will not decrease, but rather become more severe and frequent, thus threatening more regions around the world. The increasing adverse worldwide impact from floods indicates that: (1) Accurate and precise flooding prediction plays an increasingly important role in early warning systems to protect human lives and properties, especially for those developing regions with sparsely hydrological gauges or even without gauge observations. (2) Flooding is not only a regional or national-level issue, but is instead a global problem that greatly motivates a global flood monitoring and forecasting system coordinated among worldwide research institutions and government decision makers. Therefore, (1) Regional hydrological predictions advanced by remote sensing techniques and data assimilation approaches, especially for those sparsely gauged or ungauged developing regions, are of great importance to provide early warning and guidance for the preparedness of flood disaster. (2) A reliable Global Flood Prediction System (GFPS) is appealing for international collaborations in the preparedness and response for water management and flood emergence.

1.2 Literature Review

1.2.1 Traditional hydrological prediction approach

Early last century, when remote sensing technique was not widespread, the hydrological prediction in the downstream was commonly calculated based on the hydrological conditions in the upstream using a hydraulic way (e.g. unit hydrograph, Muskingum method). However, the lead time for those approaches is often limited by the water concentration time in the river channel. Then the physical based hydrological models were developed to better represent the hydrological process and increasingly applied for flood monitoring and forecasting in order to provide early warnings of impending disasters. Conventionally, a hydrological model is set up at natural river basins with meteorological gauges which can provide temperature, precipitation, etc., and hydrological gauge observations such as streamflow. For distributed hydrological model, the input rain gauge observations are usually interpolated into grids and taken as the forcing data to the model. And then the model parameters are tuned manually based on the modelers' experiences or via sophisticated auto-calibration algorithms. There are some commonly applied calibration methods for improving the accuracy of streamflow simulation and prediction, such as SLS (Stepwise Line Search) (Kuzmin et al. 2008), SCE-UA (Shuffling Complex Evolution-University of Arizona) (Duan et al. 1994), and DREAM (DiffeRential Evolution Adaptive Metropolis) (Vrugt et al. 2009). Please refer to the citations for detailed information about the auto-calibration algorithms.

1.2.2 Advanced remote sensing techniques for hydrological modeling

In addition to calibration techniques, the recent development of remote-sensing technology from space-borne sensors, provided new insights into global rainfall patterns

and runoff response, and the real-time availability of these data over vast regions, has spawned the capability for systematic rainfall monitoring and subsequent flood modeling especially for those poorly gauged or ungauged basin, and for global hydrological forecasting. (e.g. (Brakenridge et al. 2007; Brakenridge et al. 2003; Hong et al. 2007b; Smith 1997)). Considering hydrological modeling in those basins with limited ground surface observation networks, a great deal of success has been achieved through the recent availability of remote-sensing precipitation data (e.g. (Hong et al. 2004; Huffman et al. 2007; Joyce et al. 2004; Khan et al. 2011a, 2011b; Sorooshian et al. 2000; Turk and Miller 2005)). However, it is recognized that the uncertainty with remote sensing data may cause additional errors to be propagated into hydrologic modeling results. For example, the TRMM (Tropical Rainfall Measurement Mission) - 3B42 RT forcing data used in this study, according to (Bitew and Gebremichael 2011; Gourley et al. 2011), can lead to biased streamflow simulations through the error propagated from the model input to the model output in several different basins. The commonly used batch calibration system for hydrologic analysis combines errors from input data and model structures into parameter uncertainties; sequential data assimilation has the potential to overcome this weakness by taking into account each source of uncertainty separately (Moradkhani et al. 2005). Recently, the Global Flood Detection System (GFDS, http://www.gdacs.org/flooddetection/), began using a passive microwave sensor, AMSR-E, together with the TRMM Microwave Imager (TMI), to measure the surface brightness temperatures, which can be used creatively to infer streamflow and thus show the potential to monitor floods over the globe (Brakenridge et al. 2007). Previous assimilation studies with AMSR-E information have only focused

on the soil moisture products but not on the remotely sensed streamflow signals. In Chapters 2, the AMSR-E remote sensing streamflow signals are converted into actual streamflow for hydrological model calibration and data assimilation; by contrast, in Chapter 3, the signals are directly utilized for calibration, and then are converted into the exceeding probability for data assimilation.

1.2.3 Advanced data assimilation techniques for improving hydrological performance

In addition to conventional calibration approaches, data assimilation can further improve the accuracy and precision of the modeling results by correcting the internal model states that are used as the initial condition of the forecasting at the next time steps via assimilating available and reliable observations.

Ensemble data assimilation was first used in engineering and aerospace applications during the 1960s. In the recent decades, ensemble data assimilation has increasingly been expanded to many fields, especially meteorology, oceanography and hydrology. Data assimilation is defined as the insertion of reliable data into the dynamical model to improve the quality and accuracy of the estimates. The Ensemble Kalman Filter (EnKF), which is a promising approach as it is robust and flexible in calculating background covariance (Reichle et al. 2002), has broadly been applied in the research area of dynamic meteorology as well as numerical prediction (e.g. (Anderson et al. 2005; Hamill et al. 2001; Houtekamer and Mitchell 1998, 2001; Mitchell et al. 2002; Wang et al. 2007， 2009.)). Results show great potential of EnKF in enhancing modeling performance thus providing more reliable forecasts.

An increasing number of studies have been exploiting the potential of assimilating different types of hydrological observations by integrating EnKF with advanced

hydrological models. One focus has been on the optimal use of soil moisture data with the EnKF (e.g. (Aubert et al. 2003; Chen et al. 2011; Crow and Ryu 2009; Crow et al. 2005; Gao et al. 2007; Pauwels et al. 2002)). By assimilating soil moisture into an appropriately physically based model (either land surface model or hydrological model), more accurate estimates of antecedent soil moisture condition result can be generated, thus enhancing the hydrologic prognostic capability of soil and streamflow states and fluxes. However, the degree of improvement in forecast skill is contingent on the model structure and the quality of the observations that are assimilated into the model. Chen et al. (2011) pointed out that the failed attempt to improve streamflow prediction via assimilating soil moisture into the SWOT model was due to the deficiency of the model structure (Chen et al. 2011). A variety of studies have examined the applicability of assimilating streamflow observations into hydrological models in order to improve the prediction skill of the streamflow and soil moisture conditions (e.g. (Aubert et al. 2003; Chen et al. 2013; Clark et al. 2008; Pauwels and De Lannoy 2006)).

1.2.4 Advanced global hydrological monitoring and forecasting system in Real Time

Flooding accounts for about one-third of all global geophysical hazards and it leads to significant human suffering, loss of life and property damage. Currently, only several satellite remote-sensing, flood-monitoring systems exist at global scales and provide forecasts in near real time (Brakenridge et al. 2007; Hong et al. 2007b; Wu et al. 2012; Yilmaz et al. 2010). Timely, recent development and improvement of global flood early warning systems are appealing to users when they provide forecasts several days in advance for better planning and responding to emerging disasters. In Chapter 4, a Real Time Global Hydrological Monitoring System, forced by NASA TRMM-based Multi-

satellite Precipitation Analysis (TMPA) at near real-time, is proposed to be systematically evaluated to prove the reliability of hydrological detection skills; in Chapter 5, a Global Hydrological Prediction System (GHPS), forced by NOAA's Global Forecast System (GFS) precipitation forecasts, was developed and evaluated thus providing global real time flood forecasting up to 7 days in advance, which is of great significance to government decision makers in emergency response.

1.3 Research Objective

The overarching goal of this dissertation is to advance the traditional hydrological prediction via multi-sensor satellite remote sensing products, numerical weather forecasts and advanced data assimilation approach in sparsely gauged or even ungauged regions and then extend this approach to global scale with enhanced efficiency for prototyping a flood early warning system on a global basis.

1.4 Hypotheses

Based on the overarching objective, the following hypotheses are made in this dissertation:

1. Spaceborne streamflow signals can compensate for the uncertainty of spaceborne precipitation data to achieve hydrologic prediction skill comparable to results benchmarked with conventional observations.
2. Remote-sensing data can complement or even replace in-situ networks to force and calibrate hydrologic models, especially over vast sparsely gauged basins throughout the world.
3. The real time global hydrological monitoring system can be enabled by multi-sensor satellite rainfall products for near real time monitoring purpose while the real time global hydrological forecasting system can be enabled by the precipitation forecasts from Numerical Weather Prediction (NWP) system for real time forecasting purpose.
4. In addition the deterministic NWP precipitation forecast which can formulate the deterministic hydrological forecast; the ensemble NWP precipitation forecasts can add additional value in probabilistic Ensemble Streamflow Predictions which can better quantify the hydrological prediction uncertainties.

1.5 Outline of the Dissertation

This dissertation consists of six Chapters: the first Chapter is the introductive Chapter which describes the problem and raises the hypotheses, Chapters 2 to 5 are the four main Chapters followed by Chapter 6 which is an overall summary of this dissertation. In order to make every chapter an independent story, there are some repetitions in the content.

For regional hydrological prediction in Chapter 2 and 3, two rainfall – runoff hydrological models: the HyMOD (Hydrological MODel, (Wagener et al. 2001)) and the simplified version of CREST (Coupled Routing and Excess Storage, (Wang et al. 2011)) Model were set up and tested in Cubango River basin, Africa. In Chapter 2, first, the AMSR-E (Advanced Microwave Scanning Radiometer for Earth observing system) signal/TMI (TRMM Microwave Imager) passive microwave streamflow signals are converted into actual streamflow domain with the unit of m^3/s by adopting the algorithm from Brakenridge et al. (2007); then the HyMOD was coupled with Ensemble Square Root Filter (EnSRF) to account for uncertainty in both forcing data and model initial conditions and thus improve the flood prediction accuracy by assimilating the signal converted streamflow, in comparison to the benchmark assimilation of in-situ streamflow observations in actual streamflow domain with the unit of m^3/s. In Chapter 3, the remote-sensing streamflow signals, without conventional in-situ hydrological measurements, was applied to force, calibrate and update the hydrologic model coupled with EnSRF data assimilation approach in the same research region, but resulting in exceedance probability-based flood prediction.

For global hydrological predictions in Chapter 4 and 5, a physical based distributed hydrological model CREST is set up at 1/8 degree from 50°N to 50°S and forms the Real Time Hydrological Prediction System (http://eos.ou.edu) which was co-developed by HyDROS (Hydrometeorology and Remote Sensing Laboratory) lab at the University of Oklahoma and NASA Goddard center. All the parameters were either directly estimated from input data (e.g. soil type) or used as a-priori parameters (for detailed information, please refer to (Wang et al. 2011; Wu et al. 2012)). The CREST model, which is forced by gridded meteorological forcing fields - nominally rainfall observed from TRMM, has been used to simulate and forecast hydrometeorological variables such as streamflow, soil moisture, and actual evapotranspiration. In Chapter 4, the CREST model is described with details and then the Real Time Global Hydrological Monitoring System (also refer to the nowcast mode of GHPS) will be comprehensively evaluated on basis of gauge based streamflow observation and gridded global runoff data from GRDC (Global Runoff Data Center, http://www.bafg.de/GRDC/EN/Home/homepage_node.html). In order to extend the hydrological forecast horizon or the lead time for the Real Time Global Hydrological Prediction System, the deterministic precipitation forecast fields from a numerical meteorological model GFS (Global Forecasting System) as well as the ensemble precipitation forecast fields (also refers to GENS –GFS Ensembles in this study) are introduced as the forcing data to be coupled into the global CREST model in order to generate the global hydrological forecasting up to around 7 days lead time in Chapter 5. The July 21, 2012 Beijing extreme flooding event is selected to evaluate the

hydrological prediction skills for extremes of both the deterministic and the ensemble GFS products.

1.6 List of Publications from the Dissertation

CHAPTER 2

Zhang, Y., Y. Hong, J.J. Gourley, X-G Wang, J-D Gao, H. Vergara, and B. Yong. 2013, Assimilation of Passive Microwave Streamflow Signals for Improving Flood Forecasting: A First Study in Okavango River Basin, Africa, IEEE Journal of Special Topics in Applied Earth Observations and Remote Sensing. DOI: 10.1109/JSTARS.2013.2251321

CHAPTER 3

Zhang, Y., Y. Hong, J.J. Gourley, X. Wang, G.R. Brakenridge, T.D. Groeve and H. Vergara. 2013. Impact of assimilating spaceborne microwave signals for improving hydrological predictions ungauged basins. AGU Chapman Remote Sensing monograph. (Accpeted)

CHAPTER 4

Zhang, Y., Hong, Y., Gao, H., Xue, X. and Gourley, J. J.. 2013. Multi-scale Evaluation of a Real Time Multi-satellite Precipitation Forced Global Hydrological Modeling System. (to be submitted to Journal of Hydrology)

CHAPTER 5

Zhang, Y., Hong, Y., Wang, X.G., Gourley, J. J. et al. 2013. Hydrometeorological Analysis and Remote Sensing of Extremes: Was 2012 July Beijing Flood Event Detectable and Predictable? Journal of Hydrometeorology. (under revision)

References

Adhikari, P., Y. Hong, K. Douglas, D. Kirschbaum, J. Gourley, R. Adler, and G. Robert Brakenridge, 2010: A digitized global flood inventory (1998–2008): compilation and preliminary results. *Natural Hazards*, **55,** 405-422.

Anderson, J. L., B. Wyman, S. Zhang, and T. Hoar, 2005: Assimilation of surface pressure observations using an ensemble filter in an idealized global atmospheric prediction system. *Journal of Atmospheric Sciences*, **62,** 2925-2938.

Aubert, D., C. Loumagne, and L. Oudin, 2003: Sequential assimilation of soil moisture and streamflow data in a conceptual rainfall–runoff model. *Journal of Hydrology*, **280,** 145-161.

Bitew, M. M., and M. Gebremichael, 2011: Evaluation of satellite rainfall products through hydrologic simulation in a fully distributed hydrologic model. *Water Resources Research*, **47,** W06526.

Brakenridge, G. R., S. V. Nghiem, E. Anderson, and R. Mic, 2007: Orbital microwave measurement of river discharge and ice status. *Water Resources Research*, **43**.

Brakenridge, G. R., E. Anderson, S. V. Nghiem, S. Caquard, and T. B. Shabaneh, 2003: Flood warnings, flood disaster assessments, and flood hazard reduction: The roles of orbital remote sensing. *30th International Symposium on Remote Sensing of Environment, Honolulu, HI, November 10-14, 2003*, Pasadena, CA: Jet Propulsion Laboratory, National Aeronautics and Space Administration, 2003.

Chen, F., W. T. Crow, P. J. Starks, and D. N. Moriasi, 2011: Improving hydrologic predictions of a catchment model via assimilation of surface soil moisture. *Advances in Water Resources*, **34,** 526-536.

Chen, H., D. Yang, Y. Hong, J. J. Gourley, and Y. Zhang, 2013: Hydrological data assimilation with the Ensemble Square-Root-Filter: Use of streamflow observations to update model states for real-time flash flood forecasting. *Advances in Water Resources*, **59,** 209-220.

Clark, M. P., and Coauthors, 2008: Hydrological data assimilation with the ensemble Kalman filter: Use of streamflow observations to update states in a distributed hydrological model. *Advances in Water Resources*, **31,** 1309-1324.

Crow, W., and D. Ryu, 2009: A new data assimilation approach for improving runoff prediction using remotely-sensed soil moisture retrievals. *Hydrology and Earth System Sciences*, **13,** 1.

Crow, W., R. Bindlish, and T. Jackson, 2005: The added value of spaceborne passive microwave soil moisture retrievals for forecasting rainfall - runoff partitioning. *Geophysical Research Letters*, **32**.

Duan, Q., S. Sorooshian, and V. K. Gupta, 1994: Optimal use of the SCE-UA global optimization method for calibrating watershed models. *Journal of Hydrology*, **158,** 265-284.

Gao, H., E. F. Wood, M. Drusch, and M. F. McCabe, 2007: Copula-derived observation operators for assimilating TMI and AMSR-E retrieved soil moisture into land surface models. *Journal of Hydrometeorology*, **8,** 413-429.

Gourley, J. J., Y. Hong, Z. L. Flamig, J. Wang, H. Vergara, and E. N. Anagnostou, 2011: Hydrologic evaluation of rainfall estimates from radar, satellite, gauge, and combinations on Ft. Cobb basin, Oklahoma. *Journal of Hydrometeorology*, **12,** 973-988.

Hamill, T. M., J. S. Whitaker, and C. Snyder, 2001: Distance-dependent filtering of background error covariance estimates in an ensemble Kalman filter. *Monthly Weather Review*, **129,** 2776-2790.

Hong, Y., K. L. Hsu, S. Sorooshian, and X. G. Gao, 2004: Precipitation Estimation from Remotely Sensed Imagery using an Artificial Neural Network Cloud Classification System. *Journal of Applied Meteorology*, **43,** 1834-1852.

Hong, Y., R. Adler, A. Negri, and G. Huffman, 2007a: Flood and landslide applications of near real-time satellite rainfall products. *Natural Hazards*, **43,** 285-294.

Hong, Y., R. F. Adler, F. Hossain, S. Curtis, and G. J. Huffman, 2007b: A first approach to global runoff simulation using satellite rainfall estimation. *Water Resources Research*, **43,** W08502.

Houtekamer, P. L., and H. L. Mitchell, 1998: Data assimilation using an ensemble Kalman filter technique. *Monthly Weather Review*, **126,** 796-811.

——, 2001: A sequential ensemble Kalman filter for atmospheric data assimilation. *Monthly Weather Review*, **129,** 123-137.

Huffman, G. J., D. T. Bolvin, E. J. Nelkin, D. B. Wolff, R. F. Adler, G. Gu, Y. Hong, K. P. Bowman, and E. F. Stocker (2007), The TRMM Multisatellite Precipitation Analysis (TMPA): Quasi-Global, Multiyear, Combined-Sensor Precipitation Estimates at Fine Scales, *Journal of Hydrometeorology*, *8*(1), 38-55.

Joyce, R. J., J. E. Janowiak, P. A. Arkin, and P. P. Xie, 2004: CMORPH: A method that produces global precipitation estimates from passive microwave and infrared data at high spatial and temporal resolution. *Journal of Hydrometeorology*, **5,** 487-503.

Khan, S. I., P. Adhikari, Y. Hong, H. Vergara, R. F Adler, F. Policelli, D. Irwin, T. Korme, and L. Okello, 2011a: Hydroclimatology of Lake Victoria region using hydrologic model and satellite remote sensing data. *Hydrology and Earth System Sciences*, **15,** 107-117.

Khan, Sadiq I., Yang Hong, Jiahu Wang, Koray K. Yilmaz, Jonathan J. Gourley, Robert F. Adler, G. Robert Brakenridge, Fritz Policelli, Shahid Habib, and Daniel Irwin, 2011b: Satellite Remote Sensing and Hydrologic Modeling for Flood Inundation Mapping in Lake Victoria Basin: Implications for Hydrologic Prediction in Ungauged Basins. *Geoscience and Remote Sensing, IEEE Transactions on*, **49,** 85-95.

Kuzmin, V., D.-J. Seo, and V. Koren, 2008: Fast and efficient optimization of hydrologic model parameters using a priori estimates and stepwise line search. *Journal of Hydrology*, **353,** 109-128.

Mitchell, H. L., P. Houtekamer, and G. Pellerin, 2002: Ensemble Size, Balance, and Model-Error Representation in an Ensemble Kalman Filter*. *Monthly Weather Review*, **130,** 2791-2808.

Moradkhani, H., S. Sorooshian, H. V. Gupta, and P. R. Houser, 2005: Dual state–parameter estimation of hydrological models using ensemble Kalman filter. *Advances in Water Resources*, **28,** 135-147.

Pauwels, V., R. Hoeben, N. E. Verhoest, F. P. De Troch, and P. A. Troch, 2002: Improvement of TOPLATS‐based discharge predictions through assimilation of ERS‐based remotely sensed soil moisture values. *Hydrological Processes*, **16,** 995-1013.

Pauwels, V. R., and G. J. De Lannoy, 2006: Improvement of modeled soil wetness conditions and turbulent fluxes through the assimilation of observed discharge. *Journal of Hydrometeorology*, **7,** 458-477.

Reichle, R. H., D. B. McLaughlin, and D. Entekhabi, 2002: Hydrologic data assimilation with the ensemble Kalman filter. *Monthly Weather Review*, **130,** 103-114.

Smith, K., and R. Ward, 1998: *Floods: physical processes and human impacts.* Vol. 408, Wiley Chichester.

Smith, L. C., 1997: Satellite remote sensing of river inundation area, stage, and discharge: A review. *Hydrological Processes*, **11,** 1427-1439.

Sorooshian, S., K.-L. Hsu, G. XIAOGANG, H. V. Gupta, B. Imam, and D. Braithwaite, 2000: Evaluation of PERSIANN system satellite-based estimates of tropical rainfall. *Bulletin of the American Meteorological Society*, **81,** 2035-2046.

Turk, F. J., and S. D. Miller, 2005: Toward improved characterization of remotely sensed precipitation regimes with MODIS/AMSR-E blended data techniques. *Geoscience and Remote Sensing, IEEE Transactions on* **43,** 1059-1069.

Vrugt, J. A., C. Ter Braak, C. Diks, B. A. Robinson, J. M. Hyman, and D. Higdon, 2009: Accelerating Markov chain Monte Carlo simulation by differential evolution with self-adaptive randomized subspace sampling. *International Journal of Nonlinear Science and Numerical Simulation*, **10,** 273-290.

Wagener, T., D. P. Boyle, M. J. Lees, H. S. Wheater, H. V. Gupta, and S. Sorooshian, 2001: A framework for development and application of hydrological models. *Hydrology and Earth System Sciences Discussions*, **5,** 13-26.

Wake, B., 2013: Flooding costs. *Nature Climate Change*, **3,** 778-778.

Wang, J., Y. Hong, L. Li, J.J. Gourley, S.I. Khan, K.K. Yilmaz, R.F. Adler, F. S. Policelli, S. Habib, D. Irwn, A. S. Limaye, T. Korme and L. Okello. 2011: The coupled routing and excess storage (CREST) distributed hydrological model. *Hydrological sciences journal*, **56,** 84-98.

Wang, X., C. Snyder, and T. M. Hamill, 2007: On the theoretical equivalence of differently proposed ensemble-3DVAR hybrid analysis schemes. *Monthly Weather Review*, **135,** 222-227.

Wang, X., T. M. Hamill, J. S. Whitaker, and C. H. Bishop, 2009: A comparison of the hybrid and EnSRF analysis schemes in the presence of model errors due to unresolved scales. *Monthly Weather Review*, **137,** 3219-3232.

Wu, H., R. F. Adler, Y. Hong, Y. Tian, and F. Policelli, 2012: Evaluation of Global Flood Detection Using Satellite-Based Rainfall and a Hydrologic Model. *Journal of Hydrometeorology*, **13,** 1268-1284.

Yilmaz, K. K., R. F. Adler, Y. Tian, Y. Hong, and H. F. Pierce, 2010: Evaluation of a satellite-based global flood monitoring system. *International Journal of Remote Sensing*, **31,** 3763-3782.

Chapter 2. Assimilation of Passive Microwave Streamflow Signals for Improving Flood Forecasting: A First Study in Cubango River Basin, Africa

Abstract

Floods are among the most frequently occurring and disastrous natural hazards in the world. The overarching goal of this study is to investigate the utility of passive microwave AMSR-E signal and TRMM based precipitation estimates in improving flood prediction at the sparsely gauged Cubango River Basin, Africa. This is accomplished by coupling a widely used conceptual rainfall-runoff hydrological model with Ensemble Square Root Filter (EnSRF) to account for uncertainty in both forcing data and model initial conditions. Three experiments were designed to quantify the contributions of the AMSR-E signal to the flood prediction accuracy, in comparison to the benchmark assimilation of in-situ streamflow observations, for both "Open Loop" and "Assimilation" modules. In general, the EnSRF assimilation of both in-situ observations and AMSR-E signal-converted-streamflow effectively improved streamflow modeling performance in terms of three statistical measures. In order to further investigate AMSR-E signals' contribution to extreme events prediction skill, the upper 10^{th} percentile daily streamflow was taken as the threshold. Results show significantly improved skill and detectability of floods as well as reduced false alarm rates. Given the global availability of satellite-based precipitation from current TRMM and future GPM, together with soil moisture information from the current AMSR-E and future SMAP mission at near real-time, this "first attempt" study at a sparsely gauged

African basin shows that opportunities exist for an integrated application of a suite of satellite data in improving flood forecasting worldwide by careful fusion of remote sensing and in-situ observations.

2.1 Introduction

Every year there are hundreds and thousands of flood events around the world that cause significant human suffering, loss of life and property damage (Adhikari et al. 2010; Hong et al. 2007a; Kugler and Groeve 2007). In a changing climate, it is reasonably anticipated that the flood risk will not decrease but become more severe and frequent, thus threatening more regions around the world (McCarthy 2001). Therefore, accurate and precise forecasting of floods plays an increasingly important role in early warning systems to protect life and property.

In order to provide early warnings of impending disasters, hydrological models are typically applied for flood detection and prediction. The traditional way to improve the accuracy of streamflow simulation and prediction is to calibrate the model using manual or automatic approaches such as SLS (Stepwise Line Search) (Kuzmin et al. 2008), SCE-UA (Shuffling Complex Evolution-University of Arizona) (Duan et al. 1994), and DREAM (DiffeRential Evolution Adaptive Metropolis) (Vrugt et al. 2009). In addition to conventional calibration approaches, data assimilation can further improve the accuracy and precision of the modeling results by correcting the internal model states that are used as the initial condition of the forecast for the next time steps via assimilating available and reliable observations.

Ensemble data assimilation was first used in engineering and aerospace applications dating back to the 1960s. In recent decades, ensemble data assimilation has increasingly been expanded to many fields, especially meteorology, oceanography and hydrology. Data assimilation is defined as the insertion of reliable data into the dynamical model to improve the quality and accuracy of the estimates (Robinson and

Lermusiaux 2000). Recently, an increasing number of studies have been exploiting the potential to assimilate different types of hydrological observations by integrating EnKF with advanced hydrological models. One focus has been on the optimal use of soil moisture data with the EnKF (e.g. (Aubert et al. 2003; Chen et al. 2011; Crow and Ryu 2009; Crow et al. 2005; Gao et al. 2007; Pauwels et al. 2002)). Besides the assimilation of soil moisture, a variety of studies have examined the applicability of assimilating streamflow observations into hydrological models in order to improve streamflow prediction and soil moisture conditions (e.g. (Aubert et al. 2003; Chen et al. 2013; Clark et al. 2008; Pauwels and De Lannoy 2006)).

In addition to calibration and data assimilation techniques, the recent development of remote-sensing technology, which provides high temporal and spatial resolution forcing data such as precipitation and soil moisture, can greatly facilitate the improvement of flood forecasting (e.g. (Brakenridge et al. 2003, 2007; Hong et al. 2007b; Smith 1997)). However, it is recognized that the uncertainty with remote sensing data may cause additional errors to be propagated into hydrologic modeling results. For example, the TRMM (Tropical Rainfall Measurement Mission) - 3B42 RT forcing data used in this study, according to (Bitew and Gebremichael 2011; Gourley et al. 2011), can lead to biased streamflow simulations through the error propagation from the model input to the model output in different basins. The commonly used batch calibration system for hydrologic analysis combines errors from input data and model structures into parameter uncertainties; sequential data assimilation has the potential to overcome this weakness by taking into account each source of uncertainty separately (Moradkhani et al. 2005).

NASA AMSR-E (Advanced Microwave Scanning Radiometer for Earth observing system)/Aqua provides both soil moisture retrievals from the brightness temperature and the approximated river streamflow signals using the techniques proposed by (Brakenridge et al. 2007). To date, however, previous assimilation studies with AMSR-E information are only focused on the soil moisture products but not on the remotely sensed streamflow signal. The overarching goal of this study is to investigate the potential utility of AMSR-E remotely-sensed signal data for hydrological model calibration and data assimilation in the Cubango River Basin, with rainfall forcing from TRMM-based satellite precipitation estimates. To do so, an ensemble square root filter (EnSRF), (also referred to as an EnKF without perturbing the observations) was applied and coupled with a widely tested rainfall-runoff hydrological model called HyMOD to overcome both the uncertainty of remotely sensed precipitation and streamflow data combined with the simplicity of the model structure.

To the best of our knowledge, this research is the first attempt to incorporate remotely-sensed streamflow, which was derived from the AMSR-E signals retrieved and provided by the Global Flood Detection System (GFDS, http://www.gdacs.org/flooddetection/), for hydrologic model parameter estimation and data assimilation. This study demonstrates the applicability of the globally-available AMSR-E signals and satellite-based precipitation estimates in enhancing the hydrologic performance via a combined calibration and data assimilation approach. It is shown that the assimilation of either gauge-observed or remote sensing-derived streamflow into the model updates all the internal model states (soil moisture content, quick and slow flow tank contents) with the expectation of thereby reducing the deviations between the

model simulation and observation of streamflow. With the increasing availability of remote-sensing data over the globe (e.g. precipitation and soil moisture) and advances in computational power, it is possible that sequential data assimilation of remotely-sensed soil moisture and streamflow signals can be implemented in a real-time hydrological prediction system for improved hydrological forecasting, especially for the vast basins of the world that are only sparsely gauged.

Section 2.2 describes the Cubango river basin and the details of the model and data sources. Section 2.3 introduces the methodology of this study. In section 2.4, the results of sensitivity analysis, calibration, data assimilation and threshold-based evaluation are discussed. Finally, a summary of results and conclusions are provided in section 2.5.

2.2 Study Region, Model and Data

2.2.1 Study Region

The Okavango River, which is the fourth longest river system in southern Africa, runs for about 1100 km from central Angola and flows through Namibia and Botswana (as shown in Figure 2.1).

The Okavango catchment is approximately 413,000 km^2, while the Okavango delta which lies downstream is about 15,000 km^2. Within the area of this catchment, Angola accounts for 48%, Nambia accounts for 37% and Botswana 15% of the land area. The Okavango river originates in the headwaters of central Angola, then the Cubango and Cuito tributaries meet to form the Cubango-Okavango River near the border of Angola and Namibia and flow into the Okavango Delta in Botswana. The upper stream region belongs to subtropical climate zone with annual precipitation around 1300mm while the downstream region, which contains the Kalahari Desert, belongs to the semi-arid climate zone with annual precipitation around 450mm (Hughes et al. 2006; Milzow et al. 2009b). The headwater region, which is the northern part of the basin, is mainly covered by the ferralsols soil with a lower hydraulic conductivity. The headwater region also has a high forest cover and contributes significantly to the river runoff (Hughes et al. 2006). The rest of the basin is dominated by arenosals soil (www.sharing-water.net), which is very porous with high hydraulic conductivity, so that water drains rapidly, leaving little moisture for plants. As mentioned in (Chen et al. 2013), around 95% of inflow is lost in the atmosphere due to high potential evapotranspiration rate and only a small portion contributes to groundwater.

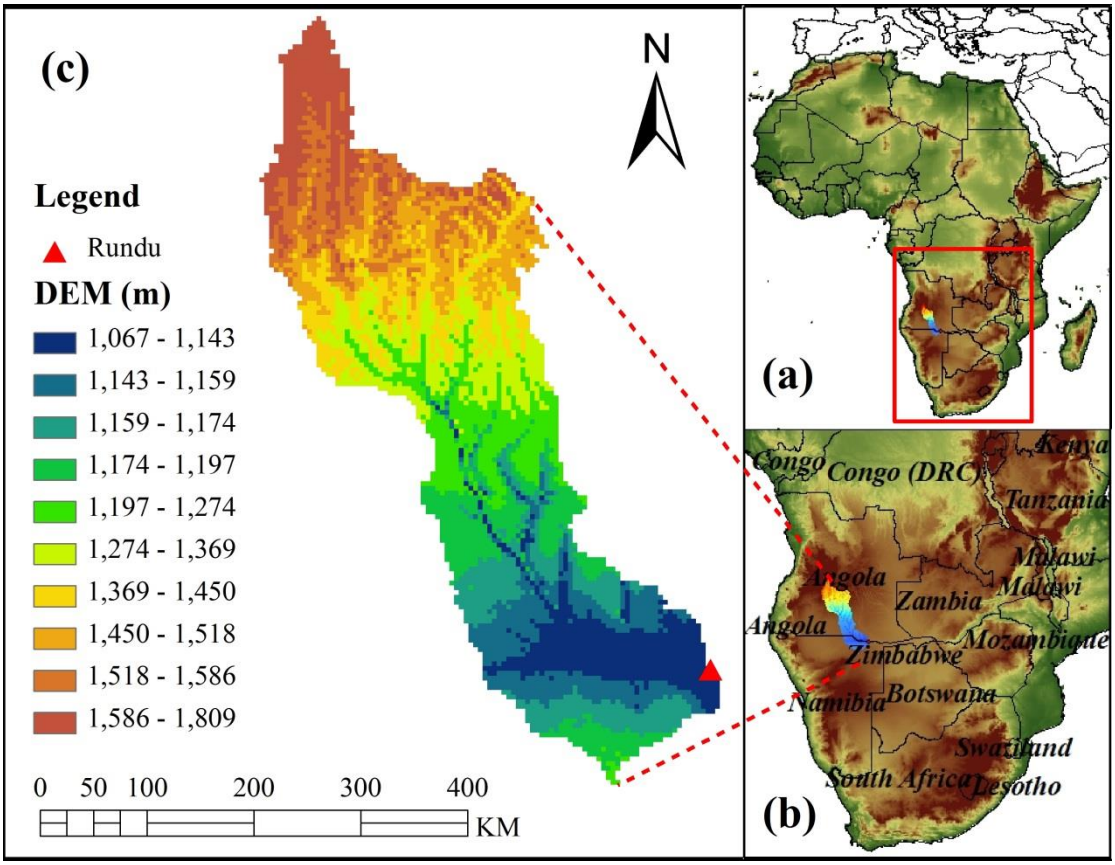

Figure 2.1 Map of research region – Cubango River Basin, South Africa (a) African; (b) Southern Part of Africa; (c) Cubango River

Several studies in the Okavango River Basin have investigated the hydrological response under climate change (Andersson et al. 2006; Hughes et al. 2006，2011; McCarthy et al. 2003; Milzow et al. 2009a). Since the Okavango River basin is one of the most important economic and water resources in southern Africa, additional studies have been solicited to assist in the decision-making for water management in this basin. The main tributary of Okavango River, the Cubango River, which is mainly located in Angola, is selected as the study basin. Figure 2.1 shows the location of the Cubango River in southwest Africa, which accounts for a majority of the available water resources in the Okavango river. The Rundu gauge station is located at the outlet of

Cubango River, a location where both the ground gauge-based streamflow observation and the remote-sensing discharge estimates (i.e., AMSR-E M/C ratio signal) are available.

2.2.2 Model

To concentrate on the effectiveness of the Ensemble Square Root Filter, the conceptually simple Hydrological MODel (HyMOD. Figure 2.2) described in (Wagener et al. 2001) was utilized. This model commonly consists of several quick flow reservoirs and one single reservoir for slow flow; the quick flow reservoirs and the slow flow reservoir operate in parallel as routing components. The parameters of HyMOD and their reasonable ranges are as shown in Table 2.1 (Wagener et al. 2001a): (1) C_{max}: maximum storage capability in the catchment; (2) b_{exp}: the degree of spatial variability of the soil moisture capacity within the catchment; (3) α: quick-slow split parameter; (4) N_q: number of quick flow routing tanks; (5) R_q: quick flow routing tanks rate parameter; and (6) R_s : slow flow routing tanks rate parameter. The internal states are (1) $S(t)$: soil moisture accounting tank state contents; (2) X_q: quickflow routing tanks state contents with dimension of 1*Nq; and (3) X_s: slowflow routing tank state contents. Following evaporation, the remaining rainfall is used to fill the soil moisture storage and then the excess rainfall splits into quickflow reservoir and slowflow reservoir by the quick-slow split parameter α. The flow in each reservoir is governed by quick flow routing tanks rate parameter R_q and slow flow routing tanks rate parameter R_s (Blasone et al. 2008; Kollat et al. 2012). In summary, the input variables should consist of the precipitation and the Potential Evapotranspiration PET, while the main output variable is the streamflow Q.

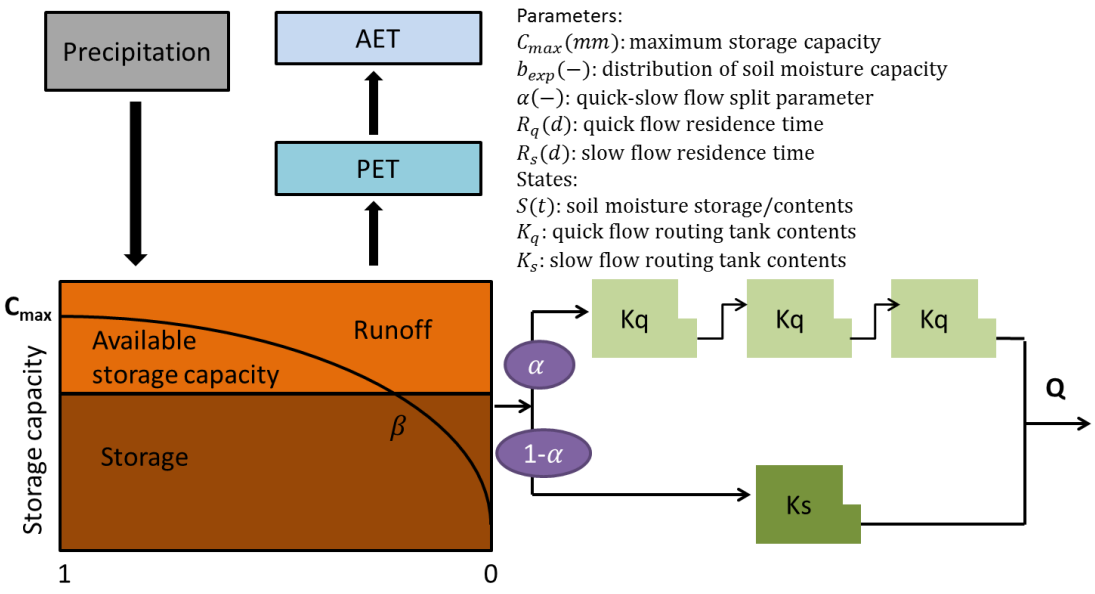

Figure 2.2 Structure of HyMOD

Table 2.1 Parameter Range of HyMOD

Parameter	Unit	Range
C_{max}	mm	1-500
b_{exp}	-	0.1-2
α	-	0-0.99
N_q	-	1-inf
R_q	day	0.1-0.99
R_s	day	0-0.1

2.2.3 Data

With the development of remote-sensing techniques, the application to distributed hydrologic modeling especially in sparse or even ungauged basins has dramatically improved. Remote-sensing data with higher spatial and temporal resolution can provide information over the globe with less cost and less manual maintenance involved. These data can be used as the forcing data (e.g., precipitation, potential evapotranspiration) to drive the hydrologic models and to calibrate the parameters as well, thus enabling the flood forecasts and water resources management tools in most of the developing countries where conventional ground-based measurements are scarce. The Okavango River Basin is considered to be poorly gauged. Sparse ground gauge-based precipitation measurements are available in the Cubango sub-basin where most runoff is generated (Milzow et al. 2011). In this study, remotely-sensed precipitation and potential evapotranspiration are incorporated to drive the model while both the gauge measurement and the remotely-sensed estimation of streamflow are adopted to calibrate the model.

TRMM Multisatellite Precipitation Analysis (TMPA) provides two standard 3B42-level products: the near-real-time 3B42 RT which uses the TRMM combined instrument dataset to calibrate the data and the post-real-time research product 3B42 V7 (level 7) which adjusts the rainfall accumulation by gauge analysis (Huffman et al. 2007). Both 3B42 RT and 3B42 V6 products are quasi-global with coverage from 50 ℃N to 50 ℃S latitude. In this study, the TRMM 3B42 RT with the spatial resolution of 0.25 ° (approximate to 25km in the tropical area) and temporal resolution of three hourly, is processed into daily accumulation as well as basin average and applied as the forcing

data to drive the hydrological model. PET (potential evapotranspiration) comes from the Famine Early Warning System Network (FEWS NET; http://igskmncnwb015.cr.usgs.gov/Global/) with a spatial resolution of 0.25°, and is likewise processed into daily and basin average as additional forcing to the model.

For the benchmarks that were used to calibrate the model, both the ground gauge-observed streamflow from the local government and the AMSR-E signal converted streamflow were applied in this study. Dartmouth Flood Observatory (DFO, http://www.dartmouth.edu/~floods/), as well as GFDS, uses the AMSR-E sensor for discharge estimation in global scope for flood monitoring. Besides these two systems, other studies also explore the possibility of estimating the discharge based on the AMSR-E sensors (Salvia et al. 2011; Temimi et al. 2007, 2011). This study uses the conventional Dartmouth algorithm (Brakenridge et al. 2007), a polynomial model (refer to part 2.3.2), to retrieve the actual streamflow (in m^3/s) from the AMSR-E C/M radiance ratio.

2.3 Methodology

2.3.1 Streamflow estimation from AMSR-E signals

The GFDS uses the near real-time satellite-based, remote-sensing data to monitor floods over the globe. In this system, a passive microwave sensor, AMSR-E, together with TRMM TMI (TRMM Microwave Imager) sensor, are used to measure the brightness temperature at 36.5GHz, descending orbit with horizontal polarization, which responds to surface wetness and thus flooding (Brakenridge et al. 2007). It should be noted that though AMSR-E-polarized measures the brightness temperature (also expressed as radiance) both horizontally and vertically at 6 frequencies from 6.9 to 89.0 GHz, only 36.5GHz at horizontal polarization is selected to measure the change of river discharge through a series of sensitivity tests (Brakenridge et al. 2007). A wet pixel (usually over the surface of a river) is selected to measure the brightness temperature of the measurement (M) area while an adjacent dry pixel is selected to measure the brightness temperature of the calibration (C) area (usually over the land near the wet pixel); the fraction of the measurement and calibration brightness temperature is referred as the M/C ratio signal (Eq. (1)).

$$M / C\ Ratio = Tb_m / Tb_c \tag{1}$$

The M/C ratio signal data are provided by GFDS. Some details about selecting the M/C pixels should be noted: (1) The calibrated dry pixel C is located near the measurement wet pixel M so that changes such as vegetation, soil texture, etc. at those locations are more likely to be correlated. In other words, those two locations are more likely to share similar conditions (e.g. vegetation, and soil texture); (2) C and M are within a short distance so that the measurement acquired by AMSR-E are effectively

contemporaneous; (3) M is selected to have the largest change in water surface area and relatively high sensitivity; (4) C is selected to be close to M but is located far enough to be not affected by flood inundation; (5) Moderate Resolution Imaging Spectroradiometer (MODIS) is applied to assist selecting M where flow area expansions occur (Brakenridge et al. 2007; Kugler and Groeve 2007). The main merit of the AMSR-E passive microwave sensor onboard the NASA EOS Aqua satellite is that it is not restricted by cloud cover and provides data availability for daily flood monitoring over the globe. In addition, since nighttime radiation is more stable than during the day, the descending (nightly) orbit with a footprint size of approximately 8× 12km is used. For additional details, refer to Figure 3. in (Kugler and Groeve 2007) which illustrates how the AMSR-E sensor can be used to detect flooding.

The C/M radiance ratio, which is the reciprocal of M/C ratio signal, is correlated at a significant level with observed streamflow as shown in Figure 2.3.

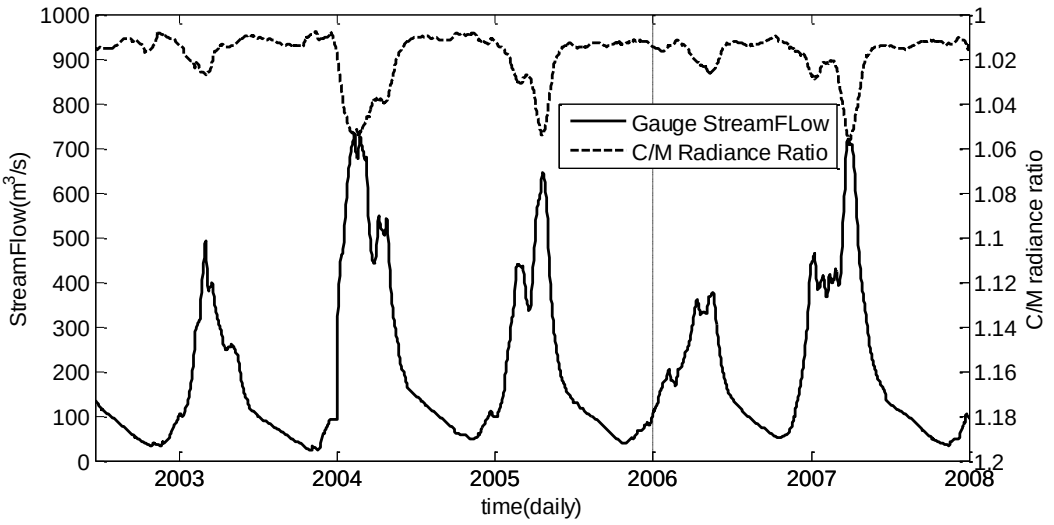

Figure 2.3 Time series plot of C/M radiance ration and observed streamflow from Jun-22-2002 to Dec-31-2007

The relationship can also be visualized by the scatter plot shown in Figure 2.4. Here, the observed streamflow is used to calibrate the orbital gauging measurements (the C/M radiance ratio signal) into in-situ discharge units (m^3/s) via a quadratic polynomial regression as shown in Figure 2.4. Some other regressions were also tested in this study but not listed in this paper; it turns out the nonlinear quadratic polynomial regression outperformed the linear regression and other polynomial regressions. This arithmetic "pair ratio" (C/M radiance ratio as shown in eq. (1)) approach proposed by Brakenridge, accounts for the inherent correlated changes between the brightness temperature ratio and river gauge data (Brakenridge et al. 2007). Brakenridge et al. (2007) also demonstrated that AMSR-E data, calibrated via the paired measurement approach, and obtained over carefully selected river reaches, can characterize river discharge changes at a useful level of accuracy (Brakenridge et al. 2007). It should be noted that the parameters of the quadratic polynomial equation as shown in Figure 2.4 are calibrated using both the gauge streamflow and AMSR-E signals data sets from 22 Jun 2002 to 31 Dec 2005. Following conversion, the correlation coefficient between the signal-converted streamflow and the observed streamflow is 0.95, the Bias is 1.91% and the RMSE (Root Mean Square Error) is 56.64m^3/s during this period [note: capitalized "Bias" in this paper refers to the statistical index that is calculated by eq.(17)].

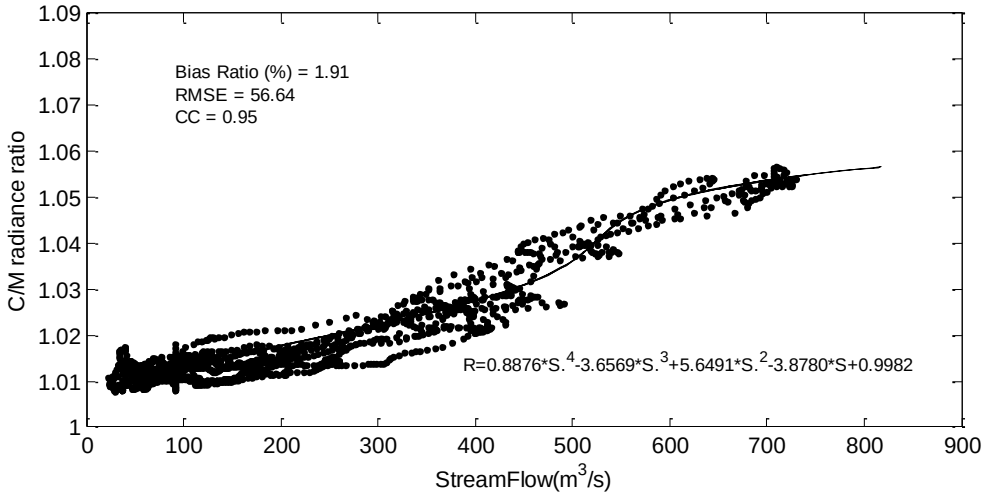

Figure 2.4 Scatter plot and rating curve equation comparing daily C/M radiance radio versus gauge based streamflows (In the equation, R refer to runoff /streamflow and S refer to signal)

The datasets from 1 Jan 2006 to 31 Dec 2007 are applied to validate the performance of this regression method. Figure 2.5 indicates that the signal-converted streamflow is well correlated with gauge observations from 2002 to 2007, especially during the peak flow periods. However, overestimation of streamflow exists during the low flow period because the AMSR-E sensors are not sensitive to low flows. In addition, this approach is applied to medium- to large-sized basins. The accuracy of the AMSR-E signals for basins with less than 50000km^2 drainage areas needs further investigation (Khan et al. 2012). Additional factors influencing the utility of AMSR-E data for streamflow estimation include the width of the river, channel geometry, water temperature relative to land, and measurement pixel resolution.

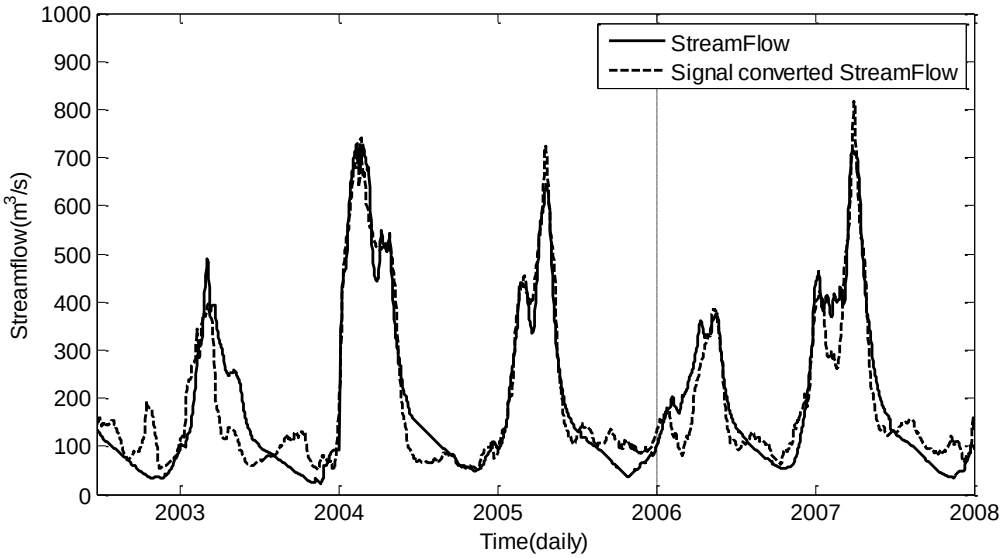

Figure 2.5 Observed streamflow V.S. signal converted streamflow from Jun-22-2002 to Dec 31-2005

2.3.2 Model Calibration and Validation

There are two general approaches for hydrologic model calibration: manual calibration and automatic calibration. The manual calibration approach, which is also expressed as "expert calibration", is largely based on the experience of the modeler. In contrast, the automatic calibration approach, which is largely dependent on the computational power and the efficiency of the algorithm, has been widely applied in hydrological calibration and it is often regarded as a quicker solution for arriving at a useful, calibrated model (Duan et al. 1994).

In this study, an automatic parameter estimation method called DREAM (Differential Evolution Adaptive Metropolis) developed by Vrugt (Vrugt et al. 2009), was applied to calibrate all the six parameters of HyMOD using gauge observations (in experiment 1&2 as described in section 2.3.4) and AMSR-E signal converted streamflow (in experiment 3 as described in section 2.3.4), respectively. DREAM, uses a sophisticated

method to estimate the posterior probability density function in complex, high–dimensional sampling problems and resulted in a successful calibration of the HyMOD model parameters. From the authors' experience, the sensitivities of the parameters C_{max} which controls the quantity of excess rainfall and the routing parameter R_q which controls the residence time of quick-flow are relatively higher, then followed by α, b_{exp} and R_s . From the previous experiences (Blasone et al. 2008; Kollat et al. 2012; Wagener et al. 2001), the number of quick-flow tanks N_q is somewhat sensitive but usually the recommended best value is three for small- to medium-sized basins.

The time series of the precipitation, PET, gauge streamflow observation, and AMSR-E signal are from 22 Jun 2002 (the starting date of the AMSR-E data) to 31 Dec 2007 due to the data availability. The calibration period spans 2003 to 2005, and the validation period is from 2006 to 2007. For each experiment, a warm-up period from 22 Jun 2002 to 31 Dec 2002 was run ahead of each experiment to initialize the internal model states.

2.3.3 Data Assimilation Approach: EnSRF

A sequential data assimilation technique called Ensemble Square Root Filter (EnSRF), which is also referred to as EnKF without perturbing observations, is applied to assimilate different streamflow observations into HyMOD. Compared to the traditional EnKF which requires perturbing both forcing data and observations, for the EnSRF, only the forcing data is perturbed and the ensemble mean is updated by the observation. Whitaker and Hamill demonstrated that there is no additional computational cost by EnSRF relative to EnKF, and EnSRF performs more accurately than EnKF for the same ensemble size (Whitaker and Hamill 2002). But it still remains a research topic to

compare the accuracy and efficiency of different sequential data assimilation approaches (e.g. EnKF, EnSRF).

Let X^b be the background model forecast, which is also called the first guess in data assimilation ($n \times 1$ dimension and n is the number of emsembles); let y be the observation ($p \times 1$ dimension and p is the number of observations), which is the streamflow measurements in this study; let H be the observation operator that converts the states in the model into observation space ($p \times n$ dimension); the estimate of the analyzed state X^a can be described by the traditional Kalman filter update function (Whitaker and Hamill 2002) ($n \times 1$ $dimension$),

$$X^a = X^b + \hat{K}(y - H(X^b)) \quad (2)$$

In Eq (2), $\hat{K}$ refers to the traditional Kalman gain. Let's denote the ensemble X^b as

$$X^b = (x_1^b, x_2^b, \dots, x_n^b) \quad (3)$$

Where we ignore time index and the subscript represents the ensemble member. The ensemble mean is then defined as

$$\overline{X^b} = \frac{1}{n}\sum_{i=1}^{n} x_i^b \quad (4)$$

The perturbation from the mean for the i th member is

$$x_i'^b = x_i^b - \overline{x^b} \quad (5)$$

Then X'^b is defined as a matrix formed from the ensemble of perturbations:

$$X'^b = (x_1'^b, x_2'^b, \dots, x_n'^b) \quad (6)$$

An estimation of background error covariance is defined as

$$\hat{P}^b = \frac{1}{n-1} X'^b (X'^b)^T \quad (7)$$

However, in practice, we do not calculate $\hat{P}^b$, but rather calculate $\hat{\mathrm{P}}^{\mathrm{b}}\mathrm{H}^{\mathrm{T}}$ and $\mathrm{H}\hat{\mathrm{P}}^{\mathrm{b}}\mathrm{H}^{\mathrm{T}}$ are evaluated by the following equations In order to estimate the Kalman gain $\hat{\mathrm{K}}$ ::

$$\hat{\mathrm{P}}^{\mathrm{b}}\mathrm{H}^{\mathrm{T}} = \frac{1}{\mathrm{m}-1}\sum_{i=1}^{m}(\mathrm{X}_{\mathrm{i}}^{\mathrm{b}} - \overline{\mathrm{X}}^{\mathrm{b}})(\mathrm{H}(\mathrm{X}_{\mathrm{i}}^{\mathrm{b}} - \overline{\mathrm{H}(\mathrm{X}^{\mathrm{b}})}))^{\mathrm{T}} \quad (8)$$

$$\mathrm{H}\hat{\mathrm{P}}^{\mathrm{b}}\mathrm{H}^{\mathrm{T}} = \frac{1}{\mathrm{m}-1}\sum_{i=1}^{m}(\mathrm{H}(\mathrm{X}_{\mathrm{i}}^{\mathrm{b}}) - \mathrm{H}(\overline{\mathrm{X}}^{\mathrm{b}}))(\mathrm{H}(\mathrm{X}_{\mathrm{i}}^{\mathrm{b}} - \overline{\mathrm{H}(\mathrm{X}^{\mathrm{b}})}))^{\mathrm{T}} \quad (9)$$

Here, m is the ensemble size. Then the traditional Kalman gain $\hat{\mathrm{K}}$ can be calculated by Eq (10),

$$\hat{\mathrm{K}} = \hat{\mathrm{P}}^{\mathrm{b}}\mathrm{H}^{\mathrm{T}}(\mathrm{H}\hat{\mathrm{P}}^{\mathrm{b}}\mathrm{H}^{\mathrm{T}} + \mathrm{R})^{-1} \quad (10)$$

R is the observation error covariance with a dimension of $p \times p$. In EnSRF, the reduced Kalman gain $\tilde{\mathrm{K}}$ is used to update the deviation from the ensemble mean as estimated by the following equation,

$$\tilde{\mathrm{K}} = (1 + \sqrt{\frac{\mathrm{R}}{\mathrm{H}\hat{\mathrm{P}}^{\mathrm{b}}\mathrm{H}^{\mathrm{T}}+\mathrm{R}}})^{-1}\hat{\mathrm{K}} \quad (11)$$

The ensemble mean can be updated by

$$\overline{\mathrm{X}}_{\mathrm{i}}^{\mathrm{a}} = \overline{\mathrm{X}}_{\mathrm{i}}^{\mathrm{b}} + \hat{\mathrm{K}}(\mathrm{y} - \mathrm{H}(\overline{\mathrm{X}}_{\mathrm{i}}^{\mathrm{b}})) \quad (12)$$

The perturbation (deviation of ensemble mean) can be updated by

$$\mathrm{X}_{\mathrm{i}}'^{\mathrm{a}} = \mathrm{X}_{\mathrm{i}}'^{\mathrm{b}} - \tilde{\mathrm{K}}\mathrm{H}(\mathrm{X}_{\mathrm{i}}'^{\mathrm{b}}) \quad (13)$$

The final analysis follows as

$$\mathrm{X}_{\mathrm{i}}^{\mathrm{a}} = \overline{\mathrm{X}}_{\mathrm{i}}^{\mathrm{a}} + \mathrm{X}_{\mathrm{i}}'^{\mathrm{a}} \quad (14)$$

As mentioned above, when the EnSRF is applied, the forcing data (which is the precipitation in this study) needs to be perturbed. Precipitation perturbations in this study are defined as

$$\mathrm{P}_{\mathrm{i}} = \mathrm{P} + \varepsilon_{\mathrm{i}} \quad (15)$$

where ε_{i} is a random noise factor drawn from a Gaussian distribution

$$\varepsilon_{\mathrm{i}} \sim \mathrm{N}(0, \mathrm{R}) \quad (16)$$

Since this study utilizes a lumped model HyMOD, the satellite-derived precipitation is aggregated into a basin average at every time step as the forcing input of the model, so no spatial error correlation is computed in the generation of the precipitation perturbation due to the feature of the lumped model. Regarding the temporal error correlations, the equation does not directly account for the temporal error correlations. At each time step, an independent rainfall error is generated by Gaussian distribution (refer to eq. (15) and (16)) and added to the original basin average precipitation.

2.3.4 Experimental Design

The primary forcing datasets for the Cubango River basin come from the TRMM RT remote-sensing product and the potential evapotranspiration data from FEWS (http://igskmncnwb015.cr.usgs.gov/Global). Three experiments were performed for testing the efficiency of improving the streamflow simulations by assimilating different sources of observations. First, rainfall and runoff observations from June 2002 to December 2005 were used to calibrate the model parameters without data assimilation following the warm-up period. Then, both the gauge-based streamflow observation and the AMSR-E signal converted streamflow were assimilated separately into HyMOD to update all the internal states at each assimilation cycle, which is daily in this study for both calibration and validation period. The modeling results of these three experiments are evaluated by the gauge-observed streamflow, which is always considered as the most accurate and reliable observation of streamflow.

In the first experiment, the model was calibrated by the gauge-observed streamflow and then the gauge observation was also assimilated into HyMOD to estimate the internal model states. This experiment is the benchmark for all experiments, which are

summarized in Table 2.2. In the second experiment, the model was similarly calibrated using the gauge-observed streamflow; however, in the assimilation step, the AMSR-E signal converted streamflow was incorporated into HyMOD in lieu of the gauge-observed streamflow data assimilated in experiment 1.

Table 2.2 Introduction of experiments design

Experiments	Calibration Benchmark	Data Assimilated into Model
Exp1	Ground Gauge Observed Streamflow	Ground Gauge Observed Streamflow
Exp2	Ground Gauge Observed Streamflow	AMSR-E M/C Ratio Signal Converted Streamflow
Exp3	AMSR-E M/C Ratio Signal converted streamflow	AMSR-E M/C Ratio Signal Converted Streamflow

In the third experiment, the model was calibrated by the AMSR-E signal converted streamflow and then it was also assimilated into model to correct the model states for each assimilation cycle, without gauge-based observations involved.

2.3.5 Sensitivity Analysis

Research has been carried out in the sensitivity analysis among the spread of precipitation ensembles, observation error, ensemble size, and their impacts on data assimilation efficiency (Pauwels and De Lannoy 2006; Whitaker and Hamill 2002). Here, the "spread of the precipitation" is the white noise that is added into the precipitation to generate the precipitation ensembles. In other words, it is a measure of the difference between the precipitation ensemble members and is represented by the standard deviation (e.g. the parameter R is eq. (11)). (Pauwels and De Lannoy 2006) analyzed the sensitivity of observation error; results show that the increase in the observation error leads to a decrease in the accuracy of the modeled discharge.

(Whitaker and Hamill 2002) pointed out that with the enlargement of the ensemble size the modeled result improved up to a point where the modeled result remained the same. Those two studies mentioned above only analyzed the sensitivity of a single factor (e.g. observation error and ensemble size) affected in the effectiveness of data assimilation. Actually, the effectiveness of EnSRF, which can be evaluated by an NSCE (Nash-Sutcliffe Coefficient of Efficiency) statistic, should be a function of several factors (i.e., observation errors, spread of precipitation and ensemble size). In this study, a joint sensitivity analysis has been carried out to evaluate the mutual impacts of various observation errors, spread of precipitation and ensemble sizes for assimilating different sources of streamflow observations. Finally an optimal and reasonable point (with certain observation error, spread of precipitation and ensemble size) that yields the best simulation results when applying EnSRF will be identified and then utilized in the data assimilation experiments. It should be noted that the sensitivity analysis is applied after the model calibration step to avoid the bias in the model, and the sensitivity analysis is only applied for the calibration period.

2.2.6 Evaluation Metrics

In this study, three commonly used statistical indicators were used to assess the long time series model performance with and without the EnSRF data assimilation technique. Bias Ratio quantifies the difference between the simulated streamflow and the observed streamflow as described by the following equation:

$$Bias(\%) = \frac{\sum (y_i - x_i)}{\sum x_i} * 100 \tag{17}$$

In Eq(12), (13) and (14), x_i is the observed streamflow and y_i is the simulated streamflow. Normalized Root Mean Square Error is used to measure random errors as follows:

$$RMSE(\%) = \frac{\sqrt{\sum (x_i - y_i)^2 / n}}{\bar{x}} * 100 \quad (18)$$

For both Bias and RMSE, the smaller their values are (i.e., closest to 0), the better the model result is. Small values of Bias and RMSE signify the modeling results are close to the corresponding observations in regards to systematic bias and random errors.

NSCE is a frequently used statistic to quantify the agreement between the model simulation and the ground observation. The perfect value of NSCE is 1. If the value of the NSCE is below 0, it indicates that the mean of the observation is a better predictor than the model.

$$NSCE = 1 - \frac{\sum (x_i - y_i)^2}{\sum (x_i - \bar{x})^2} \quad (19)$$

In order to further evaluate the performance of EnSRF-coupled-HyMOD in flood detection during the peak flow period, a high flow threshold is defined as the top 10% daily streamflow quantile, and the categorical verification statistics of Probability of Detection (POD), False Alarm Ratio (FAR), Critical Success Index (CSI) and Equitable Threat Score (ETS) are used to evaluate the correspondence between the simulated and observed runoff above the high flow threshold. For specific descriptions of POD, FAR, CSI and ETS, please refer to Appendix.

2.4 Results

2.4.1 Sensitivity Analysis of the Ensemble Size, Observation Error and Spread of Precipitation

As shown by Figure 2.6., observation errors of 5%, 8%, 10%, 13%, 15%, 18%, and 20%, spreads of precipitation of 0.10, 0.20, 0.30,…1.90, and 2.00, and ensemble sizes of 10, 30, 50, 70, and 90 were tested to carry out the sensitivity analysis on the impact of assimilating different sources of streamflow observations to the improvement of modeled streamflow. In the sensitivity analysis for the three experiments, NSCE was taken as the evaluation metric.

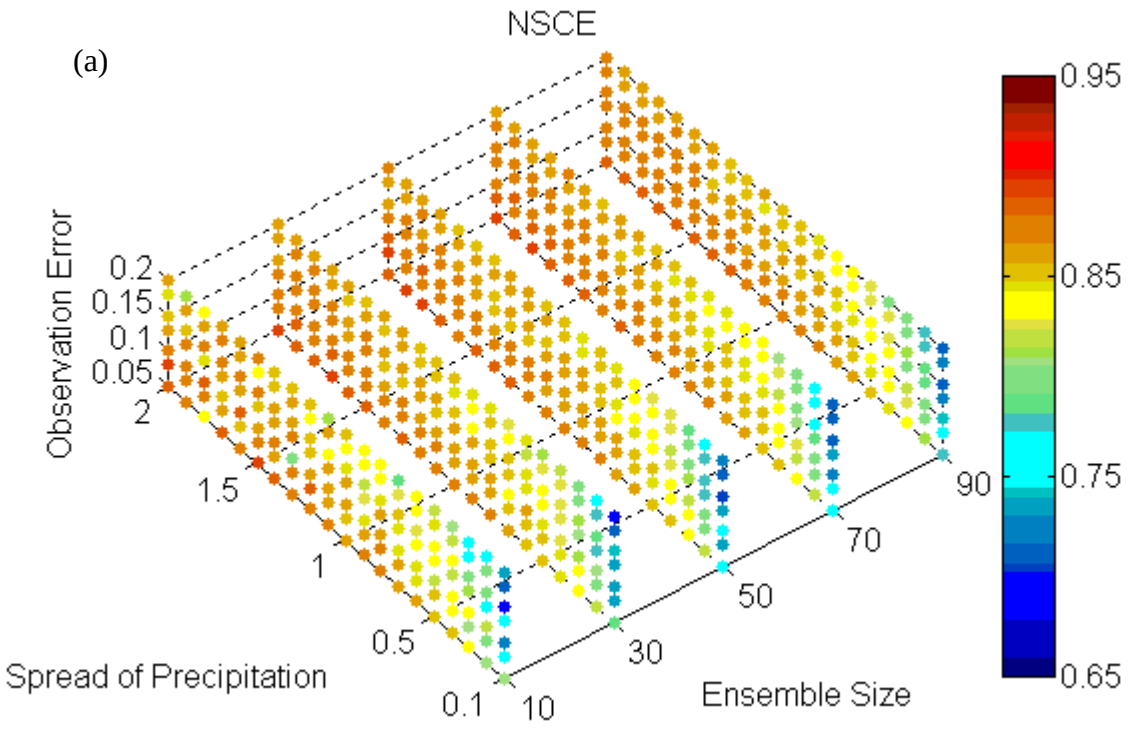

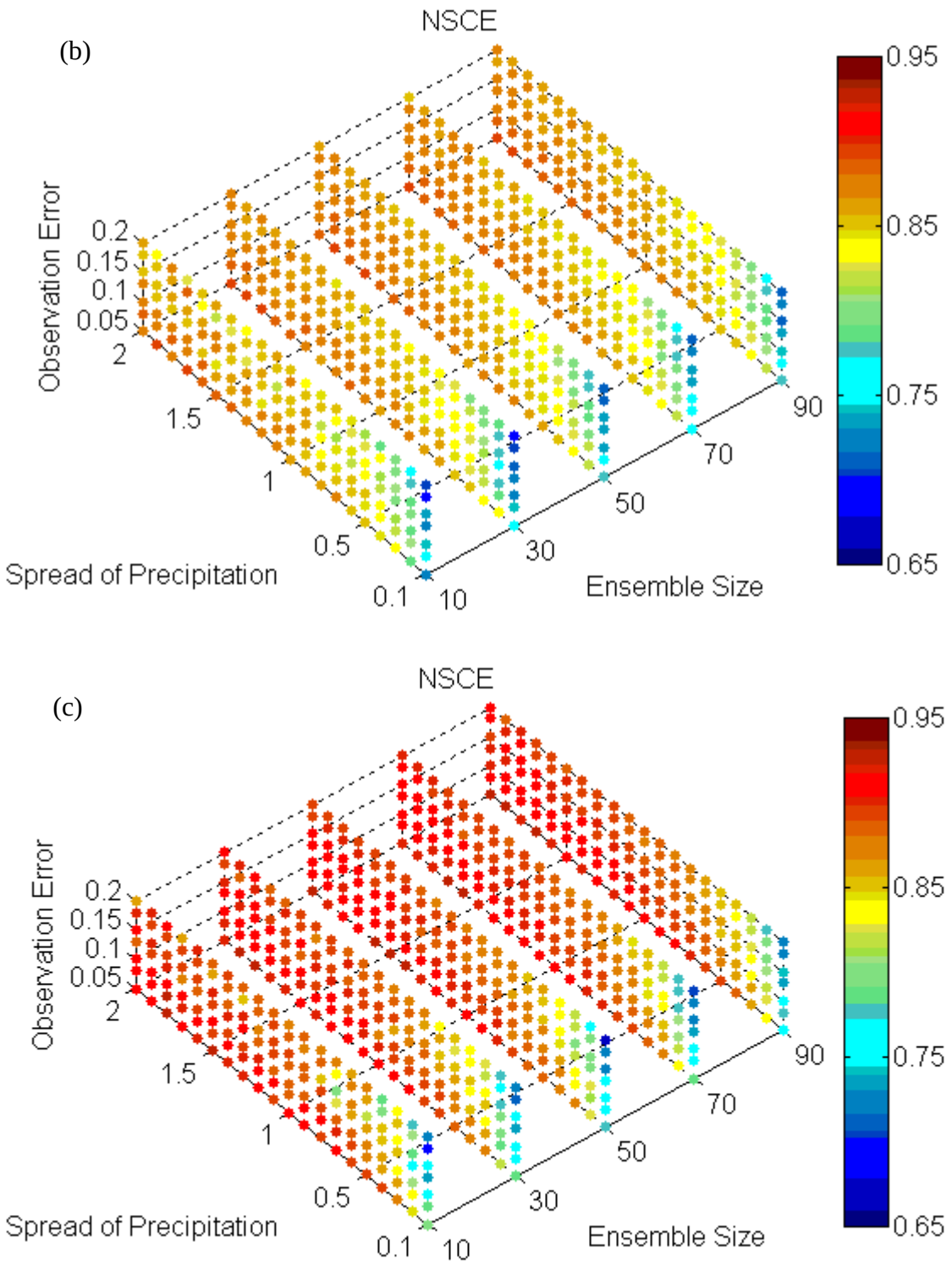

Figure 2.6 Sensitivity analysis regarding observation error spread of precipitation, and ensemble size taking NSCE as the evaluation index (a) Experiment 1; (b) Experiment 2; (c) Experiment 3

Figure 2.6(a), which shows the sensitivity analysis results for experiment 1, indicates increasing the observation error leads to a decrease in the accuracy of the modeled streamflow, which corresponds to the conclusion in (Pauwels and De Lannoy 2006). From the sensitivity plot, it appears a value of 5% is an appropriate assumption describing the observation error. As the observation error goes up from 5% to 20%, the NSCE decreases (see from the vertical direction from Figure 2.6(a)). It may go down below 5% for a better NSCE value, but actually the NSCE does not change much when observation error goes below 10%, which indicates the model performance is not sensitive when the observation error is smaller than 10%. In addition, based on previous experiences from USGS (U.S. Geological Survey), the error of streamflow that is from the gauge observation is usually around 8% (Sauer and Meyer 1992), which is within the reasonable observation error range: 5%-10%. Due to the deficiencies within the simple structure of HyMOD, a larger background covariance was generated thus making the results much more dependent on the observation. In other words, during the assimilation procedure when the observation error is assumed to be smaller, the Kalman gain is increasing, which makes more corrections from the first guess to the observations. Based on the previous experience form USGS, in this case, for the time series assimilation experiment, 8% is assumed as the observation error for experiment 1 to produce the result in Figure 2.6(a). Regarding the ensemble size, the NSCE increases when the ensemble size is enlarged from 10 to 50. However, when the ensemble size is further increased from 50 to 90, it does not lead to a further improvement in NSCE, which means the ensemble size of 50 members was large enough to produce the optimal modeling results. In addition, increasing the spread of precipitation also contributes to

the improvement of the modeling result. By increasing the spread of precipitation from 10% to 170% the modeled streamflow becomes more and more accurate (NSCE becomes closer to 1); however, increasing the spread beyond the value 170% results in no further improvement in the NSCE values.

For experiments 2 and 3, similar sensitivity tests were conducted and are shown in Figure 2.6(b) and Figure 2.6(c). Regarding the observation error, since the remotely-sensed AMSR-E signal converted streamflow shows an overestimate during the low-flow, dry seasons (Figure 2.5), a relatively larger observation error of 10% (compared to ground gauge-based streamflow observation error of 8% in experiment 1) is assumed. These results are shown for experiments 2 and 3 in Figure 2.7(b) and Figure 2.7(c) respectively, both of which assimilate the AMSR-E observations. The optimal ensemble size for experiment 2 and 3 is the same as experiment 1. When fixing the ensemble size to 50 members, the simulated discharge skill reaches maximum values when the spread of precipitation approaches around 140% for both experiment 2 and experiment 3.

Of all the three factors potentially impacting data assimilation efficiency, ensemble size was the least sensitive while the spread of precipitation was the most sensitive. The sensitivity analysis shows that the error in the remotely-sensed precipitation estimates was around 140% to 170%. As mentioned in the introduction, studies show that the TRMM RT precipitation product can lead to bias and random errors that propagate into hydrologic modeling outputs. For hydrological forecasting, the error usually comes from a combination of uncertainties in the input data (TRMM RT and PET in this study), the model structure, and the initial conditions. In this study, the model structural errors were not quantified so that the inability of the model to generate accurate

streamflow was translated into the input forcing data uncertainty. In other words, a larger spread of precipitation is selected in this study to compensate for the modeling error in this case.

2.4.2 Calibration Analysis

As shown in Figure 2.7, model calibration results are quite similar to one another, even when the gauge streamflow observation (experiment 1 & 2) or AMSR-E signal converted streamflow (experiment 3) was applied for calibration. When model parameters are adjusted using gauge-observed streamflow (experiments 1 and 2), the value of Bias, RMSE and NSCE are -11.08%, 68.33% and 0.61, respectively. When the model parameters are adjusted using the AMSR-E signal converted streamflow (experiment 3), the value of Bias, RMSE and NSCE are -8.11%, 75.78% and 0.61, respectively. The striking similarity of the calibration results using different streamflow data sources is a result of high consistency between the signal-converted streamflow and the gauge-observed streamflow. As shown in Figure 2.5, the signal-converted streamflow matches quite well with the gauge observation especially during high flow periods. Moreover, the statistic used to compare the simulations and observations, NSCE, is much more sensitive to high flows compared to low flows. However, it is noted that because of the insensitivity of the AMSR-E sensor to low flows, there is significant overestimation of the signal-converted streamflow for dry periods. The apparent capability to use the AMSR-E signal to calibrate a hydrologic model while achieving nearly the same degree of high skill as using in-situ gauge observations highlights its great potential to be used in tandem with remotely-sensed precipitation

data and PET for providing real-time flood detection and forecasts in sparsely gauged or ungauged basins.

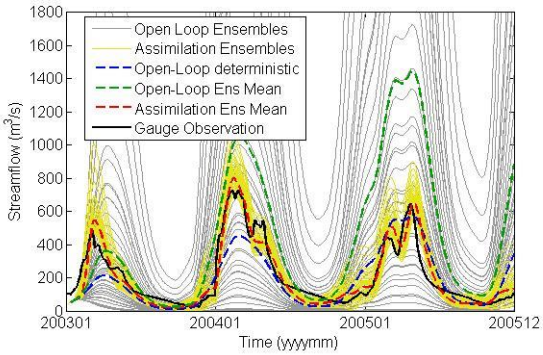

Fig. 2.7 (a1)

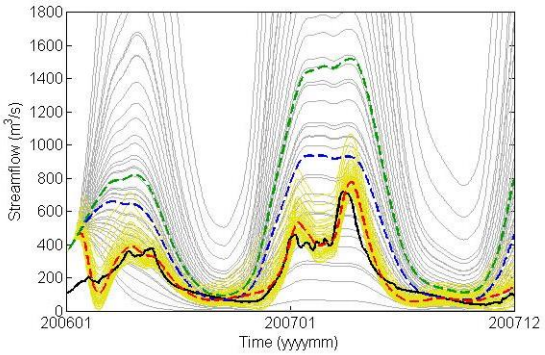

Fig. 2.7 (a2)

exp1	Calibration			Validation		
	Bias(%)	RMSE(%)	NSCE	Bias(%)	RMSE(%)	NSCE
Open Loop	-11.08	68.33	0.61	104.25	140.62	-2.01
Assimilation	-1.39	29.50	0.91	-7.02	34.59	0.92

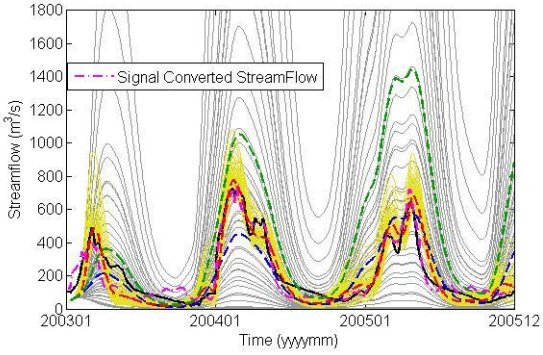

Fig. 2.7 (b1)

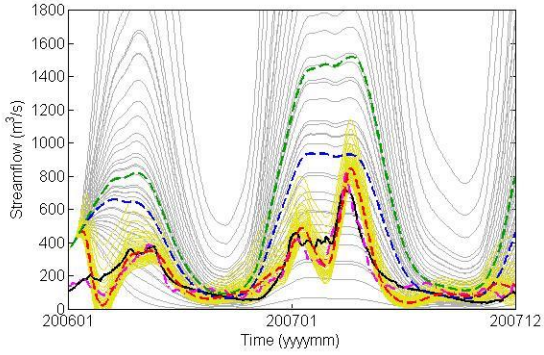

Fig. 2.7 (b2)

exp2	Calibration			Validation		
	Bias(%)	RMSE(%)	NSCE	Bias(%)	RMSE(%)	NSCE
Open Loop	-11.08	68.33	0.61	104.25	140.62	-2.01
Assimilation	2.65	37.27	0.87	-4.93	62.43	0.85

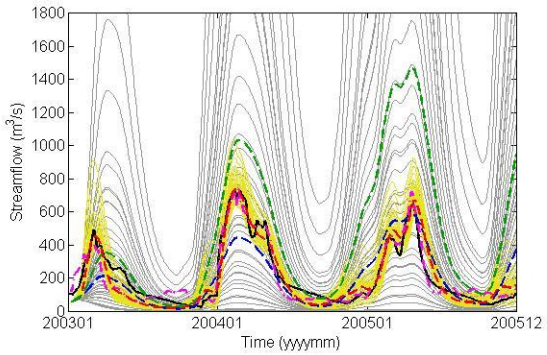

Fig. 2.7 (c1)

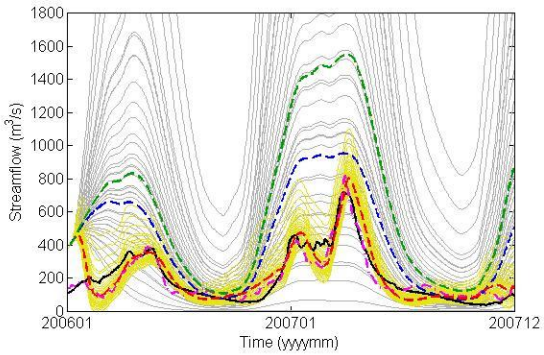

Fig. 2.7 (c2)

exp3	Calibration			Validation		
	Bias(%)	RMSE(%)	NSCE	Bias(%)	RMSE(%)	NSCE
Open Loop	-8.11	75.78	0.61	109.90	161.43	-2.18
Assimilation	1.37	33.02	0.89	-7.21	36.88	0.87

Figure 2.7 Comparisons between streamflows predictions before (open loop) and after (assimilation) data assimilation

(a) Experiment 1: model was calibrated by gauge streamflow and the data that used to be assimilated into the model was also gauge streamflow: (a1) for calibration period and (a2) for validation period

(b) Experiment 2: model was calibrated by gauge streamflow and the data that used to be assimilated into the model was the AMSR-E signal converted streamflow: (b1) for calibration period and (b2) for validation period

(c) Experiment 3: model was calibrated by AMSR-E signal converted streamflow and the data that used to be assimilated into the model was also the AMSR-E signal conversion: (c1) for calibration period and (c2) for validation period

2.4.3 Impact of Data Assimilation

- Impact of data assimilation during calibration period

EnSRF is used to assimilate different sources of streamflow observations into the hydrological model and to estimate all the internal states, thus potentially improving the model outputs of discharge. In order to make the results comparable among those three experiments, the same ensemble size (50) and spread of precipitation (150%) were assumed during the implementation of the assimilation procedures into HyMOD. Since the observation error of the AMSR-E signal converted streamflow shows significant overestimation during low flows, a larger observation error of 10% (in experiment 2 & 3) was assumed while 8% was assumed with the gauge observation error (in experiment 1). The precipitation forcing was perturbed by adding Gaussian white noise through multiplying the TRMM RT daily data by a multiplier of which the mean is 1.0 and the standard deviation is 150%. If negative values appear during the random multiplier generating, the code will automatically re-conduct the Gaussian distributed multiplier generation until they are all positive values.

Overall, Figure 2.7 shows the streamflow "Open Loop" ensembles (grey lines), data "Assimilation" ensembles (yellow lines), Open Loop Ensemble Mean (green dash line), Assimilation Ensemble Mean (red dash line), Open Loop deterministic model run (blue dash line), gauge observation (dark solid line), and signal converted streamflow (magenta dash-dot line). Compared to streamflow ensembles before data assimilation (grey lines), the streamflow ensemble spread after data assimilation (yellow lines) is much reduced, and the ensemble mean after the assimilation is also much closer to the observations. This result reflects the effectiveness of the EnSRF. Compared with the

deterministic Open Loop run, which is the modeled streamflow driven by the original TRMM RT precipitation data without perturbation, the Open Loop ensemble mean is overestimated due to the discard of negative values during the precipitation perturbation procedure as mentioned in the end of last paragraph.

For the assimilation module, the statistical evaluation excludes the first three month for both calibration and validation period due to the bad first guesses at the beginning of each period; in order to make a "fair" comparison between Open-Loop and Assimilation, for Open Loop module, statistics were also calculated excluding the first three months of each period. Experiment 1 is the benchmark for the experiments as it represents a traditional calibration using rainfall and gauged runoff observations while including a streamflow data assimilation step. Figure 2.7(a) shows the impact of the assimilation procedure on the modeled streamflow in the benchmark experiment 1. By assimilating the gauge-based streamflow observation into the gauge-calibrated HyMOD, the Bias is improved from -11.08% to -1.39%, RMSE reduces from 68.33% to 29.50%, while NSCE goes up from 0.61 to 0.91. These statistical results all indicate significant improvement in the modeled streamflow following the assimilation of gauge-based streamflow during the calibration period from 2003 to 2005.

In the second and third experiments, the effectiveness of assimilating AMSR-E signal converted streamflow into HyMOD, conditioned on calibrations from different streamflow sources was assessed. In the second experiment, the model was calibrated by gauge streamflow and then the AMSR-E signal converted to streamflow was assimilated into HyMOD. In the third experiment, the AMSR-E signal converted to streamflow was used as the source for both model calibration and assimilation. Similar

results were obtained in experiments 2 and 3 compared to the first experiment. Specifically, after the EnSRF data assimilation technique was applied, values of RMSE dropped while NSCE rose. This justifies its use for improving discharge simulations.

Furthermore, in order to further evaluate the potential advantage of using data assimilation approach, ensemble spread before (blue solid line) and after (red solid line) data assimilation and the absolute error between modeled streamflow and observed streamflow for both Open Loop module (blue dotted line) and Assimilation module (red dotted line) were plotted in Figure 2.8. As expected, the ensemble spread is greatly reduced using the EnSRF relative to the Open-Loop, and the absolute error is also reduced after applying the EnSRF compared to the Open-Loop, especially during the validation period.

- Impact of data assimilation during validation period

During the validation period from 2006 to 2007, the modeling performance without streamflow assimilation has deteriorated at a significant level compared to the calibration period in terms of Bias, RMSE and NSCE in all three experiments as shown in the tables located in the lower panels in Figure 2.7 (a), (b), and (c), respectively. Both the simplicity of the model structure and the inter-annual uncertainties in the remotely-sensed TRMM RT precipitation contribute to this deterioration.

However, the application of EnSRF to assimilate different sources of streamflow observation improves the 1-day streamflow prediction. All the experiments' modeling results have been remarkably enhanced for the "Assimilation" component compared to the "Open Loop" during the validation period. In comparing the statistics in the three

experiments, experiment 2 reveals a slight degradation in all three scores in comparison to the benchmark in the first experiment. Nonetheless, the degradation isn't significant indicating the potential application of assimilating the AMSR-E signal even into a hydrologic model that has been previously calibrated from gauge observations. As expected, the best statistical results were associated to experiment 1. Experiment 3, which was based on calibration and assimilation using the AMSR-E signal alone, outperformed experiment 2 and has competitive results to experiment 1 as well. The comparable modeling performance of experiment 3 compared to experiment 1 clearly highlights the potential of using the remote-sensing data as a proxy for streamflow with application for flood early warning in sparsely-gauged or ungauged basins. The above results demonstrate that even using a simple hydrological model, when coupled with the EnSRF data assimilation approach, together with large perturbations of precipitation to compensate for the model structural deficiencies, a satisfactory modeling performance can be produced for streamflow forecasting. Further evaluations based on extreme events are conducted in the next section.

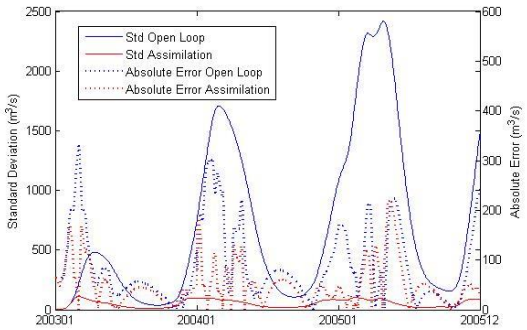

Fig. 2.8 (a1)

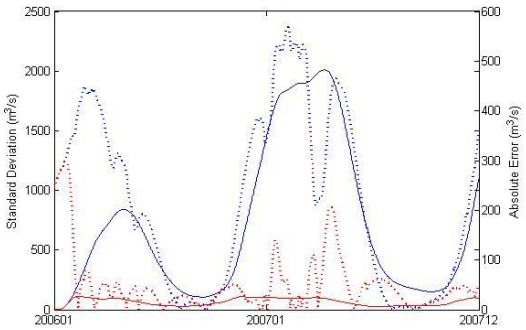

Fig. 2.8 (a2)

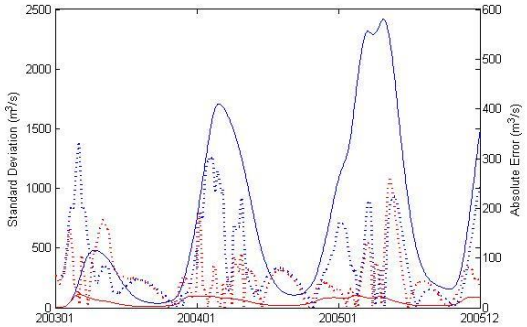

Fig. 2.8 (b1)

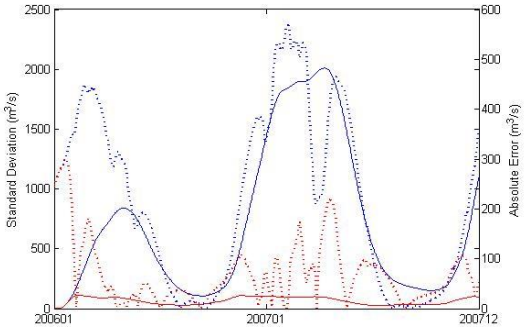

Fig. 2.8 (b2)

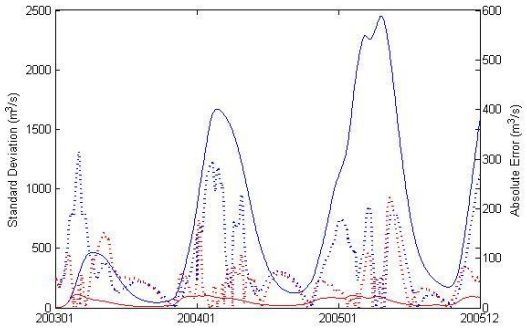

Fig. 2.8 (c1)

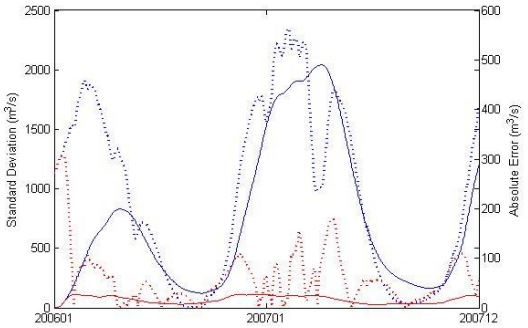

Fig. 2.8 (c2)

Figure 2.8 Time series error analysis for Experiment 1 (Fig.2.8. a), Experiment 2 (Fig.2.8. b) and Experiment 3 (Fig.2.8 c). The left panels are corresponding to calibration period, the right panels are corresponding to validation period. The blue and red solid lines are the ensemble standard deviation for Open Loop module and Assimilation module respectively. The blue and red dash lines are the absolute error between the model simulated streamflow and the observed streamflow.

2.4.4 Threshold-based Evaluation and Analysis

As shown in Figure 2.9, a threshold for high flow is calculated by ranking the daily streamflow data from 1946 to 2005 (50 years) at the Rundu gauge station from highest to lowest. The discharge corresponding to the top 10% daily streamflow quantile, with a value of 402 m^3/s, is identified as the high flow threshold.

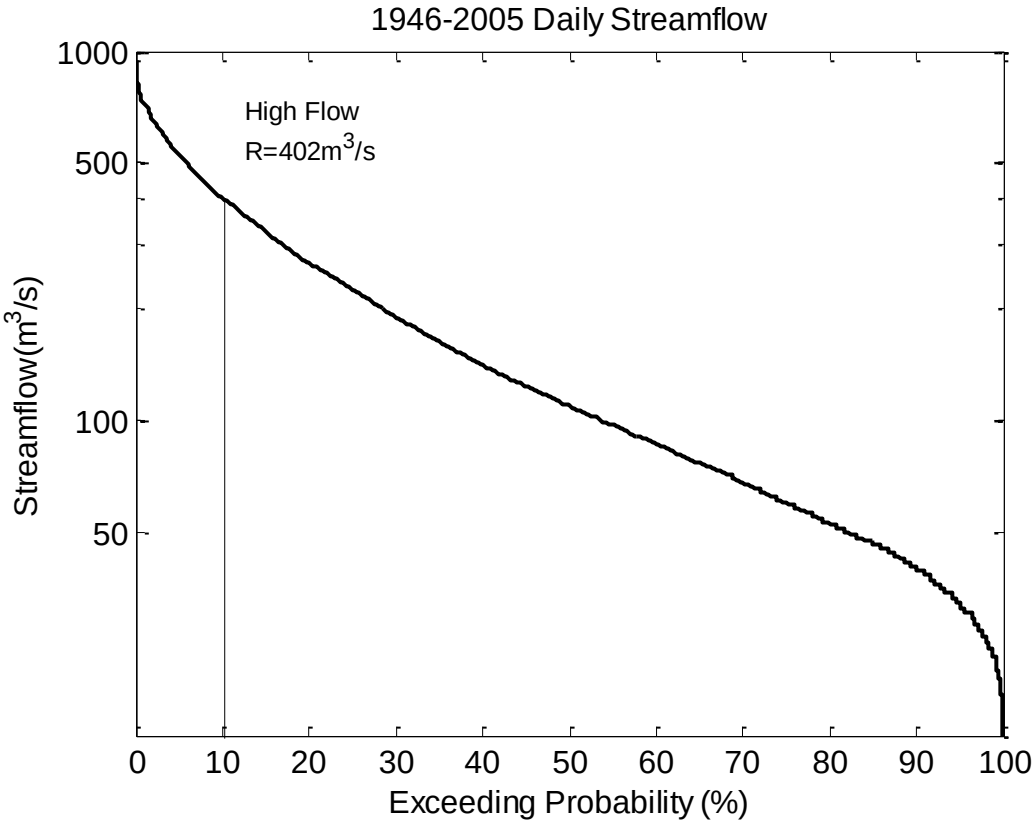

Figure 2.9 Identification of high flow threshold

POD, FAR, CSI and ETS were calculated to further evaluate the filter's performance focused on the detection-capability of the top 10% daily streamflow quantile for the three experiments as before. Figure 2.10 indicates that after data assimilation, POD, CSI and ETS increase while FAR decreases for all experiments during both calibration (left panel in Figure 2.10) and validation (right panel in Figure 2.10) period experiments

except for the POD in the validation period. The POD values without data assimilation are equal to one for the reason that the modeled streamflow is significantly overestimated during the validation period (as shown in Figure 2.7) with all "hits" and no "misses". Nonetheless, the major improvements of POD, FAR, CSI and ETS during both the calibration and validation period highlight the efficiency of high flow detection following data assimilation. These categorical verification statistics together with Bias, RMSE, and NSCE indicate that the impact of the data assimilation procedure to the modeled streamflow is beneficial, especially for improving the model simulation skill during flood events mainly due to the fact that the AMSR-E sensor is quite sensitive to high flow events. During these flooding cases the difference between the brightness temperature for the calibration pixel and the measurement pixel is more acute due to the expansion of the river's surface area.

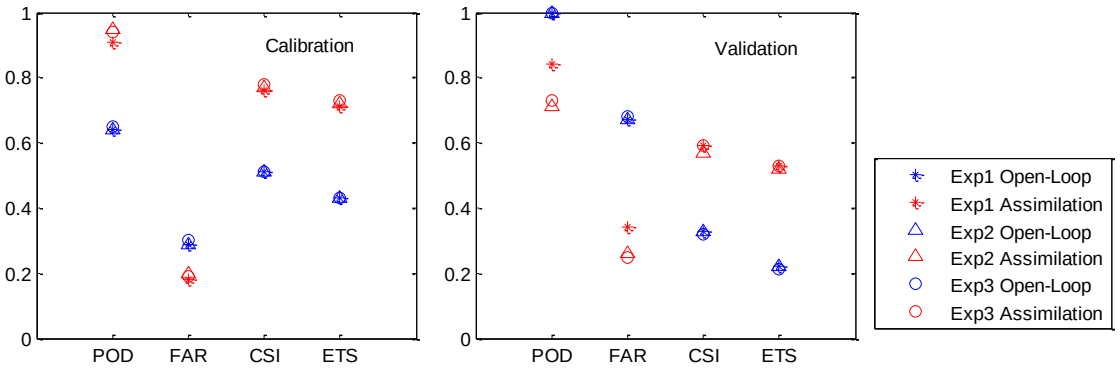

Figure 2.10 Statistics (POD, FAR, CSI, ETS) plot during high flow

For experiment 3, which fully depends on the remote-sensing inputs and highlights the potential of flood prediction in ungauged basins, POD, CSI, and ETS showed improvements after implementing the data assimilation approach during the high flow

period. Compared with experiment 1 during the calibration period, all the categorical verification statistics show improvements to POD, FAR, CSI, and ETS following data assimilation. When it comes to the validation period, the flood detection capability of experiment 3 is better than experiment 2, but slightly degraded yet comparable to experiment 1, which indicates the AMSR-E signal converted to streamflow was apparently well adapted to the model. These experiments highlight the potential use of the AMSR-E signal for streamflow prediction during flooding seasons, especially in ungauged basins.

2.5 Conclusion

Though data scarcity remains a big challenge in hydrologic modeling, remote-sensing data provide a promising perspective on advancements in this research area. In addition, data assimilation techniques incorporate the uncertainties from both the input data and initial conditions and also have the potential to enhance modeling performance. In this study, the deterministic Ensemble Kalman Filter - Ensemble Square Root Filter was coupled with a widely used conceptual rainfall-runoff model to assimilate streamflow data from either in-situ or remote sensing sources to update all the internal states in the model, thus providing the potential to improve modeling results. The following conclusions are reached in this study:

(1) AMSR-E brightness temperature signals can be successfully used to estimate streamflow, highly consistent with the in-situ observation. In particular, the signal converted to streamflow matches well with the observation over relatively high flow periods due to its high sensitivity to land surface wetness.

(2) The traditional model calibration technique is subject to uncertainties in the data, parameters, internal states and model structure. The general poor performance of the calibrated model can be attributed to the weakness of traditional calibration techniques that are normally constrained or limited from the inaccuracy of input remote sensing precipitation data and the simplification of the model structure. Data assimilation can account for both the uncertainties in the input data and the model structure by updating the internal model states, so it is a promising tool in improving hydrological modeling performance, especially for applications of real-time forecasts for decision-makers.

(3) The modeling results have been found to be insensitive to the ensemble size since the model used is a lumped model and there are only a total of five internal states in this conceptual rainfall-runoff model. In contrast, the spread of the precipitation is more sensitive to the improvements of the modeled streamflow.

(4) The three experiments show that through the assimilation of either the gauged streamflow or the AMSR-E signal converted to streamflow into the hydrological model by EnSRF, the difference between the streamflow simulation and observation can be reduced. This demonstrates that EnSRF is effective and efficient in improving modeling performance by assimilating different sources of high-quality streamflow data. The first experiment is the benchmark to verify the feasibility and effectiveness of the data assimilation approach. The second experiment proves the modeling improvement via assimilating a different source of streamflow (i.e. satellite-based streamflow) into a hydrological model that was calibrated by the in-situ streamflow observations. In the third experiment, the AMSR-E streamflow signals were used first to calibrate the model and then assimilated into the model without in-situ streamflow data, thus demonstrating the potential usefulness of the AMSR-E signal data to benchmark and improve hydrological predictions in ungauged or undergauged basins.

(5) When taking the corresponding value to the upper 10th percentile of daily streamflow observations for the recent 50 years as the high flow threshold, the assimilation of both gauge-based streamflow and AMSR-E signal converted to streamflow into HyMOD not only increases POD, CSI, and ETS but also decreases FAR, thus further improving the modeling results for flood forecasting in the Cubango river basin.

(6) Previous studies on hydrological data assimilation commonly take the traditional observation as assimilation data sources, i.e., gauge-observed soil moisture (Aubert et al. 2003; Chen et al. 2011) and observed streamflow (Aubert et al. 2003; Clark et al. 2008; Pauwels and De Lannoy 2006). Benefitting from remote-sensing techniques, recent studies incorporated remotely sensed soil moisture as assimilation sources to improve the discharge prediction (Crow and Ryu 2009; Crow et al. 2005; Gao et al. 2007; Pauwels et al. 2002). So far, no remotely sensed streamflow information has been applied for hydrological data assimilation. As mentioned in (Wagener et al. 2001), currently, river discharge cannot be directly measured by satellite sensors. However, passive microwave sensors - AMSR-E together with TRMM TMI have been used to detect river discharge changes, and those information can be converted into streamflow by using the algorithm mentioned in (Brakenridge et al. 2007). This study is the "first attempt" to exploit and demonstrate the applicability of assimilating spaceborne passive microwave streamflow signals to improve flood prediction in the sparsely gauged Cubango River basin in Africa. Compared to the closest previous publication (Khan et al. 2012) which has also investigated the applicability of the AMSR-E signals in hydrological modeling in the same research region, this study used a simple yet robust model and conducted competitive results. A data assimilation technique is used in this study in addition to the traditional calibration compared to (Khan et al. 2012). Ensemble streamflow simulations are generated and then the ensemble mean is calculated as the final output to represent the streamflow simulation; When combined with EnSRF data assimilation approach HyMOD has similar results compared to a complex, distributed CREST hydrologic model.

In closing, this study is the "first attempt" to exploit and demonstrate the applicability of assimilating spaceborne AMSR-E streamflow signals to improve flood prediction in the Cubango River basin. It also shows that opportunities and challenges exist for an integrated application of a suite of satellite data to flood prediction by careful fusion of remote sensing and in-situ observations and further effective assimilation of the information into a hydrological model. Given the global availability of satellite-based precipitation and AMSR-E signal information in near real-time, we argue that this work will also contribute to the decadal initiative of Prediction in Ungauged Basins: a paradigm shift in the streamflow prediction methods away from traditional methods reliant on statistical analysis and calibrated models, and towards new techniques and new kind of observations, particularly imperative for the vast ungauged or undergauged basins around the world. More promising, data assimilation of remote sensing information for improving hydrological prediction can be increasingly appreciated and supported by the current TRMM and future GPM (Global Precipitation Mission, to be launched in July 2013) together with the current Aqua/AMSR-E and future SMAP (Soil Moisture Active and Passive, to be launched in 2014). Both the new missions are anticipated to provide better precipitation and soil moisture data in terms of coverage, accuracy, and resolutions.

Appendix:

Table A1 shows the contingency table for streamflow simulation and ground gauge observation comparisons. For the case that both the streamflow simulation and ground gauge observation are higher than a certain threshold, it is "hit"; for the case that the streamflow simulation is lower than the certain threshold when ground gauge observation is higher than the same threshold, it is "miss"; for the case that the streamflow simulation is higher than the certain threshold but mean while ground gauge observation is lower than the same threshold, it is "false alarm"; for the case that both the streamflow simulation and ground gauge observation are lower than the certain threshold, it is "Correct Rejection". The desirable values for POD, FAR, CSI and ETS are 1, 0, 1 and 1, respectively.

Table A1

Contingency Table for Simulated Steamflow (Before and After) Data Assimilation Applied and Ground Gauge Observed Streamflow

		Ground Gauge Streamflow Observation	
		Yes	No
Simulate Streamflow Before/After DA	Yes	Hit	False Alarm
	No	Miss	Correct Rejection

Probability of Detection measures the fraction of observed events that exceeded the top 10% daily streamflow quantile that were correctly simulated:

$$POD = \frac{hit}{hit + miss} \tag{A1}$$

False Alarm Ratio calculates the fraction of simulated events that exceeded the top 10% daily streamflow quantile that were not observed:

$$FAR = \frac{false\ alarm}{hit + false\ alarm} \tag{A2}$$

The Critical Success Index, which is also called Threat score, gives the overall fraction of correctly detected events that exceeded the top 10% daily streamflow quantile:

$$CSI = \frac{hit}{hit + miss + falsealarm} \tag{A3}$$

The Equitable Threat Score, which describes how well the simulated "yes" events are corresponding to the observed "yes" events that exceeded the top 10% daily streamflow quantile:

$$ETS = \frac{Hits - E}{Hits + Miss + False\ Alarm}$$
$$E = \frac{\#Forecast\ \ points \times \#Observed\ \ points}{\#\ of\ \ Total\ \ points\ \ possible} \tag{A4}$$

References

Adhikari, P., Y. Hong, K. Douglas, D. Kirschbaum, J. Gourley, R. Adler, and G. Robert Brakenridge (2010), A digitized global flood inventory (1998–2008): compilation and preliminary results, *Natural Hazards*, *55*(2), 405-422.

Andersson, L., J. Wilk, M. C. Todd, D. A. Hughes, A. Earle, D. Kniveton, R. Layberry, and H. H. Savenije (2006), Impact of climate change and development scenarios on flow patterns in the Okavango River, *Journal of Hydrology*, *331*(1), 43-57.

Aubert, D., C. Loumagne, and L. Oudin (2003), Sequential assimilation of soil moisture and streamflow data in a conceptual rainfall–runoff model, *Journal of Hydrology*, *280*(1), 145-161.

Bitew, M. M., and M. Gebremichael (2011), Evaluation of satellite rainfall products through hydrologic simulation in a fully distributed hydrologic model, *Water Resources Research*, *47*(6), W06526.

Blasone, R.-S., J. A. Vrugt, H. Madsen, D. Rosbjerg, B. A. Robinson, and G. A. Zyvoloski (2008), Generalized likelihood uncertainty estimation (GLUE) using adaptive Markov Chain Monte Carlo sampling, *Advances in Water Resources*, *31*(4), 630-648.

Brakenridge, G. R., S. V. Nghiem, E. Anderson, and R. Mic (2007), Orbital microwave measurement of river discharge and ice status, *Water Resources Research*, *43*(4).

Brakenridge, G. R., E. Anderson, S. V. Nghiem, S. Caquard, and T. B. Shabaneh (2003), Flood warnings, flood disaster assessments, and flood hazard reduction: The roles of orbital remote sensing, paper presented at 30th International Symposium on Remote Sensing of Environment, Honolulu, HI, November 10-14, 2003, Pasadena, CA: Jet Propulsion Laboratory, National Aeronautics and Space Administration, 2003.

Chen, F., W. T. Crow, P. J. Starks, and D. N. Moriasi (2011), Improving hydrologic predictions of a catchment model via assimilation of surface soil moisture, *Advances in Water Resources*, *34*(4), 526-536.

Chen, H., D. Yang, Y. Hong, J. J. Gourley, and Y. Zhang (2013), Hydrological data assimilation with the Ensemble Square-Root-Filter: Use of streamflow observations to update model states for real-time flash flood forecasting, *Advances in Water Resources*, *59*, 209-220.

Clark, M. P., D. E. Rupp, R. A. Woods, X. Zheng, R. P. Ibbitt, A. G. Slater, J. Schmidt, and M. J. Uddstrom (2008), Hydrological data assimilation with the ensemble Kalman filter: Use of streamflow observations to update states in a distributed hydrological model, *Advances in Water Resources*, *31*(10), 1309-1324.

Crow, W., and D. Ryu (2009), A new data assimilation approach for improving runoff prediction using remotely-sensed soil moisture retrievals, *Hydrology and Earth System Sciences*, *13*(1), 1.

Crow, W., R. Bindlish, and T. Jackson (2005), The added value of spaceborne passive microwave soil moisture retrievals for forecasting rainfall - runoff partitioning, *Geophysical Research Letters*, *32*(18).

Duan, Q., S. Sorooshian, and V. K. Gupta (1994), Optimal use of the SCE-UA global optimization method for calibrating watershed models, *Journal of Hydrology*, *158*(3–4), 265-284.

Gao, H., E. F. Wood, M. Drusch, and M. F. McCabe (2007), Copula-derived observation operators for assimilating TMI and AMSR-E retrieved soil moisture into land surface models, *Journal of Hydrometeorology*, *8*(3), 413-429.

Gourley, J. J., Y. Hong, Z. L. Flamig, J. Wang, H. Vergara, and E. N. Anagnostou (2011), Hydrologic evaluation of rainfall estimates from radar, satellite, gauge, and combinations on Ft. Cobb basin, Oklahoma, *Journal of Hydrometeorology*, *12*(5), 973-988.

Hong, Y., R. Adler, A. Negri, and G. Huffman (2007a), Flood and landslide applications of near real-time satellite rainfall products, *Natural Hazards*, *43*(2), 285-294.

Hong, Y., R. F. Adler, F. Hossain, S. Curtis, and G. J. Huffman (2007b), A first approach to global runoff simulation using satellite rainfall estimation, *Water Resources Research*, *43*(8), W08502.

Huffman, G. J., D. T. Bolvin, E. J. Nelkin, D. B. Wolff, R. F. Adler, G. Gu, Y. Hong, K. P. Bowman, and E. F. Stocker (2007), The TRMM Multisatellite Precipitation Analysis (TMPA): Quasi-Global, Multiyear, Combined-Sensor Precipitation Estimates at Fine Scales, *Journal of Hydrometeorology*, *8*(1), 38-55.

Hughes, D. A., D. G. Kingston, and M. C. Todd (2011), Uncertainty in water resources availability in the Okavango River basin as a result of climate change, *Hydrology and Earth System Sciences*, *15*(3), 931-941.

Hughes, D. A., L. Andersson, J. Wilk, and H. H. Savenije (2006), Regional calibration of the Pitman model for the Okavango River, *Journal of Hydrology*, *331*(1), 30-42.

Khan, S. I., H. Yang, H. J. Vergara, J. J. Gourley, G. R. Brakenridge, T. De Groeve, Z. L. Flamig, F. Policelli, and Y. Bin (2012), Microwave Satellite Data for Hydrologic Modeling in Ungauged Basins, *Geoscience and Remote Sensing Letters, IEEE*, *9*(4), 663-667.

Kollat, J., P. Reed, and T. Wagener (2012), When are multiobjective calibration trade - offs in hydrologic models meaningful?, *Water Resources Research*, *48*(3).

Kugler, Z., and T. D. Groeve (2007), The global flood detection system, *JRC Scientific and Technical Reports, EUR 23303 EN*

Kuzmin, V., D.-J. Seo, and V. Koren (2008), Fast and efficient optimization of hydrologic model parameters using a priori estimates and stepwise line search, *Journal of Hydrology*, *353*(1–2), 109-128.

McCarthy, J. J. (2001), *Climate change 2001: impacts, adaptation, and vulnerability: contribution of Working Group II to the third assessment report of the Intergovernmental Panel on Climate Change*, Cambridge University Press.

McCarthy, J. M., T. Gumbricht, T. McCarthy, P. Frost, K. Wessels, and F. Seidel (2003), Flooding patterns of the Okavango wetland in Botswana between 1972 and 2000, *AMBIO: A Journal of the Human Environment*, *32*(7), 453-457.

Milzow, C., P. E. Krogh, and P. Bauer-Gottwein (2011), Combining satellite radar altimetry, SAR surface soil moisture and GRACE total storage changes for hydrological model calibration in a large poorly gauged catchment, *Hydrology and Earth System Sciences*, *15*(6), 1729-1743.

Milzow, C., L. Kgotlhang, P. Bauer-Gottwein, P. Meier, and W. Kinzelbach (2009a), Regional review: the hydrology of the Okavango Delta, Botswana—processes, data and modelling, *Hydrogeology Journal*, *17*(6), 1297-1328.

Milzow, C., L. Kgotlhang, W. Kinzelbach, P. Meier, and P. Bauer-Gottwein (2009b), The role of remote sensing in hydrological modelling of the Okavango Delta, Botswana, *Journal of Environmental Management*, *90*(7), 2252-2260.

Moradkhani, H., S. Sorooshian, H. V. Gupta, and P. R. Houser (2005), Dual state–parameter estimation of hydrological models using ensemble Kalman filter, *Advances in Water Resources*, *28*(2), 135-147.

Pauwels, V., R. Hoeben, N. E. Verhoest, F. P. De Troch, and P. A. Troch (2002), Improvement of TOPLATS ‐ based discharge predictions through assimilation of ERS ‐ based remotely sensed soil moisture values, *Hydrological Processes*, *16*(5), 995-1013.

Pauwels, V. R., and G. J. De Lannoy (2006), Improvement of modeled soil wetness conditions and turbulent fluxes through the assimilation of observed discharge, *Journal of Hydrometeorology*, *7*(3), 458-477.

Robinson, A. R., and P. F. Lermusiaux, 2000: Overview of data assimilation. *Harvard reports in physical/interdisciplinary ocean science*, **62**.

Salvia, M., F. Grings, P. Ferrazzoli, V. Barraza, V. Douna, P. Perna, C. Bruscantini, and H. Karszenbaum (2011), Estimating flooded area and mean water level using active and passive microwaves: the example of Paran á River Delta floodplain, *Hydrology and Earth System Sciences*, *15*(8), 2679-2692.

Sauer, V. B., and R. W. Meyer (1992), Determination of error in individual discharge measurements, *U.S. Geological Survey. Open-File Report* 92-144.

Smith, L. C. (1997), Satellite remote sensing of river inundation area, stage, and discharge: A review, *Hydrological Processes*, *11*(10), 1427-1439.

Temimi, M., R. Leconte, F. Brissette, and N. Chaouch (2007), Flood and soil wetness monitoring over the Mackenzie River Basin using AMSR-E 37 GHz brightness temperature, *Journal of Hydrology*, *333*(2–4), 317-328.

Temimi, M., T. Lacava, T. Lakhankar, V. Tramutoli, H. Ghedira, R. Ata, and R. Khanbilvardi (2011), A multi-temporal analysis of AMSR-E data for flood and discharge monitoring during the 2008 flood in Iowa, *Hydrological Processes*, *25*(16), 2623-2634.

Vrugt, J. A., C. Ter Braak, C. Diks, B. A. Robinson, J. M. Hyman, and D. Higdon (2009), Accelerating Markov chain Monte Carlo simulation by differential evolution with self-adaptive randomized subspace sampling, *International Journal of Nonlinear Science and Numerical Simulation*, *10*(3), 273-290.

Wagener, T., D. P. Boyle, M. J. Lees, H. S. Wheater, H. V. Gupta, and S. Sorooshian (2001), A framework for development and application of hydrological models, *Hydrology and Earth System Sciences*, *5*(1), 13-26.

Whitaker, J. S., and T. M. Hamill (2002), Ensemble data assimilation without perturbed observations, *Monthly Weather Review*, *130*(7), 1913-1924.

Chapter 3. Impact of assimilating spaceborne microwave signals for improving hydrological prediction in ungauged basins

Abstract

The availability of in-situ data has been a constraining issue in hydrological prediction, especially in those regions that are only sparsely monitored or completely ungauged. The application of remote-sensing data, without conventional in-situ hydrological measurements, to force, calibrate and update a hydrologic model is a major contribution of this study. First, a rainfall-runoff hydrological model called CREST, coupled with an Ensemble Square Root Filter, is used for exceedance probability-based flood prediction. Then, this advanced flood-prediction framework, with different experimental designs, is forced by TRMM precipitation while Aqua AMSR-E microwave brightness temperature signals are used for model calibration and data assimilation for progressively improved river discharge prediction. Results indicate that solely relying on remote-sensing data for model forcing, parameter calibration, and state updating with EnSRF, the designed framework can adequately predict flooding events. A high flow threshold was applied and has further improved modeling performance, particularly in the flooding seasons, with a flood warning lead-time of one day. Given the anticipated global availability of satellite-based precipitation (i.e. GPM) and AMSR-E like passive microwave signal information (i.e. SMAP) in near real-time, this proposed research framework could potentially contribute to the exceedance

probability-based flood prediction in the vast sparsely gauged or ungauged basins around the world.

3.1 Introduction

Insufficient ground gauge observations have been historical barriers in hydrological predictions. Over the globe, especially in Africa, it is much more common for a given basin to be only sparsely or not monitored at all by in-situ observation networks. However, recent advancement in satellite remote-sensing technology bears the promising potential to overcome the limited spatial coverage of in-situ observation networks, thus providing the potential for hydrological predictions by being creatively used as the forcing (e.g. satellite precipitation estimation), calibration basis (e.g. passive microwave streamflow signal), and sources for assimilation (e.g. satellite-detected soil moisture estimation and passive microwave streamflow signals). This forecast system based entirely on remote-sensing information thus enhances the reliability of streamflow prediction in poorly-gauged basins, and makes streamflow prediction possible even in ungauged basins.

Considering hydrological modeling in those basins with limited ground surface observation networks, a great deal of success has been achieved through the recent availability of remote-sensing precipitation data (e.g. (Hong et al. 2004; Huffman et al. 2007; Joyce et al. 2004; Sorooshian et al. 2000; Turk and Miller 2005)). Besides utilizing the remote-sensing precipitation data as forcing, remote-sensing soil moisture data can also facilitate hydrological prediction by data assimilation approaches (e.g. (Brocca et al. 2010, 2012; Crow and Ryu 2009; Crow et al. 2005; Gao et al. 2007; Matgen et al. 2012; Pauwels et al. 2002)), which is promising for those basins with sparsely or even without in-situ soil moisture observations. As a traditional way, the hydrological prediction accuracy is commonly improved by calibrating hydrologic

models and through assimilating in-situ soil moisture observations and gauge-based streamflow measurements into hydrological models. (e.g. (Aubert et al. 2003; Clark et al. 2008; Pauwels and De Lannoy 2006)). The use of streamflow estimates from remote-sensing methods is a new area being explored, also for model calibration and data assimilation. Recently, the Global Flood Detection System (GFDS, http://www.gdacs.org/flooddetection/), began using a passive microwave sensor, AMSR-E, together with the Tropical Rainfall Measurement Mission (TRMM) Microwave Imager (TMI), to measure surface brightness temperatures, which can be used creatively to infer streamflow and thus show the potential to monitor floods over the globe (Brakenridge et al. 2007). While prior studies have evaluated the potential application of the AMSR-E sensor for discharge estimation and flood detection (Salvia et al. 2011; Temimi et al. 2007, 2011), they all required in-situ streamflow information. In addition to AMSR-E, very recently, Moderate resolution Imaging Spectroradiometer (MODIS) has also been applied by (Tarpanelli et al. 2013) to estimate the streamflows in medium-sized basins adopting the same methodology developed by (Brakenridge et al. 2007) at daily scale; good results show the potential to apply this for smaller basins thanks to the higher spatial resolution of MODIS data (250m) compared to the spatial resolution of AMSR-E at 25km; likewise the discharge estimation from AMSR-E, this approach using MODIS also requires in-situ discharge observations.

In this study, the passive microwave streamflow signals from AMSR-E are utilized directly, without in-situ streamflow observations, in a hydrologic model to calibrate the hydrological model based on the approach in (Khan et al. 2012). Then, the frequency (exceedance probability) of the remote-sensing streamflow signals is assimilated into

the hydrological model through the data assimilation approach that was applied in (Zhang et al. 2013) in order to demonstrate probabilistic flood prediction for an African basin. Though conducted in the same research region – Cubango river basin with the same forcing data (refer to section 2.2 data sources for detailed information) and a similar data assimilation approach (refer to section 2.4 for detailed information), this study is conducted in the frequency domain and is independent from the in-situ streamflow observation. The application of in-situ steamflow observation in this study is set up as the benchmarks to evaluate the hydrological performance of the remote sensing streamflow signals, which demonstrates an innovative way for improving the hydrological prediction in ungauged basins with outcomes as probabilistic based predictions. In contrast, (Zhang et al. 2013) was conducted in the actual streamflow domain. It firstly converted the remote sensing streamflow signals into streamflow based on the in-situ streamflow observation by adopting the algorithm that was developed by (Brakenridge et al. 2007). Then, the remote sensing signal converted streamflow was applied to calibrate and update the model, thus providing hydrological predictions in actual streamflow domain (i.e., in units of m^3/s).

Section 2 describes the study basin, the data applied and the algorithm. Then section 3 discusses the results of both calibration and data assimilation in frequency domain conducted by the streamflow signals (Experiment 3) compared to the results obtained by the in-situ streamflow in both actual domain (Experiment 1) and frequency domain (Experiment 2). Finally, the conclusion is drawn in section 4.

3.2 Study Basin, Data Sources and Methodology

3.2.1 Study Basin

The Okavango River, which runs for about 1100 km from central Angola and flows through Namibia and Botswana, is the fourth longest river in southern Africa (Figure 3.1). The Okavango catchment is approximately 413,000 km^2; it originates in the headwaters of central Angola, then the Cubango and Cuito tributaries meet to form the Cubango-Okavango River near the border of Angola and Namibia and flow into the Okavango Delta in Botswana. The upper stream region belongs in a subtropical climate zone with annual precipitation around 1300mm while the downstream region, which contains the Kalahari Desert, belongs to the semi-arid climate zone with annual precipitation around 450mm (Hughes et al. 2006; Milzow et al. 2009b). The headwater region, which is the northern part of the basin, is mainly covered by the ferralsols soil with a lower hydraulic conductivity. The headwater region also has a high forest cover and contributes significantly to the river runoff (Hughes et al. 2006). The rest of the basin is dominated by arenosals soil (www.sharing-water.net), which is very porous with high hydraulic conductivity, so that water drains rapidly, leaving little moisture for plants. As mentioned by (Hughes et al. 2006), around 95% of inflow is lost in the atmosphere due to high potential evapotranspiration rate and only a small portion contributes to groundwater.

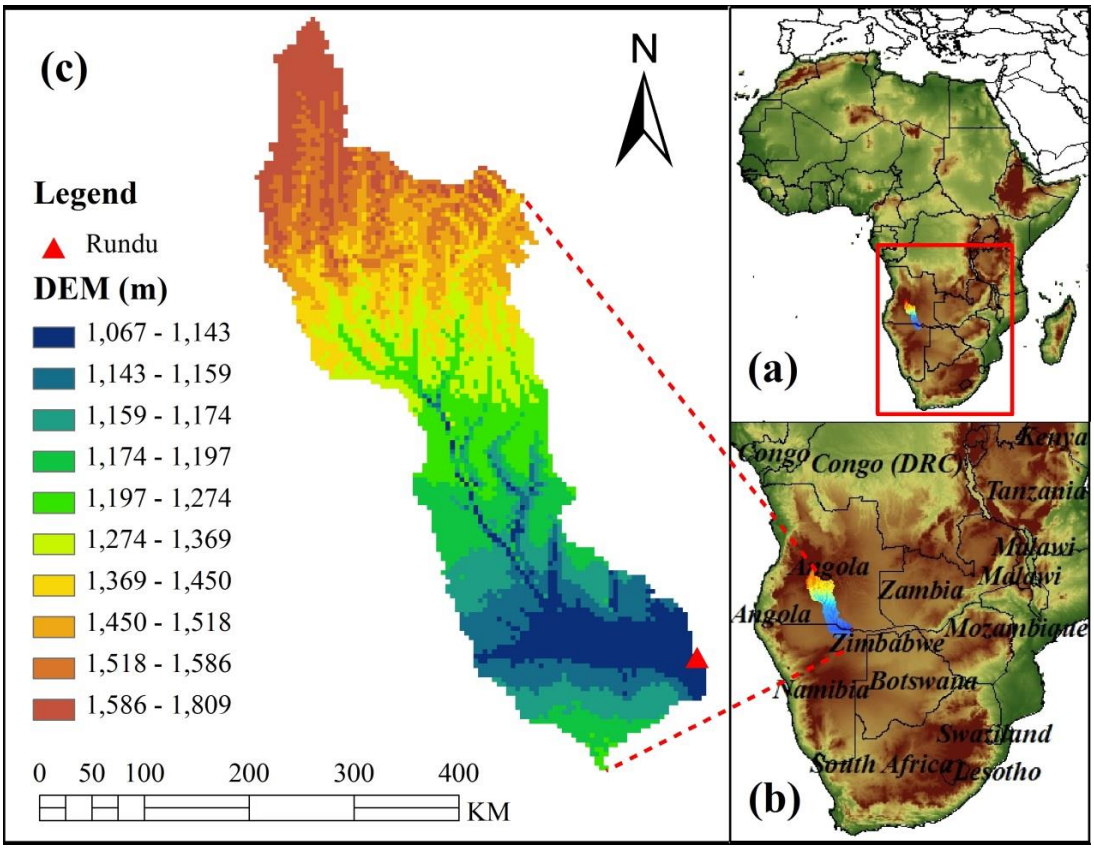

Figure 3.1 Research Region – Cubango River Basin

Several studies in the Okavango River Basin have investigated the hydrological response under climate change (Andersson et al. 2006; Hughes et al. 2006, 2011; McCarthy et al. 2003; Milzow et al. 2009a). Since the Okavango River basin is one of the most important economic and water resources in southern Africa, additional studies have been solicited to assist in the decision-making for water management in this basin. The main tributary of Okavango River - the Cubango River, which is mainly located in Angola, is selected as the study basin. It accounts for a majority of the available water resources in the Okavango river. The Rundu gauge station is the outlet of the Cubango River; at Rundu Gauge, both gauge-based streamflow and the remote-sensing discharge estimates (i.e., the AMSR-E & TMI streamflow signals) are available.

3.2.2 Data Sources

This study develops an advanced exceedance probability-based, flood-prediction framework, which is based entirely on satellite remote-sensing data without a requirement of conventional in-situ hydrological measurements. The in-situ streamflow observation, with daily temporal resolution, is only used in this study to evaluate the exceedance probability-based hydrological prediction algorithm. The proposed data sets that were applied in this study include:

TRMM RT Satellite Precipitation Estimates

Tropical Rainfall Measuring Mission (TRMM) satellite precipitation estimates are taken as forcing data into hydrological modeling in this study since the Okavango River Basin is poorly gauged (Milzow et al. 2011). TRMM Multi-satellite Precipitation Analysis (TMPA) provides two standard 3B42-level products: the near-real-time 3B42 RT which uses the TRMM combined instrument dataset to calibrate the data and the post-real-time research product 3B42 V7 (level 7) which adjusts the rainfall accumulation by gauge analysis (Huffman et al. 2007). Both 3B42 RT and 3B42 V7 products are quasi-global with coverage from 50°N to 50°S latitude. In this study, the TRMM 3B42 RT with a spatial resolution of 0.25°(approximate to 25km in the tropical area) and temporal resolution of three hourly, is processed into daily accumulations as well as basin averages and applied as the forcing data to drive the hydrological model.

FEWS PET

PET (Potential Evapotranspiration) comes from the Famine Early Warning System Network (FEWS NET; http://igskmncnwb015.cr.usgs.gov/Global/) with a temporal

resolution of monthly and spatial resolution of 0.25°, and is likewise processed into daily and basin averages as additional forcing to the model.

The Passive Microwave Streamflow signal from TRMM and Aqua

The Global Flood Detection System uses near-real-time, satellite-based, remote-sensing data to monitor floods over the globe at daily scale. In this system, a passive microwave sensor, AMSR-E, together with TRMM TMI (TRMM Microwave Imager) sensor (Note: TMI was applied after Oct 4, 2011 when AMSR-E stopped working), is used to measure the brightness temperature at 36.5GHz, descending orbit with horizontal polarization, which responds to surface wetness and thus flooding (Brakenridge et al. 2007b). A wet pixel (usually over the surface of a river) is selected to measure the brightness temperature of the measurement (M) area while an adjacent dry pixel is selected to measure the brightness temperature of the calibration (C) area (usually over the land near the wet pixel); the ratio of the measurement and calibration brightness temperature is referred as the streamflow signal (Eq. (1)).

$$M / C\ Ratio = Tb_m / Tb_c \quad (1)$$

The main merit of the AMSR-E passive microwave sensor onboard the NASA EOS Aqua satellite is that it is not restricted by cloud cover and provides data availability for daily flood monitoring over the globe. For further detailed information regarding the GFDS streamflow signals, please refer to (Brakenridge et al. 2007; Kugler and Groeve 2007).

Ground-based streamflow observation

Besides the passive microwave streamflow signal data at Rundu for both calibration and assimilation (will be specified in 2.5 Experiment design), ground-based streamflow observation at Rundu, Namibia, was used to evaluate the performance of the proposed "exceedance probability based flood-prediction framework" (Khan et al. 2012) in an upstream catchment – Cubango of around 95000km^2

3.2.3 Model

In this study, a simplified and lumped version of the CREST (**C**oupled **R**outing and **E**xcess **ST**orage , (Wang et al. 2011)) was applied, together with the satellite data and the EnSRF (Ensemble Square Root Filter) data assimilation approach, to provide exceedance probability-based hydrological predictions over the Cubango basin. The model structure is shown in Figure 3.2. After precipitation passes the canopy layer, the excess precipitation that reaches the soil surface is P_{soil}. P_{soil} is divided into excess rainfall R and infiltration water I through the Variable Infiltration Curve (VIC, (Liang et al. 1994)). After that, the excess rainfall R is further separated into overland excess rainfall R_o and interface excess rainfall, and this procedure is governed by K,which is closely related to the saturated soil hydraulic conductivity (the interface excess rainfall = $K\frac{R}{P_{soil}}$ when $P_{soil} > k$, the interface excess rainfall = R when $P_{soil} \leq k$). Next, the interface excess rainfall is evapotranspired through three soil layers and then the interface excess rainfall reduces to R_I. The overland excess rainfall R_o flows through three overland flow linear reservoirs while the interface excess rainfall R_I flows through one interflow reservoir; those two procedures are governed by the overland reservoir discharge multiplier LEAKO ($R_{o,out} = LEAKO * R_o$) and the interflow reservoir

discharge multiplier LEAKI ($R_{I,out} = LEAKI * R_I$), respectively, and then form the total runoff as Q ($Q = R_{o,out} + R_{I,out}$).

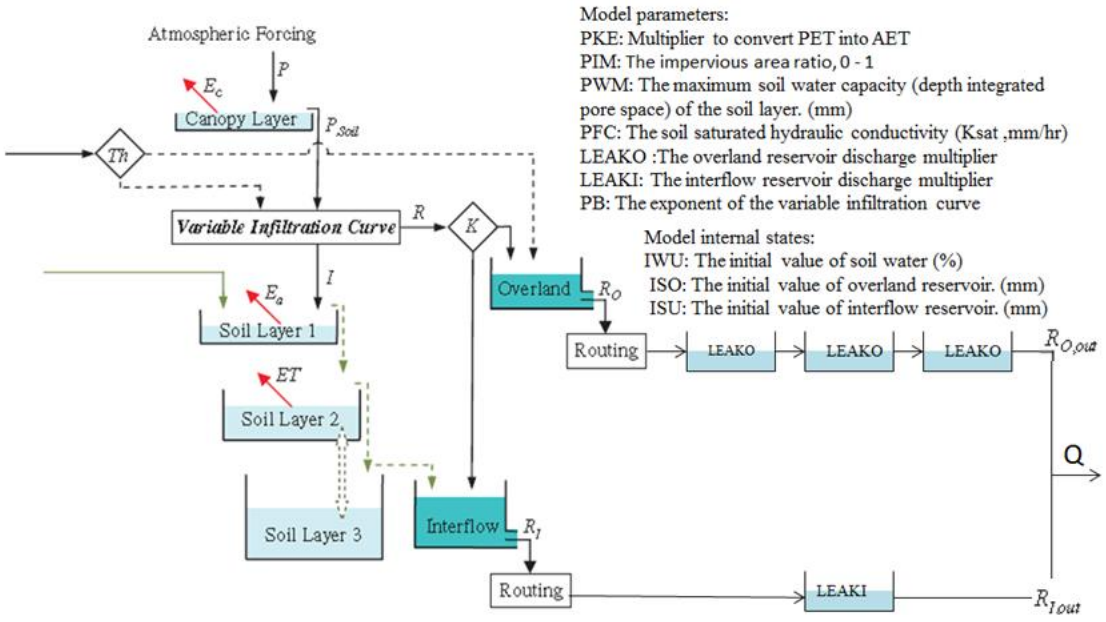

Figure 3.2 Structure of CREST Model

3.2.4 EnSRF

A sequential data assimilation technique, the Ensemble Square Root Filter (EnSRF), is applied to assimilate passive microwave streamflow signals into CREST. Unlike the traditional EnKF which requires perturbing both forcing data and observations, the EnSRF only perturbs the forcing data and the ensemble mean is updated by the observation. (Whitaker and Hamill 2002) demonstrated that there is no additional computational cost by EnSRF relative to EnKF, and EnSRF performs more accurately than EnKF for the same ensemble size. But it still remains a research topic to compare

the accuracy and efficiency of different sequential data assimilation approaches (e.g. EnKF, EnSRF). The major equations of EnSRF are listed below:

$$\mathrm{X^a} = \mathrm{X^b} + \widehat{\mathrm{K}}(\mathrm{y} - \mathrm{H}(\mathrm{X^b})) \tag{2}$$

X^a is the updated estimate of the analyzed state ($n \times 1$ dimension and n is the number of ensembles);

X^b is the background model forecast, which is also referred to the first guess in data assimilation ($n \times 1$ dimension);

y is the observation ($p \times 1$ dimension and p is the number of observations), which is the streamflow measurements in this study;

H is the observation operator that converts the states in the model into observation space ($p \times n$ dimension);

$\widehat{\mathrm{K}}$ refers to the traditional Kalman gain.

Let's denote the ensemble X^b as

$$X^b=(x_1^b, x_2^b, \dots, x_n^b) \tag{3}$$

Where we ignore time index and the subscript represents the ensemble member. The ensemble mean is then defined as

$$\overline{X^b} = \frac{1}{n}\sum_{i=1}^{n} x_i^b \tag{4}$$

The perturbation from the mean for the i th member is

$$x_i'^b = x_i^b - \overline{x^b} \tag{5}$$

Then X'^b is defined as a matrix formed from the ensemble of perturbations:

$$X'^b = (x_1'^b, x_2'^b, \dots, x_n'^b) \tag{6}$$

An estimation of background error covariance is defined as

$$\hat{P}^b = \frac{1}{n-1} X'^b (X'^b)^T \tag{7}$$

However, in practice, we do not calculate $\hat{P}^b$, but rather calculate $\hat{\mathrm{P}}^{\mathrm{b}}\mathrm{H}^{\mathrm{T}}$ and $\mathrm{H}\hat{\mathrm{P}}^{\mathrm{b}}\mathrm{H}^{\mathrm{T}}$ are evaluated by the following equations:

$$\hat{\mathrm{P}}^{\mathrm{b}}\mathrm{H}^{\mathrm{T}} = \frac{1}{\mathrm{m}-1}\sum_{i=1}^{m}(\mathrm{X}_{\mathrm{i}}^{\mathrm{b}} - \overline{\mathrm{X}}^{\mathrm{b}})(\mathrm{H}(\mathrm{X}_{\mathrm{i}}^{\mathrm{b}} - \overline{\mathrm{H}(\mathrm{X}^{\mathrm{b}})}))^{\mathrm{T}} \tag{8}$$

$$\mathrm{H}\hat{\mathrm{P}}^{\mathrm{b}}\mathrm{H}^{\mathrm{T}} = \frac{1}{\mathrm{m}-1}\sum_{i=1}^{m}(\mathrm{H}(\mathrm{X}_{\mathrm{i}}^{\mathrm{b}}) - \mathrm{H}(\overline{\mathrm{X}}^{\mathrm{b}}))(\mathrm{H}(\mathrm{X}_{\mathrm{i}}^{\mathrm{b}} - \overline{\mathrm{H}(\mathrm{X}^{\mathrm{b}})}))^{\mathrm{T}} \tag{9}$$

Here, m is the ensemble size. Then the traditional Kalman gain $\hat{\mathrm{K}}$ can be calculated by Eq (10),

$$\hat{\mathrm{K}} = \hat{\mathrm{P}}^{\mathrm{b}}\mathrm{H}^{\mathrm{T}}(\mathrm{H}\hat{\mathrm{P}}^{\mathrm{b}}\mathrm{H}^{\mathrm{T}} + \mathrm{R})^{-1} \tag{10}$$

R is the observation error covariance with a dimension of $p \times p$. In EnSRF, the reduced Kalman gain $\tilde{\mathrm{K}}$ is used to update the deviation from the ensemble mean as estimated by the following equation,

$$\tilde{\mathrm{K}} = (1 + \sqrt{\frac{\mathrm{R}}{\mathrm{H}\hat{\mathrm{P}}^{\mathrm{b}}\mathrm{H}^{\mathrm{T}}+\mathrm{R}}})^{-1}\hat{\mathrm{K}} \tag{11}$$

The ensemble mean can be updated by

$$\overline{\mathrm{X}}_{\mathrm{i}}^{\mathrm{a}} = \overline{\mathrm{X}}_{\mathrm{i}}^{\mathrm{b}} + \hat{\mathrm{K}}(\mathrm{y} - \mathrm{H}(\overline{\mathrm{X}}_{\mathrm{i}}^{\mathrm{b}})) \tag{12}$$

The perturbation (deviation of ensemble mean) can be updated by

$$X_i'^{a} = X_i'^{b} - \tilde{K}H(X_i'^{b}) \tag{13}$$

The final analysis follows as

$$X_i^a = \overline{X}_i^a + X_i'^{a} \tag{14}$$

As mentioned above, when the EnSRF is applied, the forcing data (which is the precipitation in this study) needs to be perturbed. Precipitation perturbations in this study are defined as

$$P_i = P + \varepsilon_i \tag{15}$$

where ε_i is a random noise factor drawn from a Gaussian distribution

$$\varepsilon_i \sim N(0, r) \tag{16}$$

At each time step, an independent rainfall error is generated by Gaussian distribution (refer to eq. (15) and (16)) and added to the original basin average precipitation.

3.2.5 Experimental design

The C/M radiance ratio, which is the reciprocal of M/C ratio signal (e.q. (1)), is correlated at a significant level with observed streamflow especially during the peak flow periods, as shown in Figure 3.3.

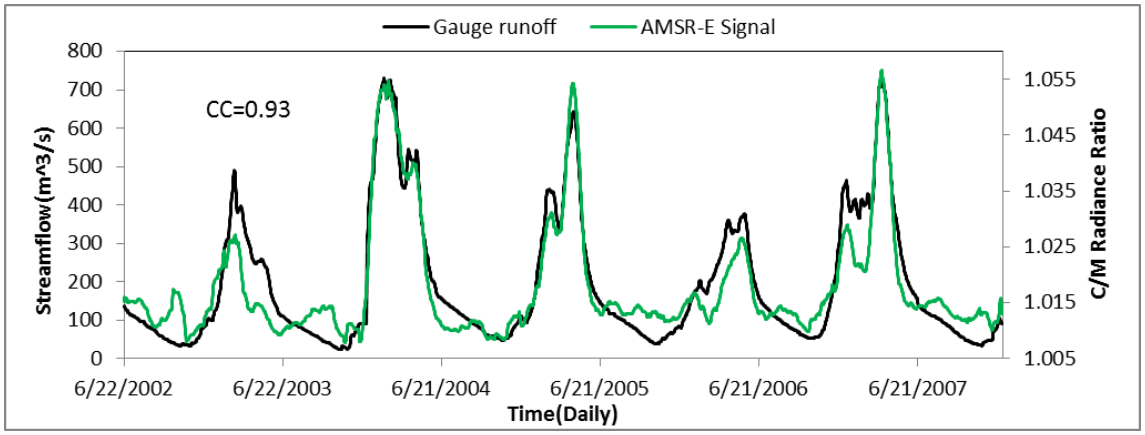

Figure 3.3 Time series of gauge streamflow observation plotted against primary y-axis and C/M Radiance Ratio plotted against secondary y-axis

Based on the high correlation coefficient between the gauge-based streamflow and the C/M radiance ratio, an innovative calibration method – the flood frequency approach, was proposed by (Khan et al. 2012), which first requires the conversion of model-simulated streamflow into exceedance probability, and then takes "max(CC)" (CC refers to Correlation Coefficient) as the objective function to conduct the automatic hydrological calibration via the algorithm Shuffled Complex Evolution – University of Arizona (SCE-UA, (Duan et al. 1994)). The flood frequency approach utilizes the period of recorded observations to compute the frequency or exceedance probability. This approach essentially normalizes the streamflow observations from absolute units (m^3/s) to dimensionless values in the frequency domain. The same approach can be applied to any time series data (i.e., passive microwave streamflow signal) as long as there is a sufficiently long record to represent climatological conditions and the signal is temporally correlated to streamflow.

As shown by Table 3.1, experiment 1, which was conducted in absolute streamflow units (m^3/s), is the traditional gauged-based approach to model calibration and data assimilation. It sets the reference to be to be compared to the frequency-based in-situ and remote-sensing approaches in Experiments 2 and 3. In Experiment 2, streamflow observations from the Rundu gauge are used to automatically calibrate the model parameters as in Experiment 1, but using the exceedance probability approach described in (Khan et al. 2012); and then the gauge streamflow frequency was assimilated into CREST model via EnSRF. Experiment 3, which represents the advanced exceedance probability-based streamflow prediction framework, is designed similarly to Experiment 2, but the exceedance probability of the observed streamflow is replaced with the frequency of the AMSR-E signals. Experiment 3 is thus based entirely on remote-sensing data and applies generally to ungauged basins. Results from the experiments with no data assimilation are referred to as "Open Loop", while the components that employ the EnSRF are referred to as "Assimilation". Results from all experiments are evaluated using gauge-observed streamflow at the Rundu station.

Table 3.1 List of Experiments Design

Exp	Calibration data source	Data Assimilated into Model	Calibration objective function
1	Gauge Streamflow	Gauge Streamflow	Min(RMSE)
2	Gauge streamflow Frequency	Gauge streamflow Frequency	Max(CC)
3 (a) Before Threshold Applied / (b) After Threshold Applied	AMSR-E Signal Frequency	AMSR-E Signal Frequency	Max(CC)

The modeling performance for both “Open Loop” and “Assimilation” was evaluated by the statistic indices normalized Root Mean Square Error (RMSE) and Nash-Sutcliffe Coefficient of Efficiency (NSCE):

$$RMSE(\%) = \frac{\sqrt{\sum(x_i - y_i)^2/n}}{\bar{x}} * 100 \quad (17)$$

$$NSCE = 1 - \frac{\sum(x_i - y_i)^2}{\sum(x_i - \bar{x})^2} \quad (18)$$

Where $x_i$is the observed streamflow and y_i is the simulated streamflow.

3.3 Results and Discussion

(Zhang et al. 2013) has conducted a sensitivity analysis in order to better understand the spread of precipitation (r in Eq. (16)), ensemble size (n in Eq. (3)) and observation error (R in Eq. (10)) and their impact to data assimilation efficiency. In this study, the same spread of precipitation (50%, as the precipitation are the same for those three experiments) and ensemble size (20) are applied to all of those three experiments. For the observation error R, it is usually assumed from the "actual" observation error based on experience. In experiment 1 and 2, the observation error is assumed as 8% according to the report (Sauer and Meyer 1992) from USGS which indicates 8% represents the common streamflow observation error; as the AMSR-E streamflow signals shows overestimation during low flows (Figure 3.3), a larger observation error of 10% is assumed in experiment 3.

Experiment 1 is the reference experiment; the model was calibrated by gauge-based streamflow observations for the period 2003 to 2005 with a computed RMSE of 34% and NSCE of 0.88. Then, the model was validated for the period 2006 to 2007, in which the RMSE shot up to 64% and the NSCE dropped to 0.33. In order to enhance the hydrological performance, the gauge streamflow observation was assimilated into the well-calibrated lumped CREST model via EnSRF at daily time step. After assimilation, the modeling performance was improved significantly during both calibration and validation periods. (Note: the statistical evaluation excludes the first half-year due to the bad first guesses at the beginning for each experiment.) The two simulations illustrated in Figure 3.4 serve as the stream gauge-based reference for the Open Loop and

Assimilation experiments focused on the use of the gauge streamflow and the microwave streamflow signals in frequency domain hereafter.

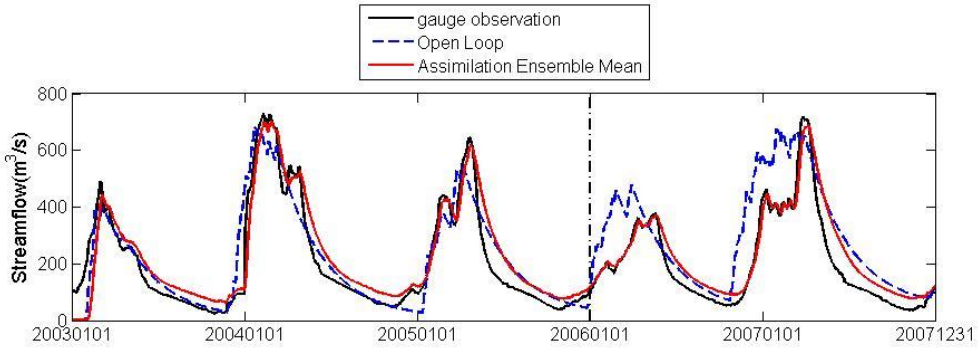

	Calibration		Validation	
	RMSE(%)	NSCE	RMSE(%)	NSCE
Open Loop	34	0.88	64	0.33
Assimilation	29	0.91	27	0.88

Figure 3.4 Impact of assimilating gauge streamflow into CREST in Experiment 1.

*Note: to the left side of the black dash line is the calibration period from 2003 to 2005; to the right side of the black dash line is the validation period from 2006 to 2007; the same for Figure 3.5 and 3.6.

In Experiment 2, the sources of data for model calibration are the same but the simulated and observed streamflow data have been converted to the frequency domain and expressed as a exceedance probability (Figure 3.5). This conversion upgraded the skill of the Open Loop simulation compared to the one in Experiment 1 in terms of RMSE; it has fallen from 34% to 22%, though with a slightly decrease of NSCE from 0.88 to 0.85 during the calibration period. For the validation period, the modeling skill improved significantly relative to Experiment 1; RMSE decreased from 64% to 29% while NSCE increased from 0.33 to 0.74. For further improvement, the Assimilation simulation, which employed the EnSRF by assimilating the gauge streamflow data in the frequency domain, resulted in a better overall skill compared to the Assimilation run in Experiment 1.

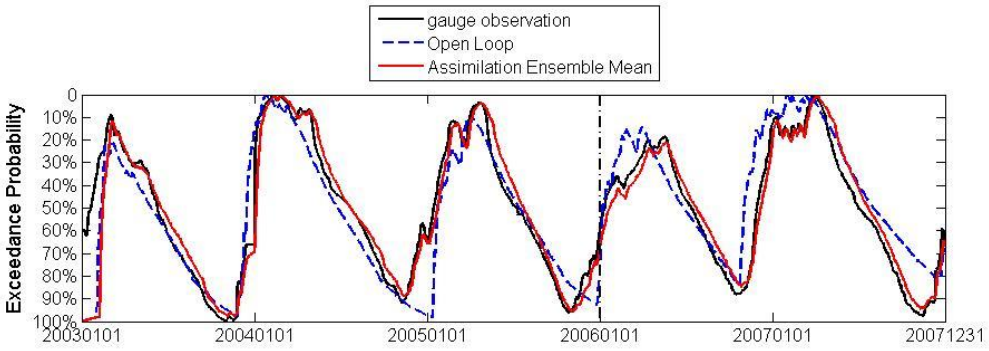

	Calibration		Validation	
	RMSE(%)	NSCE	RMSE(%)	NSCE
Open Loop	22	0.85	29	0.74
Assimilation	12	0.96	12	0.95

Figure 3.5 Impact of assimilating gauge streamflow frequency into CREST in Experiment 2.

Figure 3.3 shows the time series of the passive microwave C/M radiance ratio (green line), which is used as the streamflow proxy for automatically estimating the model parameters. The C/M radiance ratio matches well with the gauge streamflow observations during the high flow period, but shows noise during the low flow period because of the insensitivity of the AMSR-E and TMI sensors to low flows. In Experiment 3(a), the sources of data for model calibration are the C/M radiance ratios, and the C/M radiance ratios have been converted into the frequency domain and also expressed as the exceedance probability (Figure 3.6(a)). The application of C/M radiance ratio frequency degraded the skill of the Open Loop simulation compared to the ones in both Experiment 1 and 2 during the calibration period, but enhanced the Open Loop simulation during the validation period with NSCE increasing from 0.33 (Experiment 1) and 0.74 (Experiment 2) to 0.81. However, after assimilation, the streamflow signal indicates a small peak near Nov 2003 that was not observed by the stream gauge (Figure 3.6(a)). This error was not reflected in the Open Loop simulation; however, by assimilating the C/M radiance ratio with noise into the model during the low flows, errors during low flows result. The performance of the simulations was poor for low flows, but remarkable for high flows. This latter feature prompted us to devise Experiment 3(b) the same as the Assimilation component of Experiment 3(a), but the radiance ratio data are assimilated only if the exceedance probability is < 30%. In other words, the C/M radiance ratio data are trusted only during high flow conditions. After application of this subjectively chosen threshold, the red curve in Figure 3.6(b) illustrates very similar performance during high flows as in Experiment 3(a) (red curve in Figure 3.6(a)), but the prior problems during low flows have been alleviated. The

RMSE (26% during calibration period and 23% during validation period) is even better than the reference simulations in Experiment 1 that assimilated gauge streamflow (in absolute units), but worse than the simulation in Experiment 2. The NSCE of 0.79 and 0.84 during calibration and validation periods, respectively, is only a slight reduction from the reference values in both Experiment 1 and 2. Nonetheless, this reduction is quite modest considering Experiment 3b is based entirely on remote-sensing data thus can provide probability-based streamflow prediction in ungauged basins.

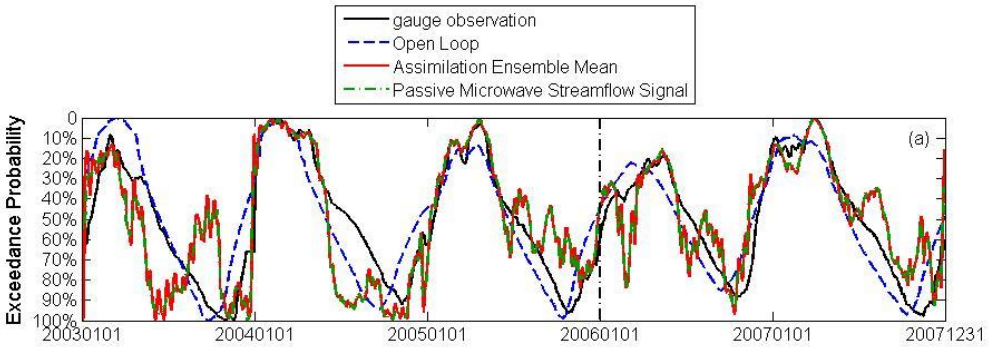

	Calibration		Validation	
	RMSE(%)	NSCE	RMSE(%)	NSCE
Open Loop	27	0.77	25	0.81
Assimilation	36	0.61	31	0.69

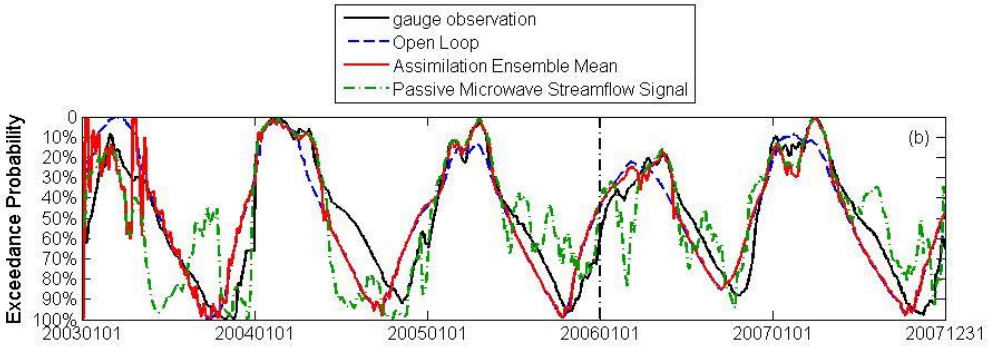

	Calibration		Validation	
	RMSE(%)	NSCE	RMSE(%)	NSCE
Open Loop	27	0.77	25	0.81
Assimilation	26	0.79	23	0.84

Figure 3.6 Impact of assimilating Passive Microwave signal frequency into CREST in Experiment 3 (a) before threshold and (b) after threshold

In addition to the improvement of hydrological prediction by assimilation of remote sensing streamflow signal frequencies, it is also interesting to explore the parameter values and ranges between those that were calibrated in the actual streamflow and frequency domains. Concerning parameter ranges, upper and lower bounds were set on all parameter values based on physical constraints and on past experience with those parameters that are more intangible. We found out that there are slight differences with the parameters PKE (multiplier to convert PET), PIM (the impervious area ratio), LEAKI (the interflow reservoir discharge multiplier), and PB (the exponent of the variable infiltration curve). However, there are large differences with the parameters PWM (the maximum soil water capacity), PFC (the soil saturated hydraulic conductivity) and LEAKO (the overland reservoir discharge multiplier). From our experience, those three parameters with the largest differences are the most sensitive parameters in this model, which control the peak volume and timing. In addition, when the parameter set calibrated from the frequency domain was applied into the actual streamflow domain, simulated streamflow showed strong overestimation compared to gauge observations. Nevertheless, the simulated streamflow and gauge observations were still well correlated, which indicates that the consistent overestimation in the actual domain does not impact its hydrological performance in the frequency domain.

Overall, the lumped CREST coupled with state estimation through an EnSRF approach can effectively improve flood prediction using remote-sensing data alone in the Cubango river basin. A limitation, as mentioned by (Khan et al. 2012) is that the use of AMSR-E signals for streamflow estimation is limited to medium- and large-scale basins. Moreover, the signal was found to be uncorrelated with observed streamflow

during low flow periods. These constraints must be considered when using the GFDS streamflow signals to infer streamflow for hydrologic model calibration and state estimation.

3.4 Conclusion

The application of remote-sensing data, alone, to force, calibrate and update a hydrologic model is a major contribution of this study. More generally, the approach developed and benchmarked herein can have great potential for predicting floods for the vast number of river basins throughout the world that are poorly gauged or even ungauged. In the Cubango River basin, data from an in-situ streamflow gauge was used for model calibration and data assimilation in a traditional manner, providing a benchmark for evaluating the use of the passive microwave sensor-derived streamflow signals as a proxy for streamflow. Then, the passive microwave streamflow signals were converted into exceedance probability; i.e., in the frequency domain, to be applied similarly as the traditional approach for calibration and assimilation.

The major outcomes from this study are summarized as follows:

(1) In the absence of data assimilation (i.e., Open Loop), model performance was limited due to the inherent deficiencies of the model structure, but was more likely dominated by bias in the rainfall forcing from the TRMM 3B42RT algorithm.

(2) The implementation of the EnSRF in all experiments resulted in a significant improvement over the Open Loop simulations except Experiment 3(a).

(3) When the GFDS streamflow signals converted to the frequency domain were substituted as the streamflow proxy for the Open Loop simulation in Experiment 3(a), there was a significant reduction in model skill compared to using gauged streamflow in both actual and frequency domains during the calibration period, but there was a significant enhancement during the validation period. However, the assimilation of the GFDS signals during the calibration period degraded the RMSE

to 36% (from 27% for Open Loop) and the NSCE to 0.61 (from 0.77 for Open Loop), which was worse than the values in the reference Experiments 1 and 2. This characteristic was found to be a result of poor sensitivity of the GFDS signal during low flow periods.

(4) The final Experiment 3(b) assimilated the AMSR-E signal only if the exceedance probability was < 30%; i.e., during high flow periods. The application of this threshold resulted in model skill that was comparable to what was obtained in the reference Experiment 1, but slightly worse than in Experiment 2. Nonetheless, this reduction is quite modest considering Experiment 3b is based entirely on remote-sensing data and this approach can be applied to those ungauged basin over the globe.

Given the real-time availability of satellite-based precipitation and AMSR-E and TMI-like passive microwave streamflow signal information, we argue that this work contributes to the decadal initiative of prediction in ungauged basins. Moreover, this study presents a potential paradigm shift in the use of streamflow exceedance probabilities, different from traditional methods reliant on in-situ streamflow observation for calibration, and towards new techniques and new types of observations. These observations and new methods are particularly imperative for the vast sparsely gauged or ungauged basins around the world. More promisingly, assimilation of remote-sensing information for improving hydrological prediction can be increasingly appreciated and supported by the current TRMM and anticipated GPM (Global Precipitation Mission, to be launched in earlier 2014), together with the future SMAP (Soil Moisture Active and Passive, to be launched in 2014). Both missions are

anticipated to provide better precipitation and surface wetness estimates in terms of coverage, accuracy, and resolutions, which bears promise to further improve flood predictions in combination with the proposed framework in this study.

References

Andersson, L., and Coauthors, 2006: Impact of climate change and development scenarios on flow patterns in the Okavango River. *Journal of Hydrology*, **331,** 43-57.

Aubert, D., C. Loumagne, and L. Oudin, 2003: Sequential assimilation of soil moisture and streamflow data in a conceptual rainfall–runoff model. *Journal of Hydrology*, **280,** 145-161.

Brakenridge, G. R., S. V. Nghiem, E. Anderson, and R. Mic, 2007: Orbital microwave measurement of river discharge and ice status. *Water Resources Research*, **43,** W04405.

Brocca, L., T. Moramarco, F. Melone, W. Wagner, S. Hasenauer, and S. Hahn, 2012: Assimilation of Surface- and Root-Zone ASCAT Soil Moisture Products Into Rainfall-Runoff Modeling. *Geoscience and Remote Sensing, IEEE Transactions on*, **50,** 2542-2555.

Brocca, L., F. Melone, T. Moramarco, W. Wagner, V. Naeimi, Z. Bartalis, and S. Hasenauer, 2010: Improving runoff prediction through the assimilation of the ASCAT soil moisture product. *Hydrology and Earth System Sciences*, **14,** 1881-1893.

Clark, M. P., and Coauthors, 2008: Hydrological data assimilation with the ensemble Kalman filter: Use of streamflow observations to update states in a distributed hydrological model. *Advances in Water Resources*, **31,** 1309-1324.

Crow, W., and D. Ryu, 2009: A new data assimilation approach for improving runoff prediction using remotely-sensed soil moisture retrievals. *Hydrology and Earth System Sciences*, **13,** 1.

Crow, W., R. Bindlish, and T. Jackson, 2005: The added value of spaceborne passive microwave soil moisture retrievals for forecasting rainfall-runoff partitioning. *Geophysical Research Letters*, **32**.

Duan, Q., S. Sorooshian, and V. K. Gupta, 1994: Optimal use of the SCE-UA global optimization method for calibrating watershed models. *Journal of Hydrology*, **158,** 265-284.

Gao, H., E. F. Wood, M. Drusch, and M. F. McCabe, 2007: Copula-derived observation operators for assimilating TMI and AMSR-E retrieved soil moisture into land surface models. *Journal of Hydrometeorology*, **8,** 413-429.

Hong, Y., K. L. Hsu, S. Sorooshian, and X. G. Gao, 2004: Precipitation Estimation from Remotely Sensed Imagery using an Artificial Neural Network Cloud Classification System. *Journal of Applied Meteorology*, **43,** 1834-1852.

Huffman, G. J., D. T. Bolvin, E. J. Nelkin, D. B. Wolff, R. F. Adler, G. Gu, Y. Hong, K. P. Bowman, and E. F. Stocker (2007), The TRMM Multisatellite Precipitation Analysis (TMPA): Quasi-Global, Multiyear, Combined-Sensor Precipitation Estimates at Fine Scales, *Journal of Hydrometeorology*, *8*(1), 38-55.

Hughes, D., D. Kingston, and M. Todd, 2011: Uncertainty in water resources availability in the Okavango River basin as a result of climate change. *Hydrology and Earth System Sciences*, **15,** 931-941.

Hughes, D. A., L. Andersson, J. Wilk, and H. H. Savenije, 2006: Regional calibration of the Pitman model for the Okavango River. *Journal of Hydrology*, **331,** 30-42.

Joyce, R. J., J. E. Janowiak, P. A. Arkin, and P. P. Xie, 2004: CMORPH: A method that produces global precipitation estimates from passive microwave and infrared data at high spatial and temporal resolution. *Journal of Hydrometeorology*, **5,** 487-503.

Khan, S. I., H. Yang, H. J. Vergara, J. J. Gourley, G. R. Brakenridge, T. De Groeve, Z. L. Flamig, F. Policelli, and Y. Bin (2012), Microwave Satellite Data for Hydrologic Modeling in Ungauged Basins, *Geoscience and Remote Sensing Letters, IEEE*, *9*(4), 663-667.

Kugler, Z., and T. D. Groeve, 2007: The global flood detection system. *JRC Scientific and Technical Reports*, EUR 23303 EN

Liang, X., D. P. Lettenmaier, E. F. Wood, and S. J. Burges, 1994: A simple hydrologically based model of land surface water and energy fluxes for general circulation models. *Journal of Geophysical Research: Atmospheres*, **99,** 14415-14428.

Matgen, P., and Coauthors, 2012: Can ASCAT-derived soil wetness indices reduce predictive uncertainty in well-gauged areas? A comparison with in situ observed soil moisture in an assimilation application. *Advances in Water Resources*, **44,** 49-65.

McCarthy, J. M., T. Gumbricht, T. McCarthy, P. Frost, K. Wessels, and F. Seidel, 2003: Flooding patterns of the Okavango wetland in Botswana between 1972 and 2000. *AMBIO: A Journal of the Human Environment*, **32,** 453-457.

Milzow, C., P. E. Krogh, and P. Bauer-Gottwein, 2011: Combining satellite radar altimetry, SAR surface soil moisture and GRACE total storage changes for hydrological model calibration in a large poorly gauged catchment. *Hydrology and Earth System Sciences*, **15,** 1729-1743.

Milzow, C., L. Kgotlhang, P. Bauer-Gottwein, P. Meier, and W. Kinzelbach, 2009a: Regional review: the hydrology of the Okavango Delta, Botswana—processes, data and modelling. *Hydrogeology Journal*, **17,** 1297-1328.

Milzow, C., L. Kgotlhang, W. Kinzelbach, P. Meier, and P. Bauer-Gottwein, 2009b: The role of remote sensing in hydrological modelling of the Okavango Delta, Botswana. *Journal of Environmental Management*, **90,** 2252-2260.

Pauwels, V., R. Hoeben, N. E. Verhoest, F. P. De Troch, and P. A. Troch, 2002: Improvement of TOPLATS-based discharge predictions through assimilation of ERS-based remotely sensed soil moisture values. *Hydrological Processes*, **16,** 995-1013.

Pauwels, V. R., and G. J. De Lannoy, 2006: Improvement of modeled soil wetness conditions and turbulent fluxes through the assimilation of observed discharge. *Journal of Hydrometeorology*, **7,** 458-477.

Salvia, M., and Coauthors, 2011: Estimating flooded area and mean water level using active and passive microwaves: the example of Parana River Delta floodplain. *Hydrology and Earth System Sciences*, **15,** 2679-2692.

Sauer, V. B., and R. W. Meyer, 1992: Determination of error in individual discharge measurements. *U.S. Geological Survey. Open-File Report* 92-144.

Sorooshian, S., K.-L. Hsu, G. XIAOGANG, H. V. Gupta, B. Imam, and D. Braithwaite, 2000: Evaluation of PERSIANN system satellite-based estimates of tropical rainfall. *Bulletin of the American Meteorological Society*, **81,** 2035-2046.

Tarpanelli, A., and Coauthors, 2013: Toward the estimation of river discharge variations using MODIS data in ungauged basins. *Remote Sensing of Environment*, **136,** 47-55.

Temimi, M., R. Leconte, F. Brissette, and N. Chaouch, 2007: Flood and soil wetness monitoring over the Mackenzie River Basin using AMSR-E 37GHz brightness temperature. *Journal of Hydrology*, **333,** 317-328.

Temimi, M., T. Lacava, T. Lakhankar, V. Tramutoli, H. Ghedira, R. Ata, and R. Khanbilvardi, 2011: A multi-temporal analysis of AMSR-E data for flood and discharge monitoring during the 2008 flood in Iowa. *Hydrological Processes*, **25,** 2623-2634.

Turk, F. J., and S. D. Miller, 2005: Toward improved characterization of remotely sensed precipitation regimes with MODIS/AMSR-E blended data techniques. *Geoscience and Remote Sensing, IEEE Transactions on* **43,** 1059-1069.

Wang, J., Y. Hong, L. Li, J.J. Gourley, S.I. Khan, K.K. Yilmaz, R.F. Adler, F. S. Policelli, S. Habib, D. Irwn, A. S. Limaye, T. Korme and L. Okello. 2011: The coupled routing and excess storage (CREST) distributed hydrological model. *Hydrological sciences journal*, **56,** 84-98.

Wang, X., T. M. Hamill, J. S. Whitaker, and C. H. Bishop, 2009: A comparison of the hybrid and EnSRF analysis schemes in the presence of model errors due to unresolved scales. *Monthly Weather Review*, **137,** 3219-3232.

Whitaker, J. S., and T. M. Hamill, 2002: Ensemble data assimilation without perturbed observations. *Monthly Weather Review*, **130,** 1913-1924.

Zhang, Y., Y. Hong, X. Wang, J. J. Gourley, J. Gao, H. J. Vergara, and B. Yong, 2013: Assimilation of Passive Microwave Streamflow Signals for Improving Flood Forecasting: A First Study in Cubango River Basin, Africa. *Selected Topics in Applied Earth Observations and Remote Sensing, IEEE Journal of*, **PP,** 1-16.

Chapter 4. Multi-scale Evaluation of the Global Hydrological Modeling System Forced by Real Time Multi-satellite Precipitation

Abstract

A near real-time Global Hydrological Simulation and Flood Monitoring Demonstration System (NR-GHSFMDS, http://eos.ou.edu/), with its core part of a physical based distributed hydrological model called Coupled Routing and Excess STorage (CREST), has been established and applied for real time global flood monitoring， thus providing early warning for decision makers and stakeholders. The latest Version 7 near real time TRMM Multi-satellite Precipitation Analysis (TMPA) was used to force the CREST model at the spatial resolution of 1/8 degree at quasi-global scale from 50°N to 50°S for a retrospective period (2002-2012). The simulated hydrological variables (e.g. runoff depth and streamflow) were compared with Global Runoff Data Center (GRDC) observations in terms of gridded global runoff climatology (mm/yr), and the selected basins based annual means, etc. The post real time TRMM product was also applied in this study to investigate how much improvement the rain gauge corrections have contributed to the hydrological simulations forced by the post real time TRMM research product compared to the real time product. At global scale, the TRMM derived gridded global runoff climatology (mm/yr), and model simulated annual streamflow means over selected basins, are in general agreement with those of the GRDC observations, though with performance variation over different continents (e.g. Africa shows relatively poor performance compared to other continents due to the sparsely in-situ networks for TMPA algorithm development). The results also indicate that the modeling performance is better with a larger basin size and a location near the equator. Given the

global availability of satellite-based precipitation in near real-time, this study demonstrates the opportunities and challenges that exist for the real time flood prediction on basis of NR-GHSFMDS, which is particularly useful for the vast ungauged regions around the globe.

4.1 Introduction

Flood is one of the major natural disasters that leads to a significant number of fatalities and economic losses. Wake (2013) recently pointed out that "the number, extent and global impact of the flood events this year (2013) is extraordinary and accounts for about 47% of global economic losses from nature disasters" (Wake 2013). Floods occurred in Europe, Canada, Asia and Australia throughout the first half of 2013, causing a total loss of around 45 billion dollars (Munich Re; http://go.nature.com/ku2qff). Then in the beginning of the second half of 2013 around early September, Colorado experienced an extreme storm and flood event, which damaged around 19,000 homes and at least 30 state highway bridges (http://en.wikipedia.org/wiki/2013_Colorado_floods). Floods, with their frequent occurrences, have become a severe and global issue. With the increasing likelihood of human impacts and climate change, it is anticipated to have more frequent, intensive, and extreme floods in the future. Hirabayashi et al. (2013) recently presented the global flood risk under climate change by the end of this century using 11 climate models and the results show that there is an increasing probability in Southeast Asia, peninsular India, eastern Africa, etc (Hirabayashi et al. 2013). Wu et al. (2013) investigated the anthropogenic impacts on the Earth's hydrological cycle and pointed out that a further rapid increase in precipitation is expected if the current air pollution trend continues (Wu et al. 2013). The frequent occurrences and increasing possibilities of flood disasters indicate the importance of the operational hydrological predictions for the purpose of "preparedness" and "mitigation", though floods cannot be entirely prevented. A lot of application of hydrological modeling are focused on the predictions at basin

scales (e.g. (Li et al. 2013; Maggioni et al. 2013; Zhang et al. 2013)). In the recent decades, the increasing development of remote sensing technique (e.g. satellite precipitation estimation) demonstrates the potential for flood estimation at macro scale, and enables the fostering of flood detection system at global scale (e.g. (Brakenridge et al. 2007; Hong et al. 2007; Proud et al. 2011; Westerhoff et al. 2013; Wu et al. 2012; Yilmaz et al. 2010)), which is of high importance for issuing an early warning for a flooding event, especially for those undeveloped regions with insufficient precipitation data. However, challenges still remain in global hydrological model parameterization, the accuracy and resolution of satellite precipitation estimates, and the computational efficiency in global hydrological modeling, etc. Among all of the satellite precipitation products, the National Aeronautic and Space Administration (NASA) Tropical Rainfall Measuring Mission (TRMM) Multi-satellite Precipitation Analysis (TMPA; (Huffman et al. 2007, 2010) has been widely applied to hydrological predictions at both regional and global scales (e.g.(Hong et al. 2007; Stisen and Sandholt 2010; Su et al. 2008; Wu et al. 2012; Yilmaz et al. 2010; Yong et al. 2010; Zhang et al. 2013)) and got positive results. However, these studies applied the old version of the TMPA product, which is Version 6. The updated Version 7 TMPA product was released on June 25, 2012 and was expected to have more reliable data quality than the old version. Motivated by the recent increasing availability of new satellite data for global precipitation estimation, this study aims at evaluating the performance of the updated Version 7 TMPA 3B42 product (both real time product, abbreviated as 3B42 V7 RT hereafter, and research product with post real time rain gauge corrections, abbreviated as 3B42 V7 RP hereafter) in the Near Realtime Global Hydrological Simulation and Flood Monitoring

Demonstration System (NR-GHSFMDS, http://eos.ou.edu/) in its initial stage without regional re-calibrations of the hydrological model. Wu et al. (2012) did a retrospective evaluation of the same Global Flooding Monitoring System (GFMS), but with Version 6 TMPA 3B42 research product as forcing. The results show that the GFMS has a Probability Of Detection (POD) around 0.7 and a False Alarm Ratio (FAR) around 0.65 for those flood events with the duration longer than 3 days and meanwhile without dams in the Well-Reported Areas (WRA), which indicate the good skill of GFMS in detecting flooding events (Wu et al. 2012).

This paper is organized as follows: section 4.2 describes the model and data for the global hydrological system; section 4.3 illustrates the evaluation of the hydrological performance of both 3B42 V7 RT and 3B42 V7 RP products; finally, in section 4.4, the conclusion is drawn with main findings, and future work is also discussed in this section.

4.2 Methodology and Data

4.2.1 Model

The Near Realtime Global Hydrological Simulation and Flood Monitoring Demonstration System (NR-GHSFMDS) forced by TRMM RT, with its core part of a physical based distributed hydrological model called Coupled Routing and Excess STorage (CREST, (Wang et al. 2011)), is currently operationally available at http://eos.ou.edu/ at the University of Oklahoma with both 3-Dimensional and 2-Dimensional Visualizations based on Google Earth (Figure 4.1).

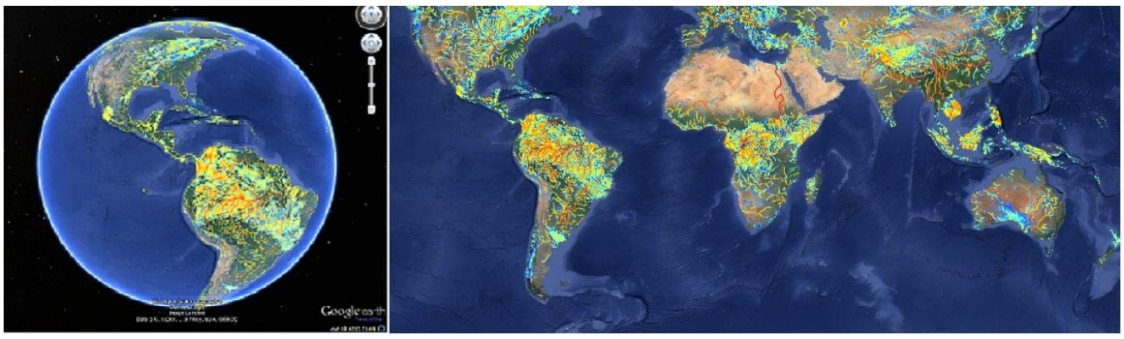

Figure 4.1 3-D and 2-D Visualizations of the streamflow from the NR-GHSFMDS

The CREST model is modified from the state-of-art Variable Infiltration Capacity (VIC) model (Liang et al. 1994; Nijssen et al. 1997) by adding a distributed grid-to-grid routing scheme, and has been successfully applied in hydrological predictions at both regional and global scales (e.g. (Khan et al. 2011a, 2011b; Wu et al. 2012; Xue et al. 2013)), proving its high cost-effectiveness in hydrological prediction. In this study, the CREST model sets up and runs at 1/8 degree based on the Digital Elevation Model (DEM) with quasi-global coverage from 50°N to 50°S at 3 hourly time interval. The model parameters are estimated from input data and used as a priori parameters, these parameter estimation details are provided in (Wang et al. 2011) and (Wu et al. 2012).

Two sets of hydrological simulations forced by 3B42 V7 RT and 3B42 V7 RP are conducted initially at 3 hourly temporal and then are converted to daily temporal scale in order to evaluate the hydrological performance based on the daily streamflow observations from the Global Runoff Data Center (GRDC) at near real time for operational application, and retrospective hydrological simulation for research purpose as well. The details of those two remote sensing satellite precipitation products are given in the next section.

Before running the model and evaluating its performance with ground streamflow observation from GRDC, the "quality control" of streamflow observations is applied:

- The locations of (i.e. latitude and longitude) of the GRDC gauge stations are specified in the CREST project file in order to generate the corresponding streamflow simulation at the specific locations. If the latitude and longitude of a certain GRDC gauge are not corresponding in the correct grid cell in the river network, a considerable underestimation of the streamflow simulation is expected. Therefore, a systematic location check has been conducted - if the GRDC gauge stations are not located on the correct grid cell in the river net which is extracted by the input 1/8 degree DEM, a manual gauge location correction is applied to correct the latitude and longitude of those GRDC gauges in order to navigate them into the river net. This quality control can prevent the underestimation due to the coarse resolution of DEM which might inaccurately represent the true river geomorphology.
- Those GRDC gauge stations with a difference above 20% between the upstream area calculated from the modeled river network and the actual upstream area

provided by GRDC are filtered out, to prevent mismatching data pairs between the model simulation and gauge observation. This usually happened in relative small river basins due to the scaling issue.

4.2.2 Forcing Data

In this study, two sets of the updated Version 7 TMPA products (Huffman et al. 2007, 2010, 2012) are applied:

- TMPA near-real-time 3B42 V7 RT, which uses a combination of active and passive microwave, infrared measurements from TRMM, and other satellites, is posted to the web about 6 hours after observation time.
- TMPA post-real-time 3B42 V7 RP, which adjusts the rainfall accumulation by gauge analysis at monthly scale and has around 2 to 3 month time delay in posting to the public on the web.

Both 3B42 V7 RT and 3B42 V7 RP products are quasi-global with coverage from 50°N to 50°S latitude with a spatial resolution of 0.25° and temporal resolution of 3 hourly. Huffman (2012) encouraged the users to investigate the potential of the TMPA 3B42 V7 RT in real time hydrological predications without gauge adjustment. The key features of 3B42 V7 RT are listed below (Huffman 2012):

- Additional satellites, such as the early parts of the Microwave Humidity Sounder (MHS) and the entire operational Special Sensor Microwave Imager/Sounder (SSMIS) are included.
- Uniformly processed input data using the current algorithms, including Advanced Microwave Sounding Unit (AMSU), MHS, TRMM Combined

Instrument (TCI), TRMM Microwave Imager (TMI), Advanced Microwave Scanning Radiometer – Earth Observation System (AMSR-E) and SSMI.

- Use of a latitude-band calibration scheme for all satellites.

4.2.3 GRDC discharge observation

Quantitative evaluations of both real-time hydrological simulations for operational applications and post-real-time hydrological simulations for research purposes are performed by benchmarking with GRDC discharge observations. The main objective of the GRDC is to collect, store and disseminate the discharge data from rivers around the world in order to facilitate hydrological research and application (http://www.bafg.de/GRDC/EN/Home/homepage_node.html). After the quality control procedure described in the above section, a total of 88 GRDC gauge stations with at least 1-year's worth of discharge data at a daily time step are used for the evaluation in this study (Figure 4.2). Besides the gauge based GRDC discharge, the GRDC observed Runoff Climatology data is also applied for the Macro-scope evaluation of gridded runoff depth. The detailed evaluation results are illustrated in section 4.3.

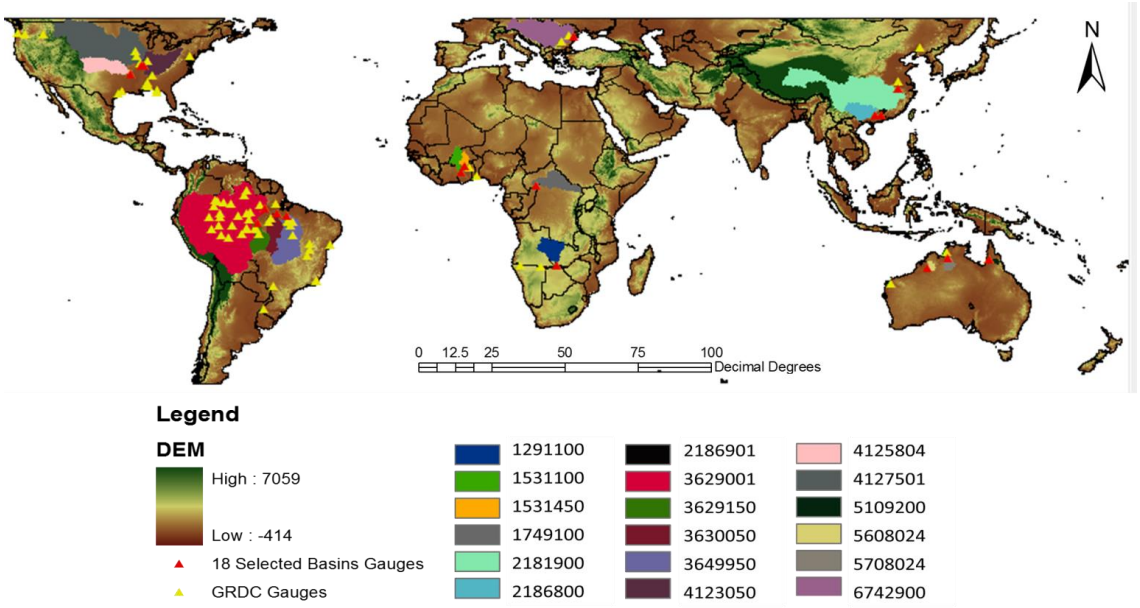

Figure 4.2 GRDC gauges distribution and the locations of the 18 selected basins

4.3 Results

In this section, first, the GRDC observed Runoff Climatology data is applied for the Macro-scope evaluation in section 4.3.1; then, a total of 88 GRDC discharge data sets (as shown by the yellow triangles in Figure 4.2) with at least 1-year's worth of data at a daily time step are used to assess the modeling performance in terms of annual mean discharge (m^3/s, section 4.3.2), modeling performance as a function of basin sizes and of latitude (section 4.3.3); to further investigate the hydrological performance of the global system at specific basins, 18 primary basins (section 4.3.4, as shown in Figure 4.2 and Table 4.1, the red triangle legends in Figure 4.2 indicate the locations of the outlets of those 18 primary basins) are selected based on the basin size and the observation availability to investigate the daily time series of streamflow simulation.

4.3.1 Macro-scope evaluation of gridded runoff depth over the quasi-globe

Figure 4.3(b) and (c) show the modeled annual mean runoff (mm/yr) driven by TRMM 3B42 V7 RT and TRMM 3B42 V7 RP 3hrly products in comparison with the GRDC observed annual mean runoff (mm/yr, Figure 4.3(a)). Please note that the blank areas indicate a lack of observation data. Figure 4.3 (b) and (c) show similar annual mean runoff estimations over the long period of 2002-2012 from RT and RP; in comparison with the GRDC observed runoff climatology, the 3B42 V7 RP derives closer annual mean runoff in central Africa around the equator, the land to the north of the Gulf of Mexico in the U.S., and the northeastern part of the U.S. (red rectangle areas ①, ②, and ③ as shown in Figure 4.3(c)) relative to GRDC rather than that of the 3B42 V7 RT.

Figure 4.3 (d) and (e) show the Bias (%) of the satellite remote sensing precipitation derived runoff climatology (RT and V7, respectively) relative to the GRDC observation. The 3B42 V7 RT forced modeled annual mean runoff relative to 3B42 V7 RP is shown in Figure 4.3(f), which provides information about the pairwise agreement of those two datasets over the period of 2002-2012 in terms of hydrological simulation at a global scale (please refer to the Appendix I. for the definitions and equations of the Bias(%), RMSE(%) and NSCE which are mentioned later).

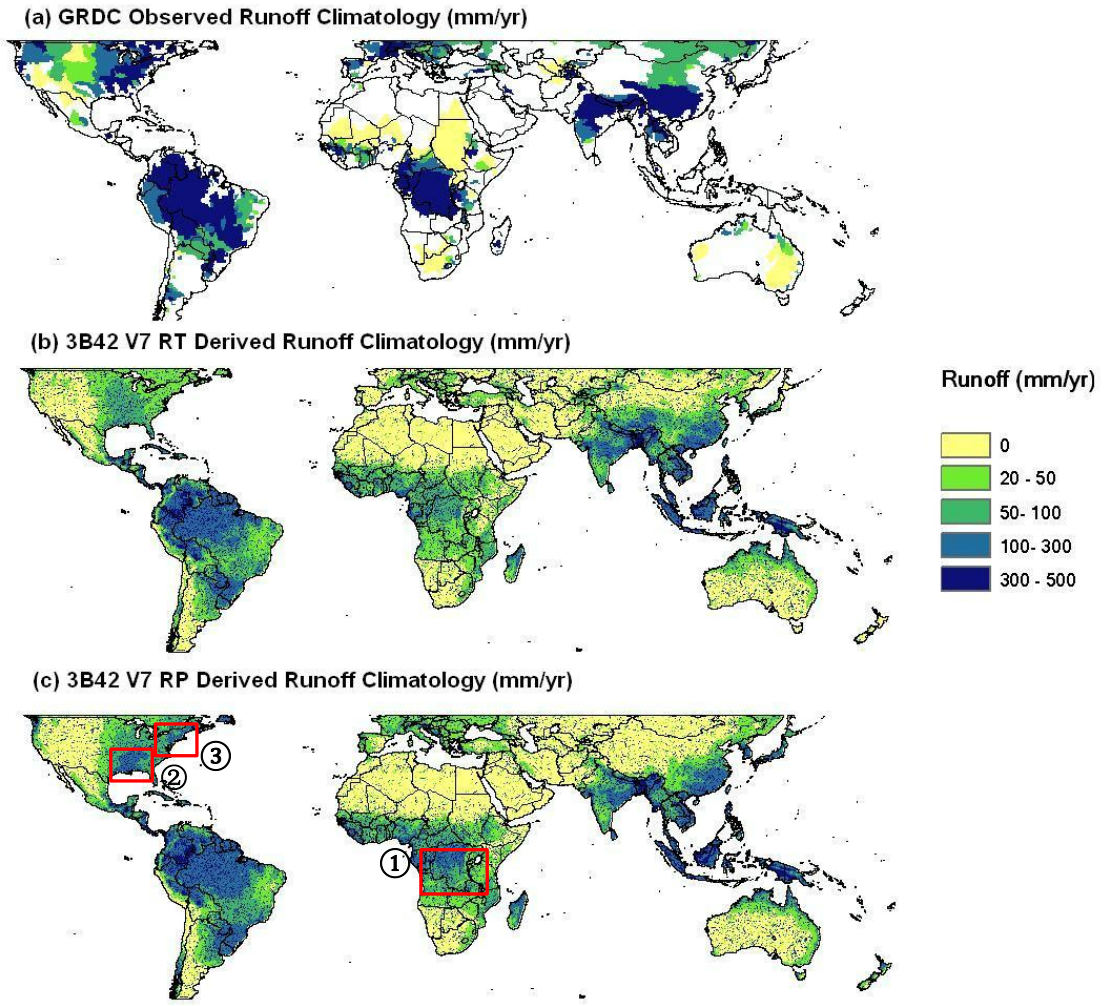
(a) GRDC Observed Runoff Climatology (mm/yr)
(b) 3B42 V7 RT Derived Runoff Climatology (mm/yr)
(c) 3B42 V7 RP Derived Runoff Climatology (mm/yr)
Runoff (mm/yr)
0
20 - 50
50- 100
100- 300
300 - 500
①
②
③

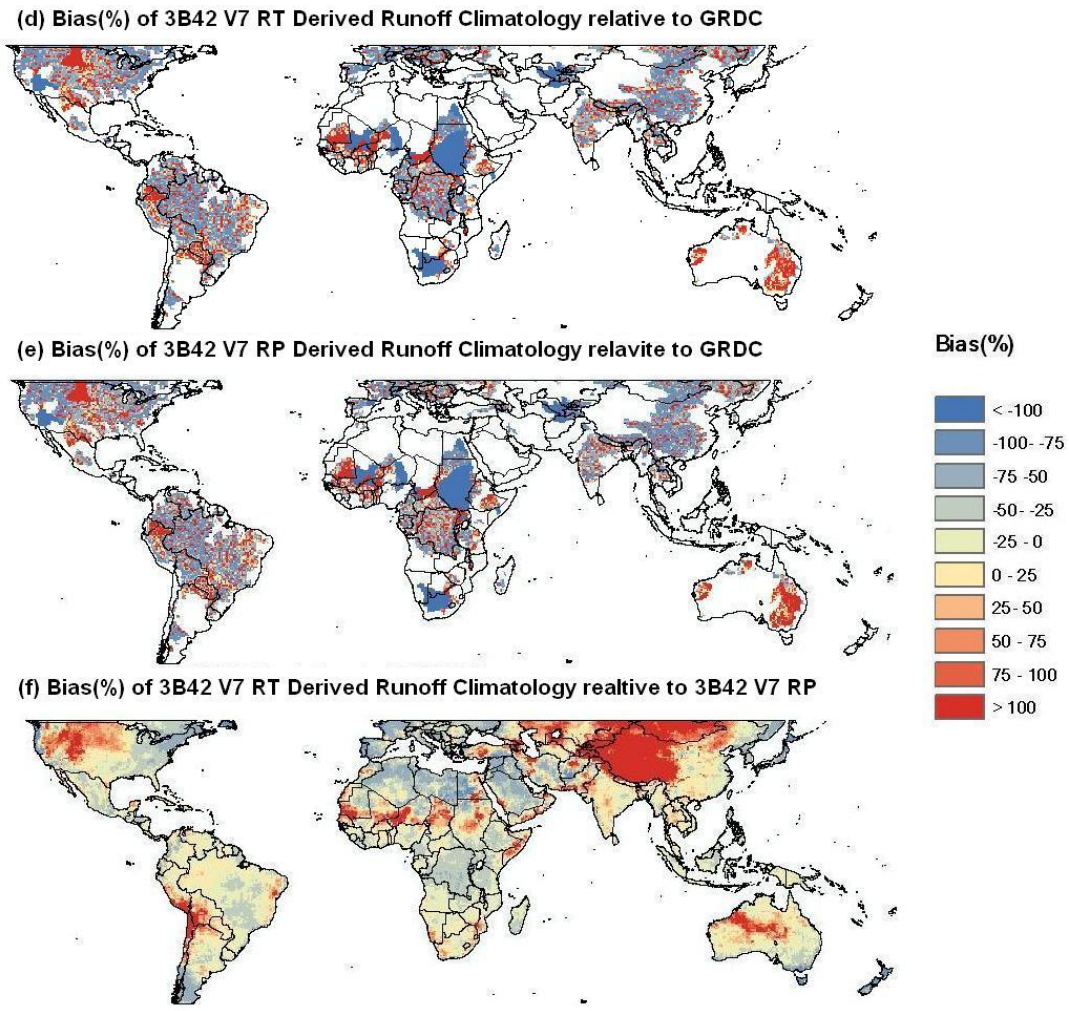

Figure 4.3 (a) GRDC observed runoff (mm/yr) (b) Annual Mean Runoff (mm/yr) simulated by CREST model forced by 3B42 V7 RT for the period 2002-2012 (c) Annual Mean Runoff (mm/yr) simulated by CREST model forced by 3B42 V7 RP for the period 2002-2012 (d) Bias(%) of 3B42 V7 RT Derived Runoff Climatology relative to GRDC (e) Bias(%) of 3B42 V7 RP Derived Runoff Climatology relative to GRDC (f) Bias(%) of 3B42 V7 RT Derived Runoff Climatology relative to 3B42 V7 RP

4.3.2 Annual streamflow evaluation

The annual means of the daily discharge simulations forced by the 3B42 V7 RT and 3B42 V7 RP over the 88 selected basins rate quite well with the GRDC observations. The GRDC observations and CREST simulations yielded a Correlation Coefficient (CC) up to 0.98 for 3B42 V7 RT and 0.99 for 3B42 V7 RP (Figure 4.4). The TMPA 3B42 V7 RP, with rain gauge correction, improved the average Bias(%) from 16.2% (forced by 3B42 V7 RT) to 2.9%; likewise with Bias(%), the RMSE(%) is improved from 74.2% to 47.7% when the forcing data is switched from 3B42 V7 RT to 3B42 V7 RP.

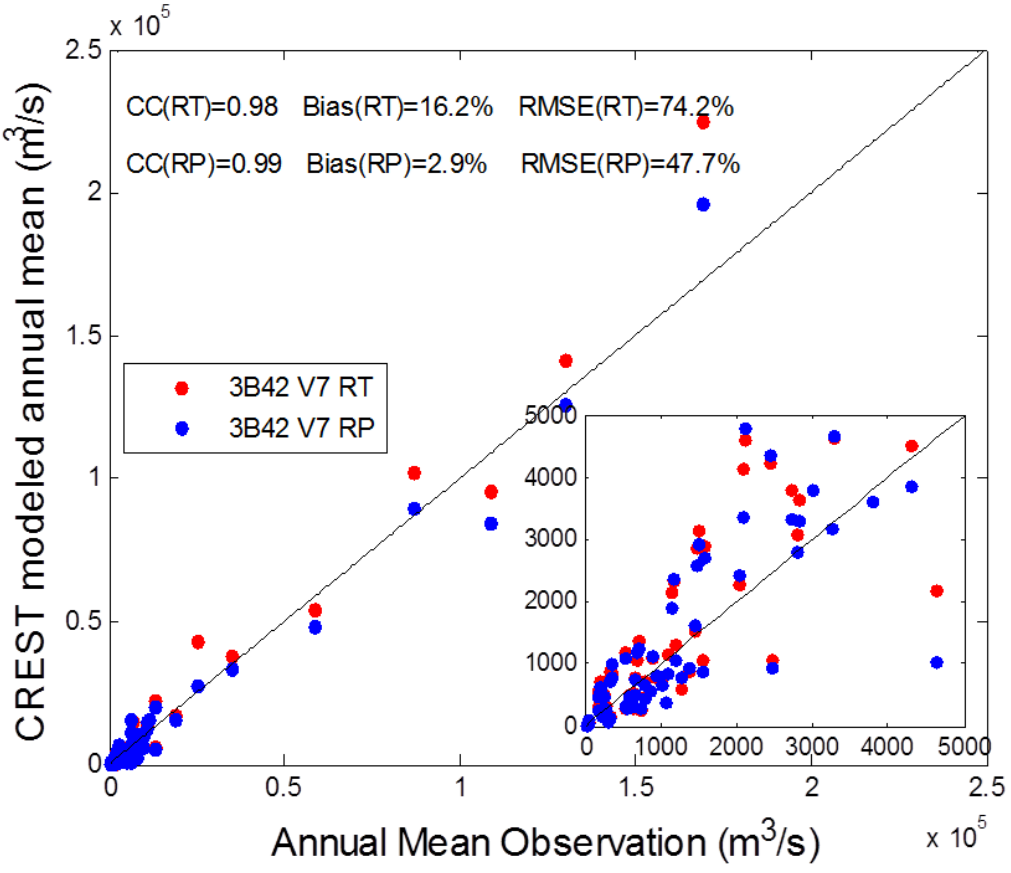

Figure 4.4 Scatter plot of streamflow annual mean between model simulation and gauge

4.3.3 Model performance as a function of basin size and of latitude

Considering the Bias(%) and RMSE(%) of the TPMA 3B42 V7 products (both RT and RP) forced daily streamflow relative to GRDC observations as the functions of basin sizes, the left panels of Figure 4.5 show an overall convergent trend to minimum errors (0% is the perfect value for both Bias(%) and RMSE(%)) with the increasing of basin sizes. The 3B42 V7 RP product, with post time rain gauge adjustment, has lower errors relative to the GRDC observation in general when compared with the 3B42 V7 RT product, as we expected.

When evaluating the hydrological performance of those two types of TMPA 3B42 V7 in terms of Bias(%) and RMSE(%) of daily streamflow simulation relative to GRDC observation as the functions of the latitude, the right panels of Figure 4.5 show a general trend of errors decreasing with the basins' outlets closer to the equator. However, there are four "odd" basins marked by the red circle in Figure 4.5 that do not have satisfactory performances even though their basin outlets are near the equator. Then a further investigation is conducted of those four basins: results show that those basins are located in Africa, and the large Bias(%) and RMSE(%) values of the daily time series of those four basins are caused by overestimation of the streamflow magnitudes from the TMPA 3B42 V7 RT and RP products and peak timing differences (Figure A1 in Appendix II). We assume that the limited number of the rain gauge stations prevents the development of the TMPA 3B42 precipitation estimation algorithms in Africa. Since the hydrological performance is highly dependent on the accuracy of rainfall input, it is anticipated that the global hydrological prediction system will be improved with further

improvement from the satellite precipitation estimation (e.g. the future GPM mission which will be discussed in Chapter 6).

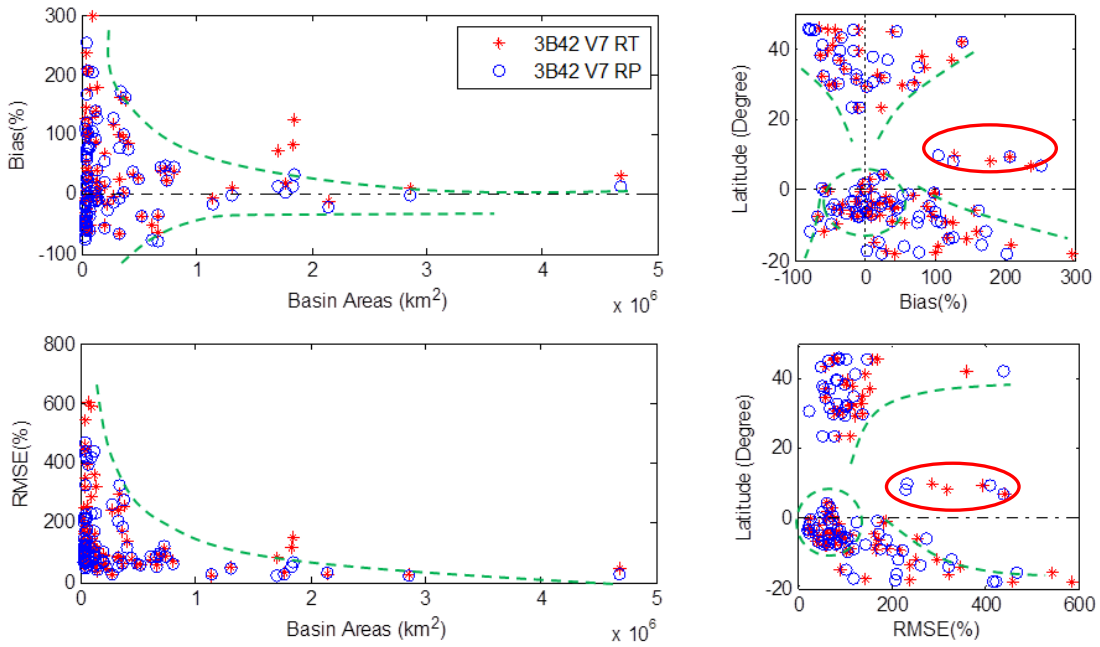

Figure 4.5 Bias(%) and RMSE(%) as a function of basin area (left panels) and latitude (right panels)

4.3.4 Evaluations of Primary Basins

(a) Information of the selected primary 18 basins

In order to further investigate the hydrological performance of the global system, 18 primary basins within the TMPA domain (50°N to 50°S) are selected for more quantitative evaluation based on the data availability and basin sizes. The selected 18 primary basins are distributed over six continents (Figure 4.2) with basin areas ranging from 38,363 km^2 (Beijiang, Asia, Table 4.1) to 4,680,000 km^2 (Amazon, South America, Table 4.1). For detailed information (i.e. the basin name, outlet, the corresponding GRDC gauge number, and basin areas) about these 18 primary basins, please refer to Table 4.1. The GRDC daily streamflow observations are used to evaluate the CREST model simulated streamflows forced by 3B42 V7 RT and RP respectively: the streamflow time series at daily scale for those 18 basins over different continents are shown by Figure 4.6 (a) – (f); and more quantitative statistic indices (i.e. Bias(%), RMSE(%), NSCE(Nash-Sutcliffe Coefficient of Efficiency) and CC) are listed in Table 4.2. Please refer to Appendix I. Equations for the definition of those statistic indices.

Table 4.1 Information of those 18 primary river basins

	GRDC ID	river	station	Basin Area (km^2)
Africa	1291100	ZAMBEZI	KATIMA MULILO	334000
	1531100	BLACK VOLTA	BAMBOI	134200
	1531450	WHITE VOLTA	NAWUNI	92950
	1749100	UBANGI	BANGUI	500000
Asia	2181900	YANGTZE RIVER	DATONG	1705383
	2186800	XI JIANG	WUZHOU 3	329705
	2186901	BEI JIANG	SHIJIAO	38363
S.America	3629001	AMAZONAS	OBIDOS - LINIGRAFO	4680000
	3629150	RIO TAPAJOS	FORTALEZA	363000
	3630050	RIO XINGU	ALTAMIRA	446203
	3649950	TOCANTINS	TUCURUI	742300
N.America	4123050	OHIO RIVER	METROPOLIS	525770
	4125804	ARKANSAS RIVER	MURRAY DAM	409297
	4127501	MISSISSIPPI RIVER	THEBES	1847188
Oceania	5109200	MITCHELL RIVER	KOOLATAH	45872
	5608024	FITZROY RIVER	FITZROY CROSSING	46133
	5708110	VICTORIA RIVER	COOLIBAH HOMESTEAD	44900
Europe	6742900	DANUBE RIVER	CEATAL IZMAIL	807000

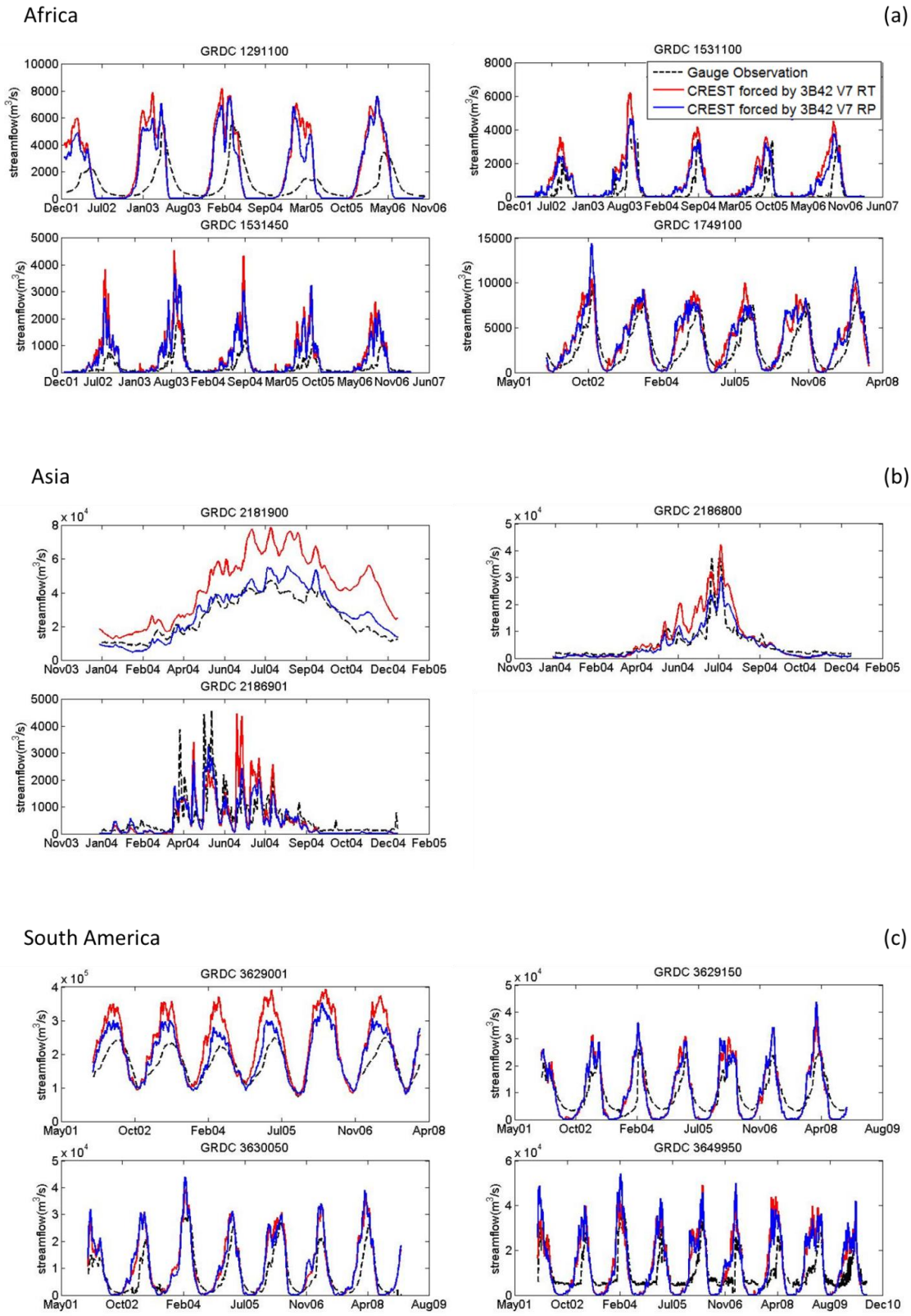
Africa
(a)
GRDC 1291100
GRDC 1531100
Gauge Observation
CREST forced by 3B42 V7 RT
CREST forced by 3B42 V7 RP
GRDC 1531450
GRDC 1749100
Asia
(b)
GRDC 2181900
GRDC 2186800
GRDC 2186901
South America
(c)
GRDC 3629001
GRDC 3629150
GRDC 3630050
GRDC 3649950
streamflow(m3/s)

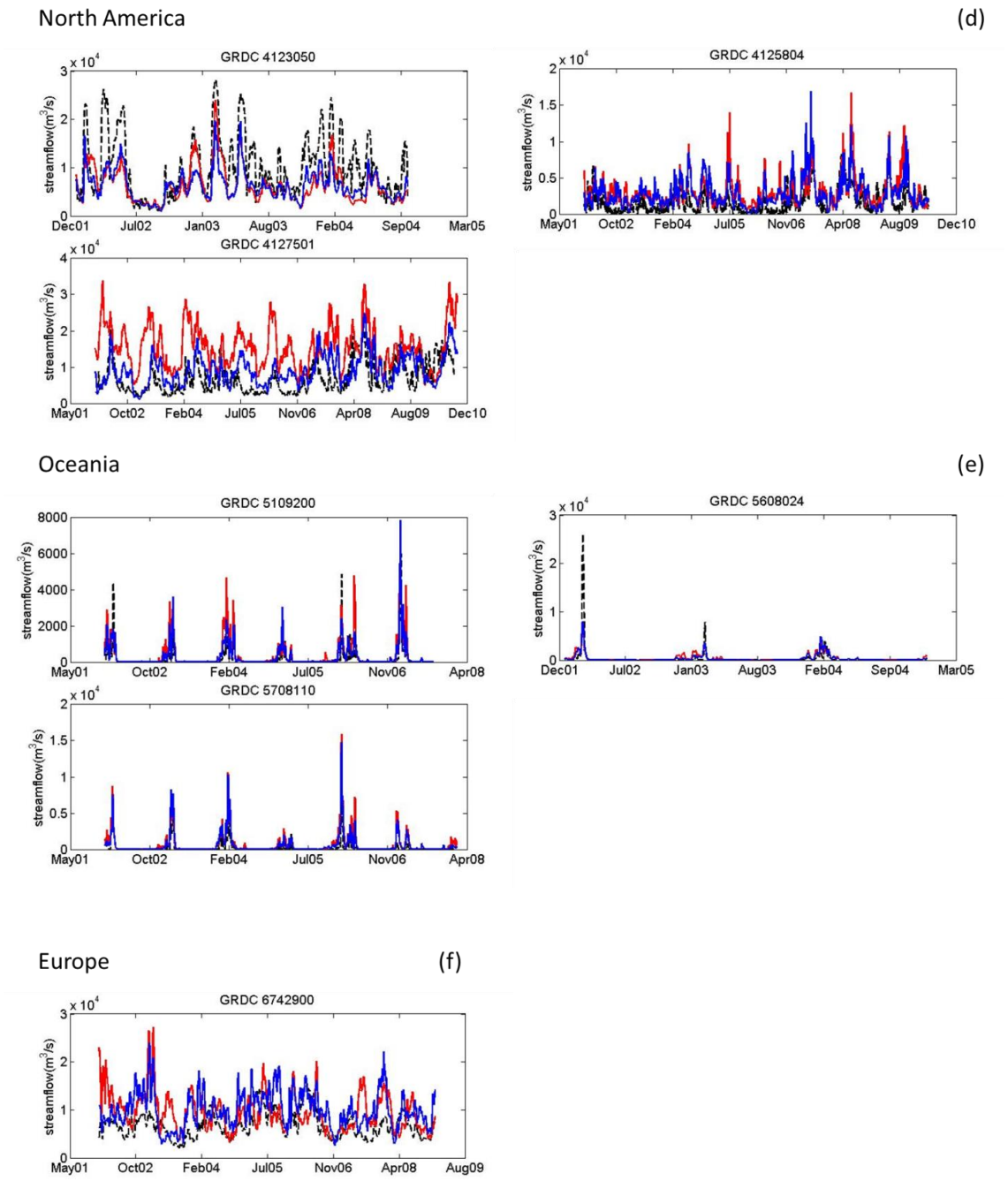

Figure 4.6 Comparison between model simulated streamflow with satellite rainfall forcing and observations at daily scale for the selected 18 basins in different continents.

Table 4.2 Statistical indices of the selected 18 primary basins.

	GRDC No.	TRMM RT				TRMM V7			
		Bias(%)	RMSE(%)	NSCE	CC	Bias(%)	RMSE(%)	NSCE	CC
Africa	1291100	101	239	-4.13	0.33	79	207	-2.86	0.36
	1531100	180	319	-0.96	0.72	127	229	-0.01	0.77
	1531450	129	286	-2.66	0.66	105	233	-1.42	0.78
	1749100	27	61	0.41	0.82	27	61	0.41	0.83
	Mean	*109*	*226*	*-1.83*	*0.63*	*84*	*183*	*-0.97*	*0.69*
Asia	2181900	72	83	-1.88	0.91	12	24	0.76	0.95
	2186800	25	87	0.44	0.89	-8	52	0.80	0.90
	2186901	-10	112	0.15	0.64	-18	78	0.59	0.79
	Mean	*29*	*94*	*-0.43*	*0.81*	*-4*	*51*	*0.72*	*0.88*
S.America	3629001	31	45	-1.57	0.84	14	25	0.20	0.87
	3629150	4	62	0.22	0.84	3	**64**	**0.17**	**0.82**
	3630050	34	76	0.45	0.88	**37**	**83**	**0.33**	**0.85**
	3649950	22	86	-0.28	0.73	**24**	**89**	**-0.35**	0.75
	Mean	*23*	*67*	*-0.29*	*0.82*	*20*	*65*	*0.09*	*0.82*
N.America	4123050	-36	58	0.17	0.71	-36	56	0.24	0.82
	4125804	86	137	-1.16	0.54	75	119	-0.61	0.67
	4127501	125	153	-5.04	0.32	33	69	-0.22	0.52
	Mean	*58*	*116*	*-2.01*	*0.52*	*24*	*81*	*-0.20*	*0.67*
Oceana	5109200	106	321	-0.09	0.74	57	210	0.53	0.83
	5608024	44	459	0.46	0.71	25	423	0.54	0.77
	5708110	209	544	-1.02	0.83	166	470	-0.50	0.87
	Mean	*119*	*441*	*-0.22*	*0.76*	*83*	*368*	*0.19*	*0.82*
Europe	6742900	39	74	-2.36	0.20	**45**	65	-1.54	0.55
	Mean	*39*	*74*	*-2.36*	*0.20*	*45*	*65*	*-1.54*	*0.55*

(b) Basins in Africa

Compared to other continents, rain gauge networks in Africa are extremely sparse and prevent hydrological modeling. Therefore, the remote sensing precipitation estimations play an important role in this region. The daily time series comparisons between the model simulated streamflow and GRDC gauge observations of the four primary basins – Zembezi, Black Volta, White Volta and Ubangi are shown by Figure

4.6(a) and the quantitative statistics (i.e. Bias(%), RMSE(%), NSCE and CC) are shown in Table 4.2. In general, the 3B42 V7 RP is generally better at hydrological predictions than 3B42 V7 RT for the four basins. However, the overall performance of the global CREST model in Africa is the worst in comparison to those basins located on other continents: three basins out of the total four have a NSCE below zero. Further research has been conducted as shown in Table A1 in Appendix III: the cross correlation coefficients are calculated with time lags in comparison to the original correlation coefficients: with time lags of 58- to 16-day, the cross correlation coefficients increase significantly when compared to the original correlation coefficients. We assume that the differences in peak timings are caused by the hydro-projects on those rivers: (1) there are two dams - Kariba and Cahora Bassa on the Zambezi River which impact the natural hydrological cycle in this river; (2) the Black Volta and White Volta are two tributaries of the river Volta which has a large reservoir downstream - Lake Volta - which is the largest in the world, and which might cause some backwater issue that leads to the peak timing errors for both the Black and White Volta Rivers; (3) several hydropower plants on the Ubangi river may lead to the peak timing differences in this river.

(c) Basins in Asia

Figure 4.6(b) and Table 4.2 show remarkable improvements for hydrological simulation forced by 3B42 V7 RP in contrast with that forced by 3B42 V7 RT in the Yangtze river: the NSCE increased from -1.88 to 0.76 after switching the forcing data from RT to RP (Table 4.2), and the differences (Bias(%)) between modeled streamflow simulation and GRDC observation is minimized down to 12% (RP) from 72% (RT). For

those two other basins – Xijiang and Beijiang, 3B42 V7 RP also outperforms 3B42 V7 RT. The average NSCE of these three basins forced by V7 RP is above 0.7, which indicates the good hydrological prediction skill in Asia.

(d) Basins in South America

Similar to Africa, the two TMPA products forced streamflow simulations in those four basins in South America also show overestimations compared to GRDC gauge observations (Figure 4.6(c)): as the Bias(%) as shown in Table 4.2 for both Africa and South America are all with positive values. Another similarity to the basins in Africa is the time lag of the model simulated streamflow in comparison to the gauge observations. The cross correlations are also investigated as shown in Table A1 in Appendix III: with the time lags around 20 days, the cross correlation coefficients increased to above 0.8 for all of these four basins compared to the original correlation coefficients which are only around 0.7. We also assume that the many dams in the three tributaries of the Amazon River - the upstream Amazon Basin, Rio Tapajos River and Rio Xingu River, and the Tucurui dam in the Tacantins River lead to the differences in peak timings between observations and model simulations in South America.

As shown by Table 4.2, for the basins Rio Xingu and Tocantins, the 3B42 V7 RP (the Bias(%) of Rio Xingu is 37% while the Bias(%) of Tocantins is 24%) shows slightly degrade from 3B42 V7 RT (the Bias(%) of Rio Xingu is 34% while the Bias(%) of Tocantins is 22%) in simulated streamflow, though the differences are within 2-3%.

(e) Basins in North America

Three basins are investigated in North America – the Ohio, Arkansas and Mississippi rivers as shown in Figure 4.6(d).

For those two medium sized basins – the Ohio River of 525,770 km^2 and the Arkansas River of 409,297 km^2, the hydrological performance of the 3B42 V7 RT and 3B42 V7 RP are quite similar (Table 4.2): the Biases(%) of the Ohio river are of the same value -36% with both RT and RP, the RMSE(%) only decreases by 2% from RT to RP; for the Arkansas river, the Bias(%) is improved from 86% to 75% from RT to RP, while the RMSE(%) is decreased from 137% to 119%.

For the largest river among these three - the Mississippi river which is within a basin area of 1,847,188 km^2, the improvement from RT to RP is significant as the Biases(%) decreased from 125% to only 33% throughout the 9 years evaluation period (2002-2010).

(f) Basins in Oceania

The three basins investigated in Oceania are all small with sizes below 50,000 km^2. As shown by Figure 4.6(e) and Table 4.2, similarly to the basins in Africa and Asia, the hydrological predictive skills improved considerably from 3B42 V7 RT to RP.

(g) Basins in Europe

The primary basin – the Danube River basin in Europe is around 807,000 km^2. Both 3B42 V7 RT and RP show obvious overestimations in the streamflow simulations in this river with low correlation coefficients. 3B42 V7 RP shows improvement in

comparison with 3B42 V7 RT in terms of RMSE(%, from 74% down to 65%), NSCE (from -2.26 up to -1.54) and CC (from 0.2 to 0.55), but the overall performance is not satisfactory even with the forcing as RP. The poor performance with both TMPA products might be due to the high latitude – the precipitation estimation is of low accuracy when IR data are combined in the high latitude precipitation estimation (Yong et al. 2010).

(h) General conclusion for these 18 primary basins

Overall, three general conclusions are drawn from the above analysis:

- The CREST modeled streamflow forced by the post real time TMPA 3B42 V7 RP generally improves the hydrological performance compared to the modeled streamflow forced by the real time TMPA 3B42 V7 RT, although in some basins the hydrological simulations with 3B42 V7 RP are still unsatisfactory, especially for those basins in Africa and Europe.

- From the mean values of those statistic indices in Table 4.2, we can draw the conclusion that the hydrological improvement from forcing with TMPA 3B42 RT to TMPA 3B42 RP is significant in those primary basins (out of 18 primary basins) in Asia and Oceana (e.g. the means NSCEs are increased from -0.43, -0.22 in Asia and Oceania to 0.72 and 0.19 respectively).

- The general poor hydrological performances (the peak timing lag as shown in Appendix III, Table A1) in Africa and South America might be caused by (a) the hydrological projects such as reservoirs and dams on top of the rivers, (b) the poor satellite precipitation data quality.

4.4 Conclusion and Future work

In this study, we present the evaluation of the Near Realtime Global Hydrological Simulation and Flood Monitoring Demonstration System forced by the updated Version 7 near real time and post real time TMPA 3B42 products:

First, a macro-scope evaluation is conducted by modeling the multiple year runoff climatology (mm/yr): the 3B42 V7 RT and RP precipitation estimation products derive similar runoff climatology over the 2002-2012 period; in contrast with RT derived annual mean runoff, RP shows higher skill in the central Africa around the equator, the land to the north of the Gulf of Mexico in the U.S., and the northeast part of the U.S. against GRDC observed runoff climatology.

Then, a total of 88 GRDC discharge gauge data with at least 1-year recond length at daily time step are used to assess the modeling performance in terms of the annual mean discharge: the results show the CREST model simulated annual mean streamflows over the 88 selected basins are in high agreement with the GRDC observation; and the annual mean streamflow driven by 3B42 V7 RP has lower errors against the GRDC observation in terms of Bias(%) and RMSE(%) and higher correlation coefficient (CC) in comparison with that driven by 3B42 V7 RT.

After that, the daily scale streamflow simulation performance in those 88 basins forced by V7 RT and V7 RP is evaluated as the functions of basin size and latitude respectively, a general role is found that the modeling performance is better with a larger basin size and a location closer to the equator.

At last, 18 primary basins are selected to examine the daily streamflow simulation effectiveness: in general, the CREST modeled streamflow forced by the post real time 3B42 V7 RP improved the hydrological performance compared to the modeled streamflow forced by the real time 3B42 V7 RT, although in some basins the hydrological simulation with 3B42 V7 RP are still unsatisfactory, especially for those basins in Africa and Europe.

Overall, this study shows the hydrological performance of the Near Realtime Global Hydrological Simulation and Flood Monitoring Demonstration System forced by the updated Version 7 real time and post real time TMPA 3B42 products in its initial stage; in other words, no local calibration has been involved in this work. This is an important aspect for future improvement: regional parameterization and collaborations with local experts are of high importance to better predict the streamflow, especially for those regions with high flood occurrence. As the evaluation results analyzed in section 4.3, the system performance is highly dependent on the quality of the input forcing data: for most of the cases, in contrast to TMPA 3B42 real time rainfall products, TMPA post real time products– the 3B42 RP with rain gauge corrections simulate more accurate streamflow against GRDC observations at both annual and daily scales. Therefore, with the promising next generation of global satellite precipitation estimation – "Global Precipitation Measurement (GPM)" with higher spatial resolution (~4km vs. ~25km with TRMM) and global-coverage (90°N to 90°S vs. 50°N to 50°S with TRMM), the CREST model can be setup at a higher spatial resolution (~4km) over the 90°N to 90°S global coverage. In addition, the GPM precipitation, which is expected to have better accuracy than the current TRMM precipitation, can be applied as the forcing data into

the current system and is expected to improve hydrological performance compared to the current TRMM mission. In addition to the parameter error and input forcing data error, human impact is another crucial factor that increasingly needs to be considered. The various hydrological projects such as hydro-power stations, dams, and reservoirs, impact the natural hydrological cycle on a basin scale, thus degrading the overall hydrological simulation skills. In order to mitigate the negative impact of the hydrological predictions skills from those hydrological projects, new model components such as the reservoir module is considered to be added into the current model.

Appendix I. Equations:

The equations of the evaluation matrices used in this paper are listed below:

$$Bias(\%) = \frac{\sum (y_i - x_i)}{\sum x_i} * 100 \quad \text{(A1)}$$

$$RMSE(\%) = \frac{\sqrt{\sum (x_i - y_i)^2 / n}}{\bar{x}} * 100 \quad \text{(A2)}$$

$$NSCE = 1 - \frac{\sum (x_i - y_i)^2}{\sum (x_i - \bar{x})^2} \quad \text{(A3)}$$

In equation A1 and A2, x_i is the observed streamflow and y_i is the simulated streamflow. For both Bias and RMSE, the smaller their values are (i.e., closest to 0), the better the model result is. Small values of Bias and RMSE signify the modeling results are close to the corresponding observations in regards to systematic bias and random errors. NSCE is a frequently used statistic to quantify the agreement between the model simulation and the ground observation. The perfect value of NSCE is 1.

Appendix II. Supplementary Figures:

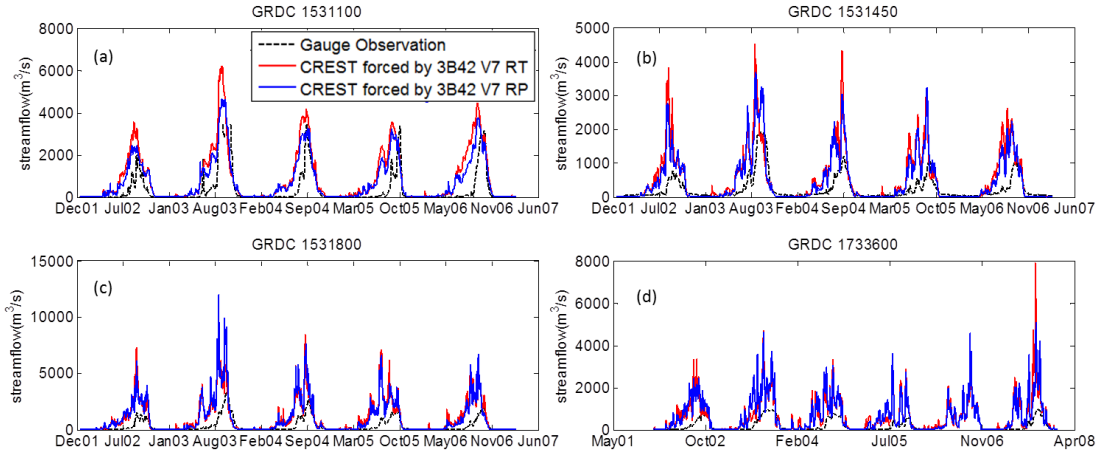

Figure A1. Time series of those four “odds” basins in Figure 4.5

Appendix III. Supplementary Tables

Table A1 Cross correlations of the rivers in Africa and South America

	GRDC No.	correlation coefficient	**cross correlation**	**time lag (days)**
Africa	1291100	0.33	**0.85**	**58**
	1531100	0.72	**0.83**	**20**
	1531450	0.66	**0.8**	**16**
	1749100	0.82	**0.93**	**23**
S.America	3629001	0.84	**0.96**	**28**
	3629150	0.84	**0.91**	**23**
	3630050	0.88	**0.94**	**18**
	3649950	0.73	**0.83**	**23**

References

Brakenridge, G. R., S. V. Nghiem, E. Anderson, and R. Mic, 2007: Orbital microwave measurement of river discharge and ice status. *Water Resources Research*, **43,** W04405.

Hirabayashi, Y., and Coauthors, 2013: Global flood risk under climate change. *Nature Climate Change*.

Hong, Y., R. F. Adler, F. Hossain, S. Curtis, and G. J. Huffman, 2007: A first approach to global runoff simulation using satellite rainfall estimation. *Water Resources Research*, **43,** W08502.

Huffman, G. J., 2012: Real-Time TRMM Multi-Satellite Precipitation Analysis Data set Documenation

Huffman, G. J., R. F. Adler, D. T. Bolvin, and E. J. Nelkin, 2010: The TRMM multi-satellite precipitation analysis (TMPA). *Satellite rainfall applications for surface hydrology*, Springer, 3-22.

Huffman, G. J., D. T. Bolvin, E. J. Nelkin, D. B. Wolff, R. F. Adler, G. Gu, Y. Hong, K. P. Bowman, and E. F. Stocker (2007), The TRMM Multisatellite Precipitation Analysis (TMPA): Quasi-Global, Multiyear, Combined-Sensor Precipitation Estimates at Fine Scales, *Journal of Hydrometeorology*, *8*(1), 38-55.

Khan, S. I., P. Adhikari, Y. Hong, H. Vergara, R. F Adler, F. Policelli, D. Irwin, T. Korme, and L. Okello, 2011a: Hydroclimatology of Lake Victoria region using hydrologic model and satellite remote sensing data. *Hydrology and Earth System Sciences*, **15,** 107-117.

Khan, Sadiq I., Yang Hong, Jiahu Wang, Koray K. Yilmaz, Jonathan J. Gourley, Robert F. Adler, G. Robert Brakenridge, Fritz Policelli, Shahid Habib, and Daniel Irwin, 2011b: Satellite Remote Sensing and Hydrologic Modeling for Flood Inundation Mapping in Lake Victoria Basin: Implications for Hydrologic Prediction in Ungauged Basins. *Geoscience and Remote Sensing, IEEE Transactions on*, **49,** 85-95.

Li, Z., D. Yang, and Y. Hong, 2013: Multi-scale evaluation of high-resolution multi-sensor blended global precipitation products over the Yangtze River. *Journal of Hydrology*, **500,** 157-169.

Liang, X., D. P. Lettenmaier, E. F. Wood, and S. J. Burges, 1994: A Simple Hydrologically Based Model of Land-Surface Water and Energy Fluxes for General-Circulation Models. *Journal of Geophyicals Research Atmospheres*, **99,** 14415-14428.

Maggioni, V., H. J. Vergara, E. N. Anagnostou, J. J. Gourley, Y. Hong, and D. Stampoulis, 2013: Investigating the Applicability of Error Correction Ensembles of Satellite Rainfall Products in River Flow Simulations. *Journal of Hydrometeorology*, **14,** 1194-1211.

Nijssen, B., D. P. Lettenmaier, X. Liang, S. W. Wetzel, and E. F. Wood, 1997: Streamflow simulation for continental-scale river basins. *Water Resources Research*, **33,** 711-724.

Proud, S. R., R. Fensholt, L. V. Rasmussen, and I. Sandholt, 2011: Rapid response flood detection using the MSG geostationary satellite. *International Journal of Applied Earth Observation and Geoinformation*, **13,** 536-544.

Stisen, S., and I. Sandholt, 2010: Evaluation of remote‐sensing‐based rainfall products through predictive capability in hydrological runoff modelling. *Hydrological Processes*, **24,** 879-891.

Su, F., Y. Hong, and D. P. Lettenmaier, 2008: Evaluation of TRMM Multisatellite Precipitation Analysis (TMPA) and its utility in hydrologic prediction in the La Plata Basin. *Journal of Hydrometeorology*, **9,** 622-640.

Wake, B., 2013: Flooding costs. *Nature Climate Change*, **3,** 778-778.

Wang, J., Y. Hong, L. Li, J.J. Gourley, S.I. Khan, K.K. Yilmaz, R.F. Adler, F. S. Policelli, S. Habib, D. Irwn, A. S. Limaye, T. Korme and L. Okello. 2011: The coupled routing and excess storage (CREST) distributed hydrological model. *Hydrological sciences journal*, **56,** 84-98.

Westerhoff, R. S., M. P. H. Kleuskens, H. C. Winsemius, H. J. Huizinga, G. R. Brakenridge, and C. Bishop, 2013: Automated global water mapping based on wide-swath orbital synthetic-aperture radar. *Hydrology and Earth System Sciences*, **17,** 651-663.

Wu, H., R. F. Adler, Y. Hong, Y. Tian, and F. Policelli, 2012: Evaluation of Global Flood Detection Using Satellite-Based Rainfall and a Hydrologic Model. *Journal of Hydrometeorology*, **13,** 1268-1284.

Wu, P., N. Christidis, and P. Stott, 2013: Anthropogenic impact on Earth/'s hydrological cycle. *Nature Climate Change*.

Xue, X., and Coauthors, 2013: Statistical and hydrological evaluation of TRMM-based Multi-satellite Precipitation Analysis over the Wangchu Basin of Bhutan: Are the latest satellite precipitation products 3B42V7 ready for use in ungauged basins? *Journal of Hydrology*, **499,** 91-99.

Yilmaz, K. K., R. F. Adler, Y. Tian, Y. Hong, and H. F. Pierce, 2010: Evaluation of a satellite-based global flood monitoring system. *International Journal of Remote Sensing*, **31,** 3763-3782.

Yong, B., and Coauthors, 2010: Hydrologic evaluation of Multisatellite Precipitation Analysis standard precipitation products in basins beyond its inclined latitude band: A case study in Laohahe basin, China. *Water Resources Research*, **46**.

Zhang, Y., Y. Hong, X. Wang, J. J. Gourley, J. Gao, H. J. Vergara, and B. Yong, 2013: Assimilation of Passive Microwave Streamflow Signals for Improving Flood Forecasting: A First Study in Cubango River Basin, Africa. *Selected Topics in Applied Earth Observations and Remote Sensing, IEEE Journal of*, **PP,** 1-16.

Chapter 5. Hydrometeorological Analysis and Remote Sensing of Extremes:Was the July 2012 Beijing Flood Event Detectable and Predictable by Global Satellite Observing and Global Weather Modeling Systems?

Abstract

Prediction and thus preparedness in advance of flood events are crucial for proactively reducing their impacts. In the summer of 2012, Beijing - the capital of China, experienced extreme rainfall and flooding, causing around 1.6 billion dollars of economic losses and up to 79 fatalities. Using rain gauge networks as a benchmark, this study investigated the detectability and predictability of the 2012 Beijing event via the Global Hydrological Prediction System (GHPS), which was forced by the NASA Tropical Rainfall Measuring Mission (TRMM) Multi-satellite Precipitation Analysis at near real-time and by the deterministic and ensemble precipitation forecast products from NOAA Global Forecast System (GFS) with around 7-day lead time. The results indicate that the disastrous flooding event was detectable by the satellite-based global observing system and predictable by the model-based global weather prediction system GFS 4 days in advance. Furthermore, the GFS ensemble precipitation forecast products from NOAA for streamflow forecasts provided additional useful information on the identification of the possibility of the extreme event. Given the global availability of satellite-based precipitation in near real-time and GFS precipitation forecast products with different lead times, this study demonstrates the opportunities and challenges that

exist for an integrated application of GHPS. These systems are particularly useful for the vast ungauged regions of the globe.

5.1 Introduction

Flooding, which is always considered as one of the most hazardous disasters in both rural and urban areas, accounts for about one-third of all global geophysical hazards (Adhikari et al. 2010; Smith and Ward 1998). Urban areas are more vulnerable to floods and their associate damages than rural areas due to high population density and intensively developed infrastructure. Urban flooding affects structures, including buildings, bridges and roadways; it may also induce severe water-borne diseases. On July 21, 2012, the capital of China, Beijing, and its surroundings experienced extreme rainfall and flooding. The storm lasted for around 16 hours and the rain rate reached as high as 215 mm/day in the urban area. It was reported as the heaviest storm event since 1951 and the return periods for flooding were estimated at 60 years in Beijing and 100 years in the surrounding Fangshan suburban area. It inundated roadways, bridges and sewage systems, causing houses collapse, cars damages, and even debris flows in Fangshan. Overall, the flooding event resulted in 79 fatalities and around 1.6 billion dollars in damages. In the same year, the Gelendzhik, Novorossiysk and the Krymsk districts in Russia were affected by the Kuban flood in July and 171 people were killed. Three months later, New York City experienced Hurricane Sandy which flooded the streets, subways, and tunnels, and cut electricity in and around the city in October. Earlier the same year, the third biggest city in Australia, Brisbane, Queensland, was inundated by floods from December 2010 to January 2011 by several separate storm events. As mentioned by (Adhikari et al. 2010), "The International Flood Network indicates that from 1995 to 2004, natural disasters caused 471,000 fatalities worldwide and economic losses totaling approximately $49 billion USD, out of which

approximately 94,000 (20%) of the fatalities and $16 billion USD (33%) of the economic damages were attributed to floods alone." In the coming decades, urban areas will likely become increasingly vulnerable to hydrometeorological extremes because urban populations are increasing, especially in fast-growing developing countries.

The increasing adverse worldwide impact from floods indicates this is not only a regional or national-level issue but also a global problem that greatly motivates a global flood detection and prediction system coordinated among worldwide research institutions and government decision makers. Currently, several satellite remote-sensing, flood-monitoring systems exist at global scales and provide forecasts in near real time (e.g. Brakenridge et al. 2007; Hong et al. 2007; Westerhoff et al. 2013; Wu et al. 2012; Yilmaz et al. 2010). Timely, recent development and improvement of global flood early warning systems are appealing to users when they provide forecasts several days in advance for better planning and responding to emerging disasters. The traditional approach to forecast streamflow at the outlet of a basin is often using a hydraulic way based on the upstream gauge observation, such as a hydrograph; for this approach, the lead time is often limited by the catchment concentration time (Bartholmes and Todini 2005). In order to extend the hydrological forecast horizon, Numerical Weather Prediction (NWP) products (e.g. temperature and precipitation) can be coupled with hydrological rainfall-runoff model, which is of high importance especially for those rivers without upstream river discharge observation and those smaller rivers with shorter response time (Hopson and Webster 2010). Besides the deterministic forecast product from NWP system, ensemble forecast products from NWP are usually applied to quantify the uncertainty in hydrologic forecast, which make NWP ensembles an

attractive product for flood forecasting system with the potential to better quantify predictability (Cloke and Pappenberger 2009). In particular, the Hydrological Ensemble Prediction Experiment (HEPEX ,(Schaake et al. 2007) http://hepex.irstea.fr), with its mission as "to demonstrate the added value of hydrological ensemble predictions (HEPS) for emergency management and water resources sectors to make decision that have important consequences for economy, public health and safety", has maintained a community from meteorology to hydrology in order to improve the ensemble forecast (e.g. Bradley et al. 2003; Bradley et al. 2004; Brown et al. 2010, 2012; Demargne et al. 2009; Demargne et al. 2013; Gneiting et al. 2007; Pappenberger et al. 2008; Seo et al. 2006; Zappa et al. 2013). Recently, a review paper (Cloke and Pappenberger 2009) showed the potential of using ensemble streamflow forecast to further improve the early warning system.

In this study, we aim at demonstrating the prototype of a Real Time Global Hydrological Prediction System (GHPS), which is driven by the NASA TRMM Multi-satellite Precipitation Analysis (TMPA) and NOAA's Global Forecast System (GFS) deterministic and ensemble precipitation forecasts. In addition, we are intending to address those questions: (1) Was the July 2012 Beijing Flood Event Detectable and Predictable by Global Satellite Observing and Global Weather Modeling Systems in its initial stage without specific calibration? (2) How much "added value" does the ensemble streamflow forecast contribute to the hydrological prediction in the probabilistic domain for this specific case study?

This study is organized as follows. In Section 5.2, the core part of GHPS - a distributed hydrological model and its set-up are described. Then the study region and

data sets applied for this particular case study are introduced in Section 5.3. In Section 5.4, the hydrologic predictions conditioned on forcing from remote-sensing datasets and model forecasts are assessed in both actual domain and probabilistic domain. Finally, results are summarized in section 5.5 along with concluding remarks.

5.2 Global Hydrological Prediction System

The Global Hydrological Prediction System (GHPS, Figure 5.1), with the Coupled Routing and Excess STorage (CREST, (Wang et al. 2011)) distributed hydrological model as its core part, is selected to evaluate the detectability and predictability of flooding using TRMM precipitation estimates and forecasts from the GFS model. The core part of GHPS, the CREST model, is modified from the state-of-art Variable Infiltration Capacity (VIC) model (Liang et al. 1994; Nijssen et al. 1997) and has added a distributed grid-to-grid routing scheme. The CREST model is currently running within the Near Realtime Global Hydrological Simulation and Flood Monitoring Demonstration System (http://eos.ou.edu) at University of Oklahoma; and this is considered as the "Real Time System" driven by TRMM 3B42 Real Time (RT, (Huffman et al. 2007)) product in the proposed GHPS. The "Retrospective System" and "Forecast System" are driven by TRMM 3B42 Level 7 (V7,(Huffman et al. 2007)) and NOAA GFS precipitation forecasts (Han and Pan 2011; Kanamitsu et al. 1991; Yang et al. 2006), respectively. For detailed information of the forcing data, please refer to section 3 and the corresponded references. In GHPS, the CREST model is set up at 1/8 degree based on the Digital Elevation Model (DEM) with quasi-global coverage from 50°N to 50°S, providing near real time runoff and streamflow simulation every 3 hours forced by TRMM RT, retrospective hydrological simulation forced by TRMM V7 since 1998 and real time flood prediction initialized at 00UTC every day with forecast lead times up to 180 hours for each initialization at each 1/8 degree grid. The model parameters are estimated from input data and used as a priori parameters (for detailed information about the parameter estimation, please refer to (Wang et al. 2011; Wu et al.

2012)): those physical parameters such as hydraulic conductivity, available water capacity, etc. in CREST model can be estimated based on the soil type map, land cover maps and digital elevation model (DEM). The CREST model, as core of the GHPS, has been warming up and partially benchmarked by 10+ years' TMPA QPE. The CREST model has been evaluated and implemented at both global and regional scales (Khan et al. 2011a; Khan et al. 2011b; Wu et al. 2012; Yilmaz et al. 2010), proving its high cost-effectiveness in hydrological prediction. Wu et al. (2013) applied the same hydrological model – CREST, but forced with TRMM V6 – the gauge corrected research product to run a retrospective streamflow simulation over the quasi-globe from 50°N to 50°S during the period 1998 – 2010. In general, the results show that the flood probability of detection (POD) is around 0.70 for the flood with the duration longer than 3 days in the no-dams areas. The general positive results indicate the potential value of this system forced with TRMM in global flood detection. However, Wu et al. (2013) did not specifically address or investigate extreme or rare events such as the studied Beijing event in this paper. Therefore, this paper is the first time prediction skill assessment of the GHPS in a local setting. In this study, the updated version TRMM data – both TRMM RT (real time product) and TRMM V7 (gauge corrected research product) are applied for flood detection. Considering the improvement satellite precipitation estimates from TRMM V6 to V7 product, the GHPS is expected to have better flood detection skills.

Other than streamflow and runoff depth, the GHPS can also provide gridded soil moisture and Actual Evapotranspiration (AET) at 1/8 degree spatial resolution as well.

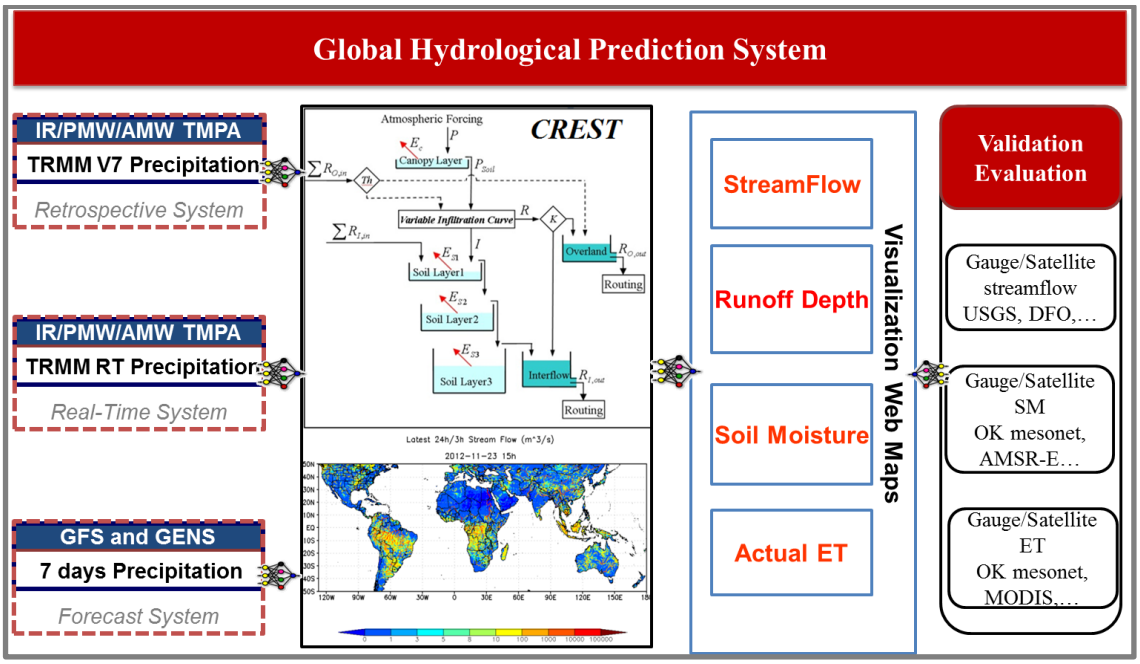

Figure 5.1 Structure of Global Hydrological Prediction System

In this study, the global CREST model is warmed up by TRMM RT from July 1st, 2012 until the initial time of each experiment. Then, the model is forced by rain gauges, TRMM RT, TRMM V7, and GFS deterministic and ensemble precipitation forecasts at different initializations (with different lead times) to generate hydrological forecasts of surface runoff in urban areas and streamflow in the watersheds. Although the CREST model includes a parameter describing the degree of imperviousness of the surface, which is quite distinct in urban regions, the model physics do not explicitly account for evapotranspiration, surface runoff generation, routing, and drainage processes that are specific to the urban environment. A detailed discussion regarding the detectability and predictability of surface runoff depths and streamflows using the GHPS, even with the simplified natural environment assumption will be discussed in section 5.4.

5.3 Research Region and Input Data

For this case study, Beijing and its upstream Juma River basin are selected as the research region as shown in Figure 5.2. Beijing, as the capital of China, is located in the northern part of China and surrounded by Heibei Province. It is the political, economic, cultural and educational center of China; it is also the metropolitan with the most-density population (20,693,000 as of 2012, http://en.wikipedia.org/wiki/Beijing) in the world. The dense population of Beijing makes it vulnerable to be highly impacted by the rainfall and flood extremes, thus leading to huge economic loss and fatalities.

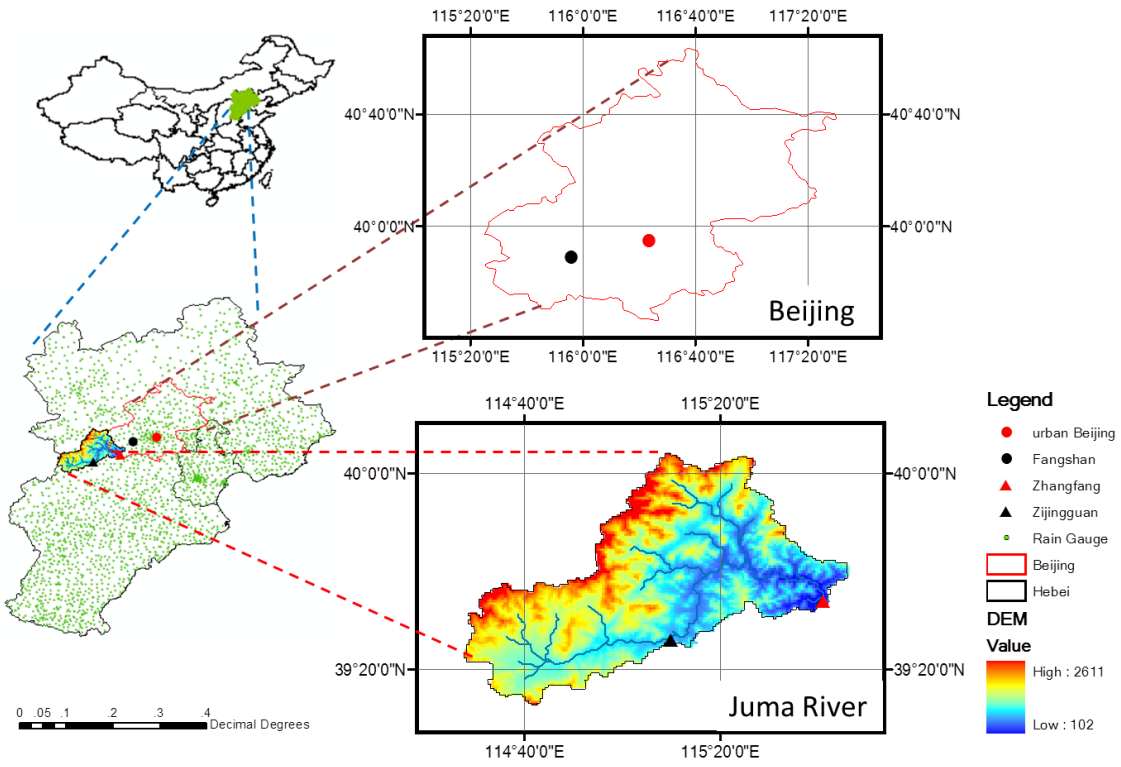

Figure 5.2 Research Region

Four precipitation data sets are used to evaluate the spatial variability of precipitation in and around Beijing on July 21, 2012: (1) High-density rain gauge observations

(Figure 5.2) with hourly temporal resolution from 03UTC on July 19, 2012 to 12UTC on July 22, 2012. There are 2041 rain gauge stations in total within Hebei province and 231 in total within Beijing city. The rain gauge data are interpolated onto a 0.25° resolution grid using kriging and accumulated into 3-hourly rainfall accumulations in order to facilitate comparison with TMPA products; (2) TRMM Multi-satellite Precipitation Analysis (TMPA) near-real-time 3B42RT, which uses a combination of active and passive microwave and infrared measurements from TRMM and other satellites (Huffman et al. 2007); (3) TMPA post-real-time 3B42 V7, which adjusts the rainfall accumulation by gauge analysis. Both 3B42RT and 3B42 V7 products are quasi-global with coverage from 50°N to 50°S latitude with a spatial resolution of 0.25° and temporal resolution of 3 hours (Huffman et al. 2007); (4) the Deterministic (GFS hereafter) and ensemble (GENS hereafter) precipitation forecast products from NOAA Global Forecast System was used to drive the hydrological forecasts. The GFS forecasts were run in near real time by NOAA Earth System Research Lab. The forecasts were initialized by the hybrid ensemble-variational data assimilation system developed based on NOAA NCEP operational data assimilation. The description of the hybrid data assimilation system for GFS can be found in (Wang 2010) and (Wang et al. 2013). The GFS forecasts were initialized four times per day (00, 06, 12, and 18UTC); and saved at 3-hourly interval up to 180-hour lead time. The spatial resolution of the forecasts data was 0.5 degrees. In this study, the GFS data and a 20-member ensemble GENS initialized at 00UTC were used to drive the hydrological forecast. Both the deterministic GFS and ensemble GENS precipitation forecasts members were

interpolated to 0.25° in order to match the spatial resolution of the TRMM rainfall estimates.

5.4 Results and Discussion

5.4.1 Rainfall evaluation

Figure 5.3 shows the total precipitation accumulation (mm/day) on July 21, 2012 over the Hebei province (dark outline), which contains the Beijing region (white outline), based on rain gauges (Figure 5.3(a)), TRMM V7 (Figure 5.3(b)), TRMM RT (Figure 5.3(c)), GFS forecast initialized 4 days to 1day in advance of the event (Figure 5.3(d,e,f,g), Please be noted that all the time information are based on UTC standard in this study). Although TRMM V7 and RT slightly underestimate the daily accumulated precipitation amounts in the center of the field compared to the gauge observations, the main characteristics of TRMM precipitation products capture the observed precipitation patterns well. The GFS daily precipitation accumulations with different lead times resemble the general patterns of the July 21 event, but they have limited spatial variability due to their coarse spatial resolution.

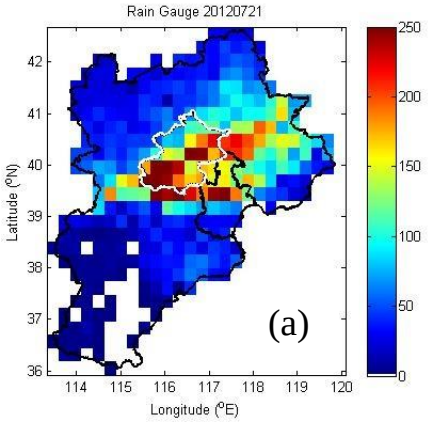
Rain Gauge 20120721
Latitude (°N)
Longitude (°E)
(a)

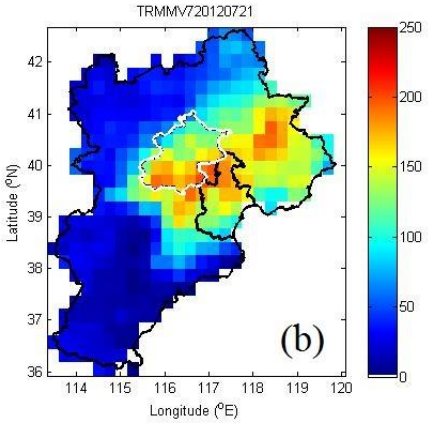
TRMMV720120721
Latitude (°N)
Longitude (°E)
(b)

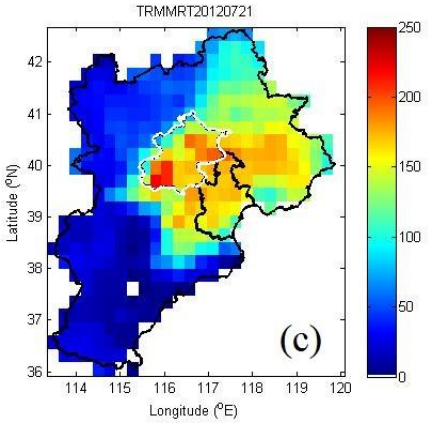
TRMMRT20120721
Latitude (°N)
Longitude (°E)
(c)

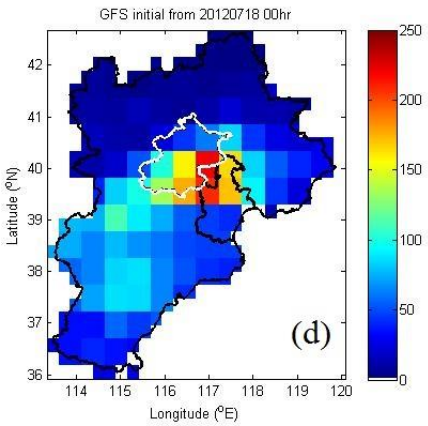
GFS initial from 20120718 00hr
Latitude (°N)
Longitude (°E)
(d)

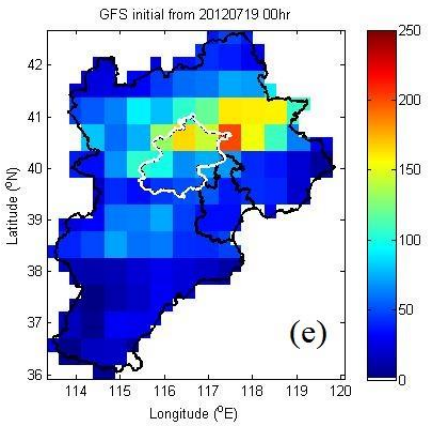
GFS initial from 20120719 00hr
Latitude (°N)
Longitude (°E)
(e)

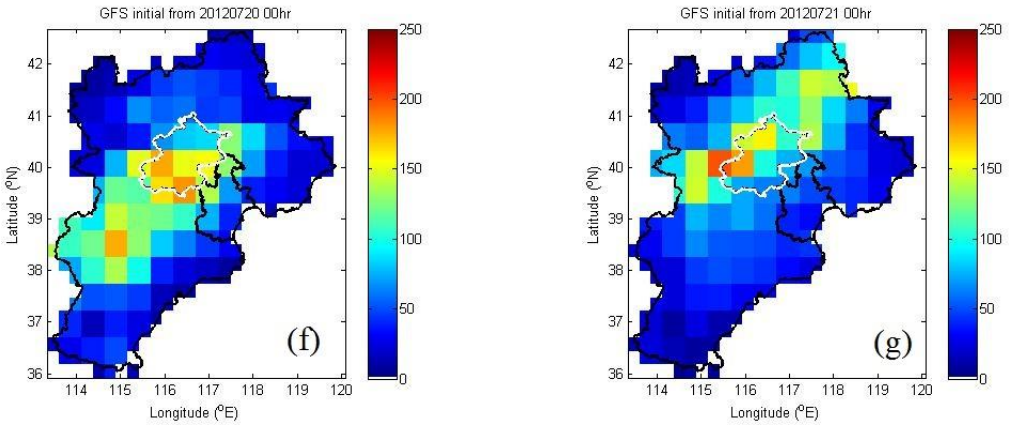

Figure 5.3 Daily precipitation accumulation (mm/day) on July 21, 2012 from (a) Rain Gauge stations; (b) TRMM V7; (c) TRMM RT; (d) GFS initialized from July 18 2012 00hr; (e) GFS initialized from July 19 2012 00hr; (f) GFS initialized from July 20 2012 00hr; (g) GFS initialized from July 21 2012 00hr.

The left panels of Figure 5.4, 5.5 5.6 and 5.7 show the rainfall accumulation time series from rain gauges, TRMM V7, TRMM RT, deterministic GFS precipitation forecasts and ensemble GFS precipitation forecasts initialized at different dates with different locations.

The performance of TRMM V7 and RT are in agreement throughout the July 21 event at urban Beijing and Fangshan: both of them captured the extreme rainfall peak, though with slight underestimation of peak volume compared to the gauge observation. GFS forecasts indicate an impending storm event over the region 4 days in advance; however, there is slightly underestimation of peak rainfall amounts compared to both the gauge observation and satellite rainfall estimates (i.e. TRMM V7 and RT). As shown by the left panels of Figure 5.4, 5.5, 5.6 and 5.7, with lead times ranging from 1 to 4 days, GFS underestimated the precipitation according to the gauge observations, but compares relatively well to the TRMM satellite rainfall estimates. However, the GFS forecast products do not indicate run-to-run consistency as the lead time decreases. For example, the GFS model predicted the rainfall accumulation accurately at 2 days in advance, with a lag of about 6-9 hours in the timing to reach the maximum rainfall accumulation following that observed by rain gauges. In contrast, for the forecast just 1 day prior to the event, the timing of the peak rainfall has improved, but there is significant underestimation with errors similar to those associated to the forecasts produced 3-4 days prior to the event.

Similar to urban Beijing and Fangshan, the performance of TRMM V7 and RT are in agreement throughout the July 21 event at Zhangfang and Zijingguan gauge station;

however, GFS, TRMM V7 and RT have obvious underestimation compared to gauge observations.

Overall, although the GFS shows underestimation of rainfall amounts and around 6-9 hours delay in reaching the maximum rainfall accumulation, it provided potentially informative prognostic skill up to 4 days in advance of the July 21 Beijing event (Figure 5.4(b)). Because GFS and GENS almost show no skills with 7-, 6- and 5-day lead time, the accumulative rainfall and runoff/streamflow simulation plots with 7-, 6- and 5-days lead time have been omitted in Figure 5.4, 5.5, 5.6 and 5.7 in this paper. But the overall statistics have been calculated from lead time 7-day to 1-day to provide a general picture of how the predictive skill propagate with shorter lead times as shown in Figure 5.8.

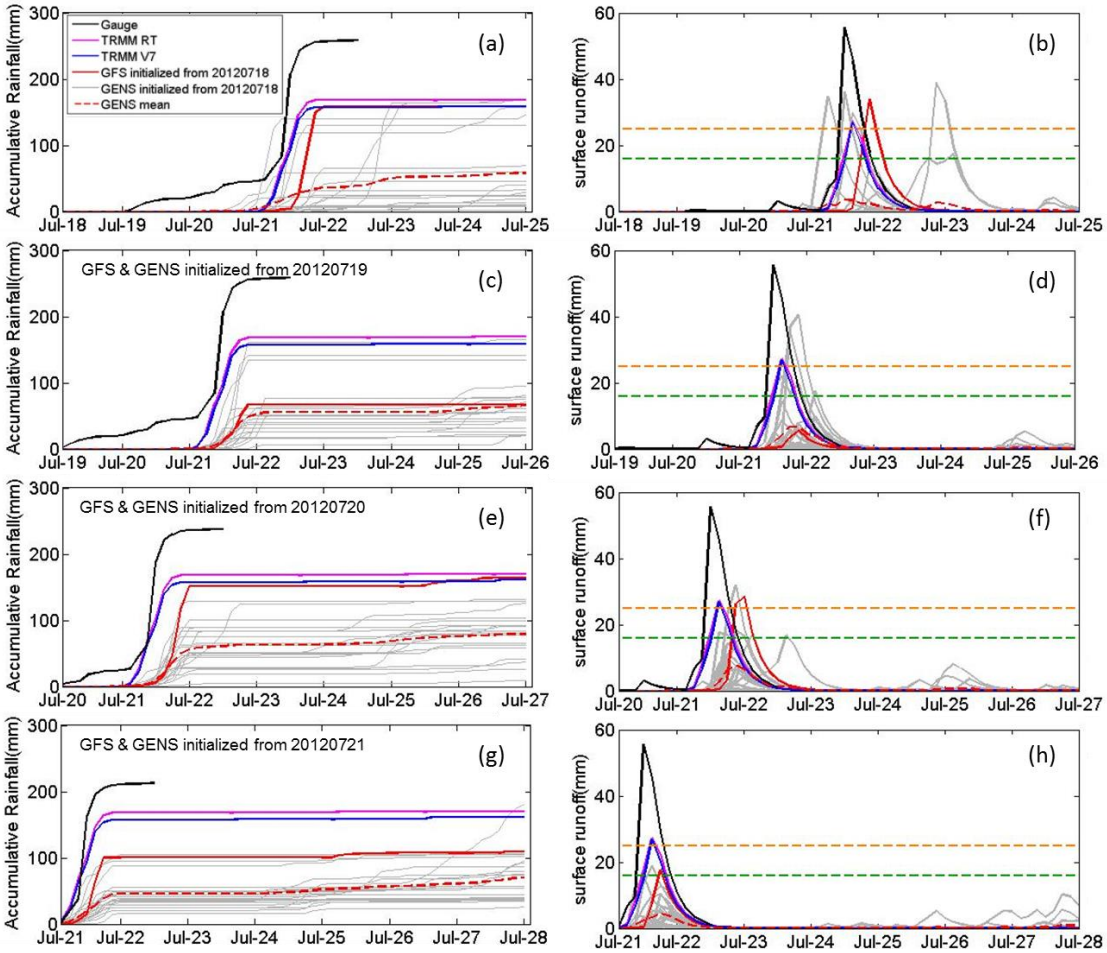

Figure 5.4 Accumulative Rainfall initialized from different date at 00UTC at Central Beijing (red dot in Figure 5.2) from different products: Gauge observation, TRMM RT, TRMM V7, GFS, GENS and GENS mean (left panel); GHPS predicted streamflow initialized from different date at 00UTC forced by different precipitation products: Gauge observation, TRMM RT, TRMM V7, GFS and GENS (right panel)

Note: Row 1 to Row 4 indicate lead time from 4 days to 1 day;

Orange dash line indicates 50 years return period surface runoff /streamflow threshold;

Green dash line indicates 20 years return period surface runoff /streamflow threshold.

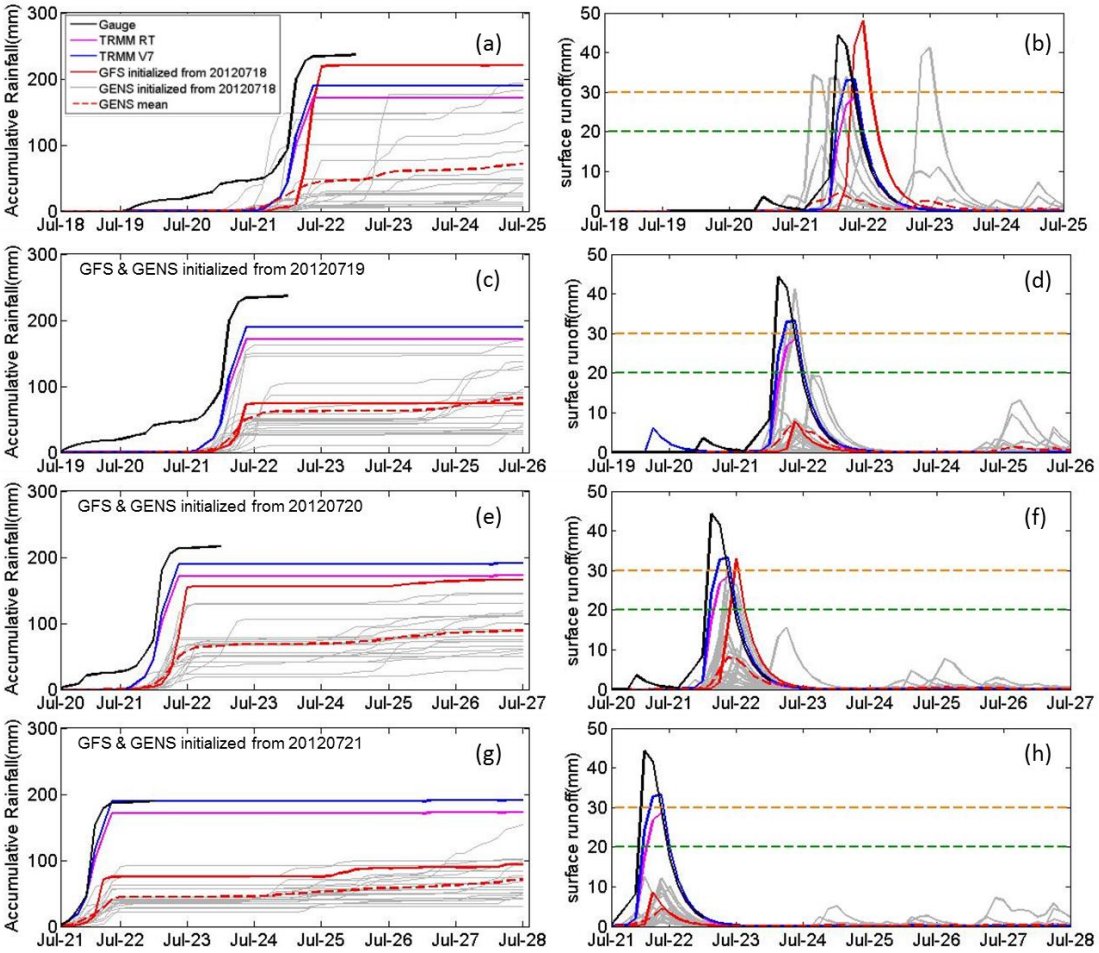

Figure 5.5 Same as Figure 5.4, but for Fangshan (dark dot in Figure 5.2)

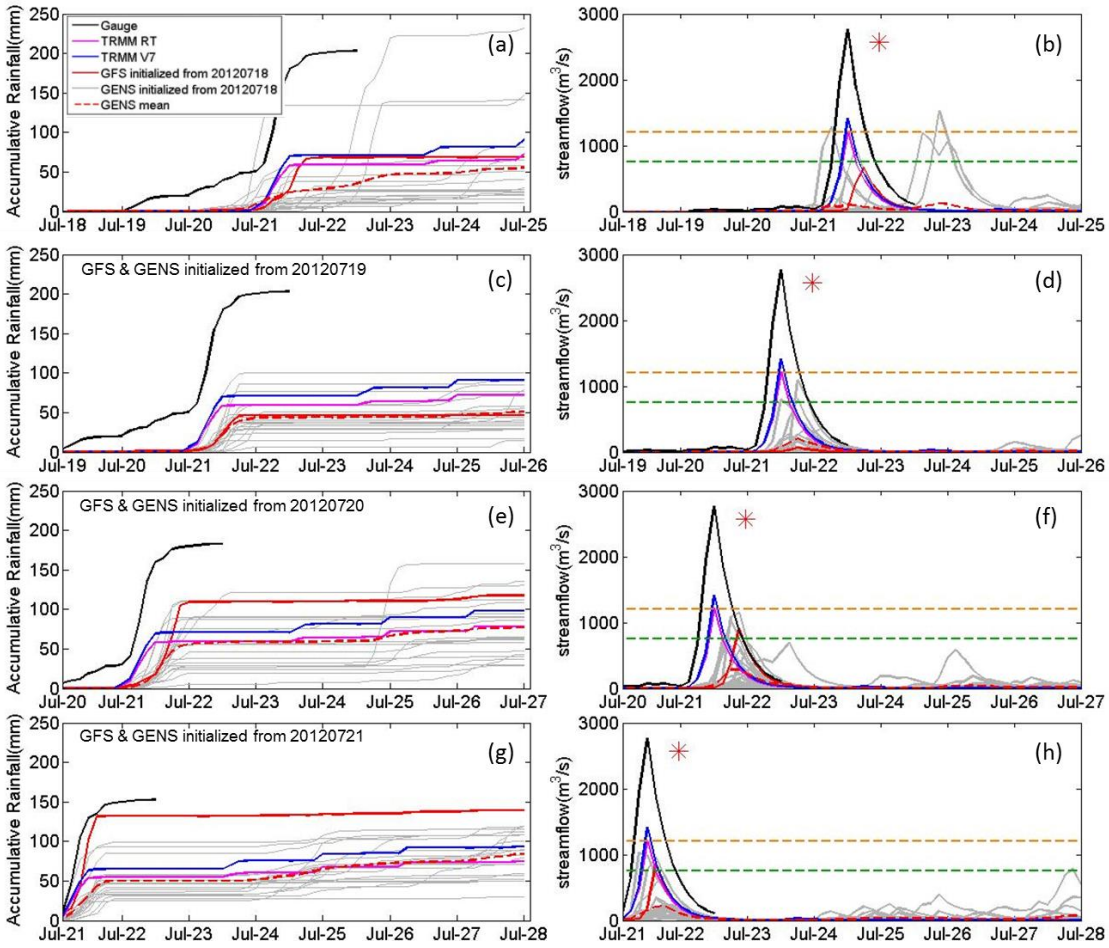

Figure 5.6 Same as Figure 5.4., but for the region over upstream of Zhangfang Gauge Station (red triangle in Figure 5.2)

Note: Red asterisk in the last two columns indicate the reported streamflow peak and timing.

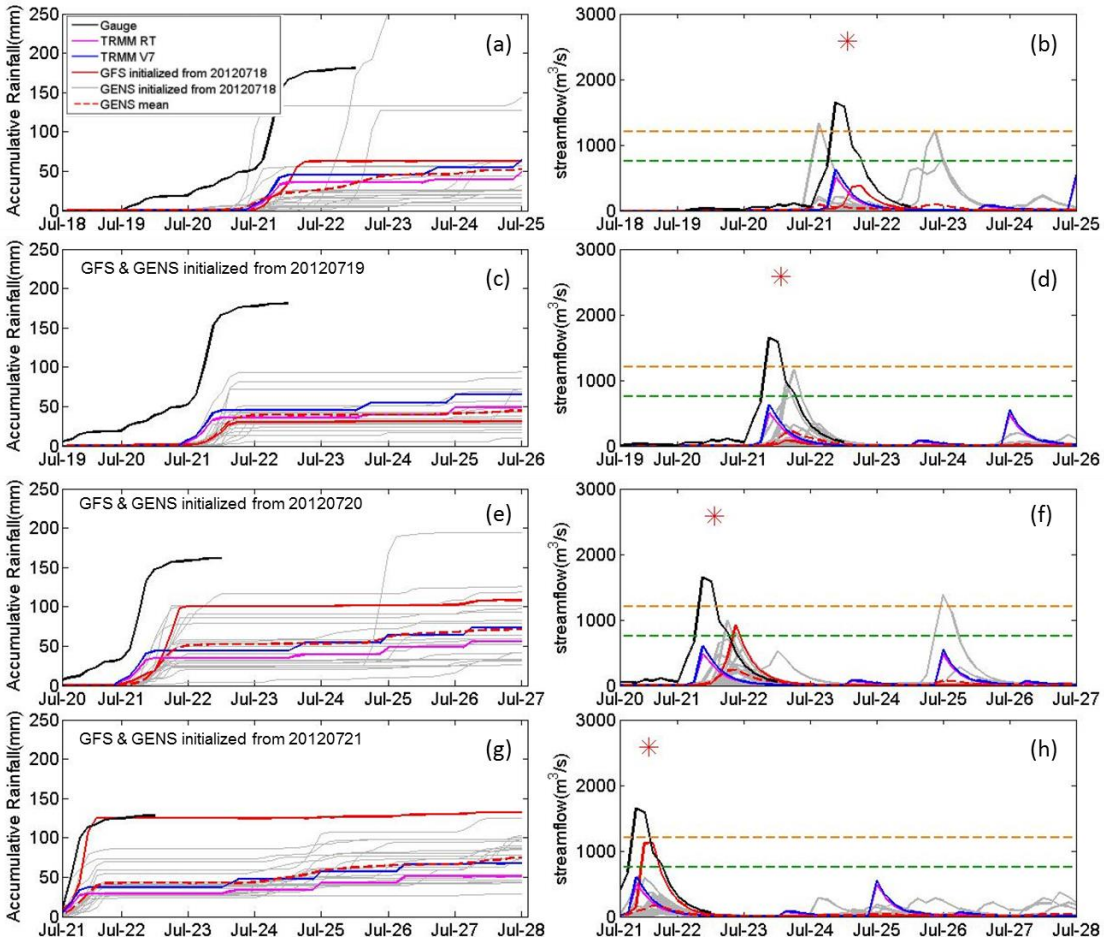

Figure 5.7 Same as Figure 5.6., but for the region over upstream of Zijingguan Gauge Station (dark triangle in Figure 5.2)

5.4.2 Time Series hydrological evaluation

Similar to rainfall evaluation, the right panels of Figure 5.4, 5.5 5.6 and 5.7 show the temporal evolution of GHPS modeled surface runoff at urban Beijing and suburban Beijing – Fangshan, and streamflow time series at Zhangfang and Zijingguan which are located at Juma River, the upstream of Beijing (as shown in Figure 5.2). In general, the modeled surface runoff and streamflow are underestimated when using the GFS forcing compared to the rain gauge-forced results on July 21 2012 over the four locations mentioned above. The GFS forced runoff at urban Beijing (~ 35mm) was underestimated around 20mm compared to gauged forced runoff (~ 55mm) at 4 days of lead time in regards to the peak flow, and there was also a slight delay in peak timing over urban Beijing (Figure 5.4(b)). For suburban Beijing - Fangshan, at the same lead time of 4 days, the GFS-forced simulations matched well with gauge-forced surface runoff on peak flow (~50mm v.s. ~45mm) but with 6-9 hours delay in the timing of the peak (Figure 5.5(b)). This indicates that the GHPS can give an early warning of up to 4 days in advance when forced with GFS rainfall forecasts, but the performance does not exhibit run-to-run consistency as the lead time decreases. Hlavcova et al. (2006) got similar conclusion that there is a considerable forecast variability with deterministic forecast – it give a clear signal at 4-day lead time but would have to be reduced in the future (Hlavcova et al. 2006). At Zhangfang gauge station, the peak volume of gauge forced modeled streamflow is in agreement with reported gauge peaks (red asterisk in Figure 5.6) with 3-6 hours lag, showing the promising potential of GHPS detectability if forced by quantitative precipitation estimation at real time. GFS-forced streamflow simulations with 4 days of lead time at Zhangfang shows an accurate prediction of the

peak timing, but with obvious underestimation in volume. For the Zijingguan gauge station, streamflow simulations conditioned on all the different forcings (i.e., gauge observations, TRMM V7, TRMM RT and GFS) underestimated the peak flow of the Beijing event compared to observed streamflow (Figure 5.7). Interestingly, at 2 days of lead time, GFS-forced simulations are more accurate than those from TRMM rainfall estimates in term of magnitude of the peak streamflow, but are poorer in terms of the timing. At 1day lead time, GFS shows advantages regarding both timing and peak volume relative to TRMM.

In order to assess the applicability of the flood detection with the GHPS to ungauged basins over the globe, we used a historical database of TRMM RT rainfall estimates. The global CREST model was driven by TRMM RT for its archive of 10 years to yield a retrospective hydrological simulation from 2002 until 2011 at each grid point. Then, the annual peaks were extracted and used to estimate the parameters of a Log Pearson Type III distribution. This enables us to estimate the simulated surface runoff and streamflow corresponding to return periods of 50 years (orange dash line in Figure 5.4 – 5.7) and 20 years (green dash line in Figure 5.4 – 5.7). This technique enables the GHPS to provide useful early detection information on the basis of its satellite remote sensing historical database without the requirement of rain gauges or stream gauges information. The results indicate there would have been flooding with a return period of approximately 50 years in both urban and suburban Beijing 4 days in advance of the event (Figure 5.4 (b), Figure 5.5(b)). This analysis also indicates the possibility of near 20-year return period flooding at Zhangfang at 4 days in advance and above 20-year return period flooding Zijingguan at 2 days in advance on the river.

In order to further assess the predictability of GHPS driven by the GFS precipitation forecasts, taking rain gauge observations as ground truth and TRMM RT as an additional benchmark, both the meteorological and hydrological predictabilities are evaluated with Bias (%) and RMSE (%) as a function of lead time. In Figure 5.8, the Bias (%) and RMSE (%) values of GFS rainfall relative to TRMM RT are calculated for 7-day period with different initialization time. For the hydrological predictability, the Bias(%) and RMSE(%) as functions of lead time are calculated for urban Beijing, suburban Beijing - Fangshan, Zhangfang and Zijingguan respectively, combined into a mean of those four series, and plotted in Figure 5.8(b). As shown in Figure 5.8, GFS has a general trend of increased prediction skill with shorter lead time in terms of both the meteorological (Figure 5.8(a)) and hydrological (Figure 5.8(b)) aspects compared with gauge observations and TRMM RT. The bias (%) of GFS-forced simulations relative to gauge-forced simulations is approximately -60% four days prior to the Jul 21 event (Figure 5.8(b)). Similarly, the Bias (%) of GFS-forced modeled streamflow relative to TRMM RT-based simulations is around -20% with 4 days lead time not only indicates useful and informative predictive skill, but also shows the competitive hydrological prognostic capability of GFS-forced GHPS relative to the detectability of TRMM RT at real time (Figure 5.4(b), 5.5(b), 5.6(b) and 5.7(b)).

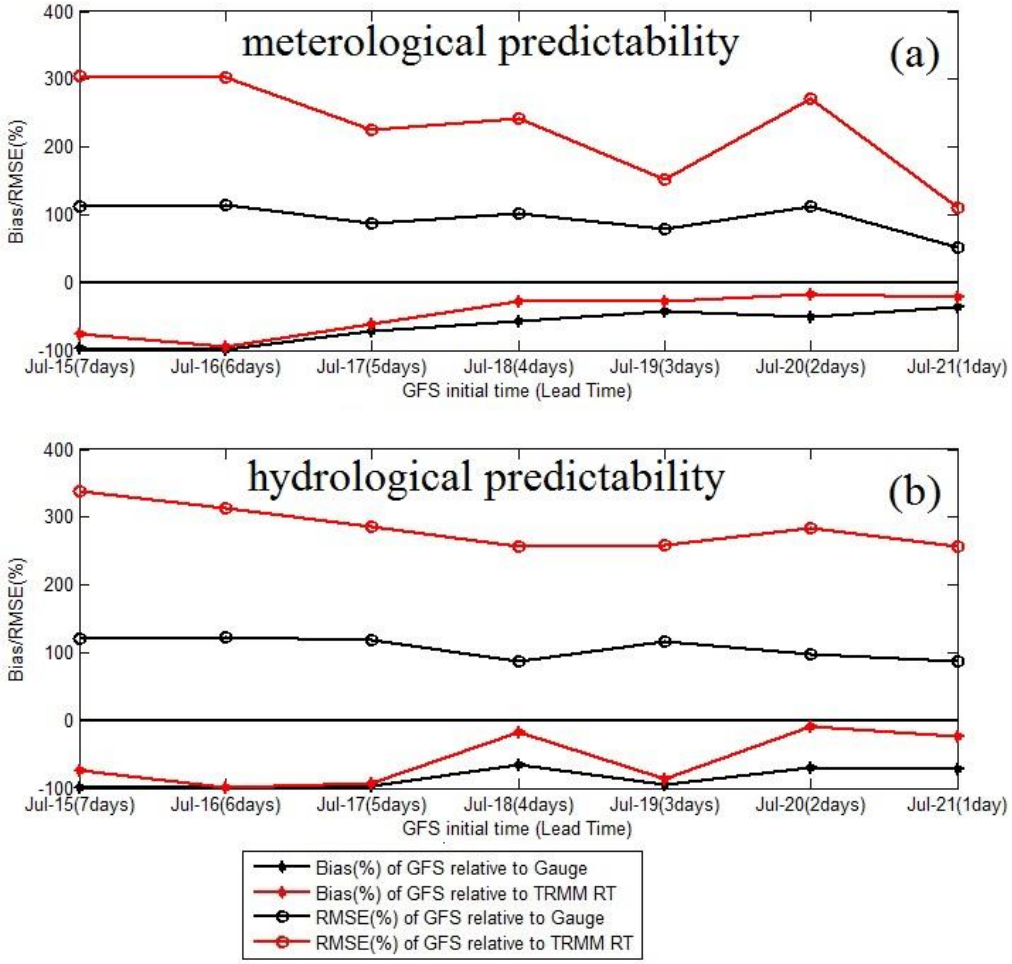

Figure 5.8 (a) Meteorological predictability of GFS relative to Gauge and TRMM RT; (b) Hydrological predictability of GFS relative to Gauge and TRMM RT.

5.4.3 Probabilistic hydrological evaluation

Probabilistic forecast derived from ensemble forecasts is considered to be much more attractive for flood forecasting system because they can provide additional information than the deterministic forecast - the identification the possibility of extreme and rare events (Buizza 2008; Gouweleeuw et al. 2005). In this section, we evaluate that how much "added value" (useful information) the ensemble streamflow forecasting contributes to the GHPS. First, the Ranking Probability Score (RPS, (Jolliffe and Stephenson 2012)) is calculated to assess the overall performance of the probabilistic forecast. The RPS for one forecast/simulation (e.g. GFS, TRMM forced modeled streamflow) is calculated via equation (1)

$$RPS = \sum_{m=1}^{J} (F_m - O_m)^2 \quad (1)$$

Where F_m is the experienced non-exceeding probability of the forecast and O_m is the experienced non-exceeding probability of the observation. For a group of n forecasts, the RPS is the mean of n RPSs:

$$\overline{RPS} = \sum_{k=1}^{n} \frac{1}{n} RPS_k \quad (2)$$

A perfect forecast is with the RPS of the value of 0.

Figure 5.9 shows the RPS of GFS, GENS, TRMM RT and TRMM V7 at different initialization with a 168hrs forecast/simulation horizon at different locations. Generally the hydrological performance with TRMM RT and V7 are very similar throughout different initial time at different locations as the purple curve and the blue curve are almost overlapped with each other. The overall performances of GFS and GENS meam are worse than the TRMM RT and V7. For Beijing, Fangshan, and Zhangfang, the RPSs of GFS are lower than the RPSs of GENS which indicate the "average" hydrological

performance of the GENS is worse than the GFS as forcing of hydrological forecasting; for Zijinguan, the forecasting forced by GENS outperforms GFS at the initial time of July 19 and 20. The results indicate that the "average performance" of GENS is not competitive with GFS, which is in agreement with the information delivered by Figure 5.4 to 5.7 that the GENS forced modeled streamflow ensemble mean is weak than the GFS forced streamflow forecast for most of the case. However, the RPSs of the GENS represent the performance of GENS central tendency (ensemble mean); for the ensemble streamflow forecast, we usually care more about if the ensemble forecast can convey the probability of occurrence of an extreme event. In this study, the traditional ensemble streamflow verification matrices (e.g. POD, FAR, Reliability Diagram, Relative Operating Characteristic) are not applicable to this study due to the low sample size limitation (Brown et al. 2010; Cloke; Pappenberger 2009); therefore, the ensemble predictive efficiency in terms of RPS, peak volume, peak timing, both peak volume and timing are developed to investigate that how many of the ensemble streamflow forecasts are "doing a better job" than the deterministic one thus delivering additional useful information.

The ensemble predictive efficiency P^* in term of RPS is defined as follow:

$$P^* = \frac{n(RPS)^*}{n} \tag{3}$$

Where n is the total number of ensembles ($n = 20$ in this study), $n(RPS)^*$ is the total number of ensemble streamflow that have a lower RPS than the GFS. The bars in Figure 5.9 shows the percentages of ensemble streamflow forecasts that "conquer" the deterministic forecast are above 25% at Beijing with different lead time; for Zijingguan gauge station, the ensemble predictive efficiency is up to 85% at 2-day in advance

(initialized at 2012072000). Despite the unstable value of the ensemble predictive efficiencies, they are all above zero for those four different locations with different lead times, which demonstrate that at least there are some ensemble forecasts that can deliver more accurate and reliable early warning information.

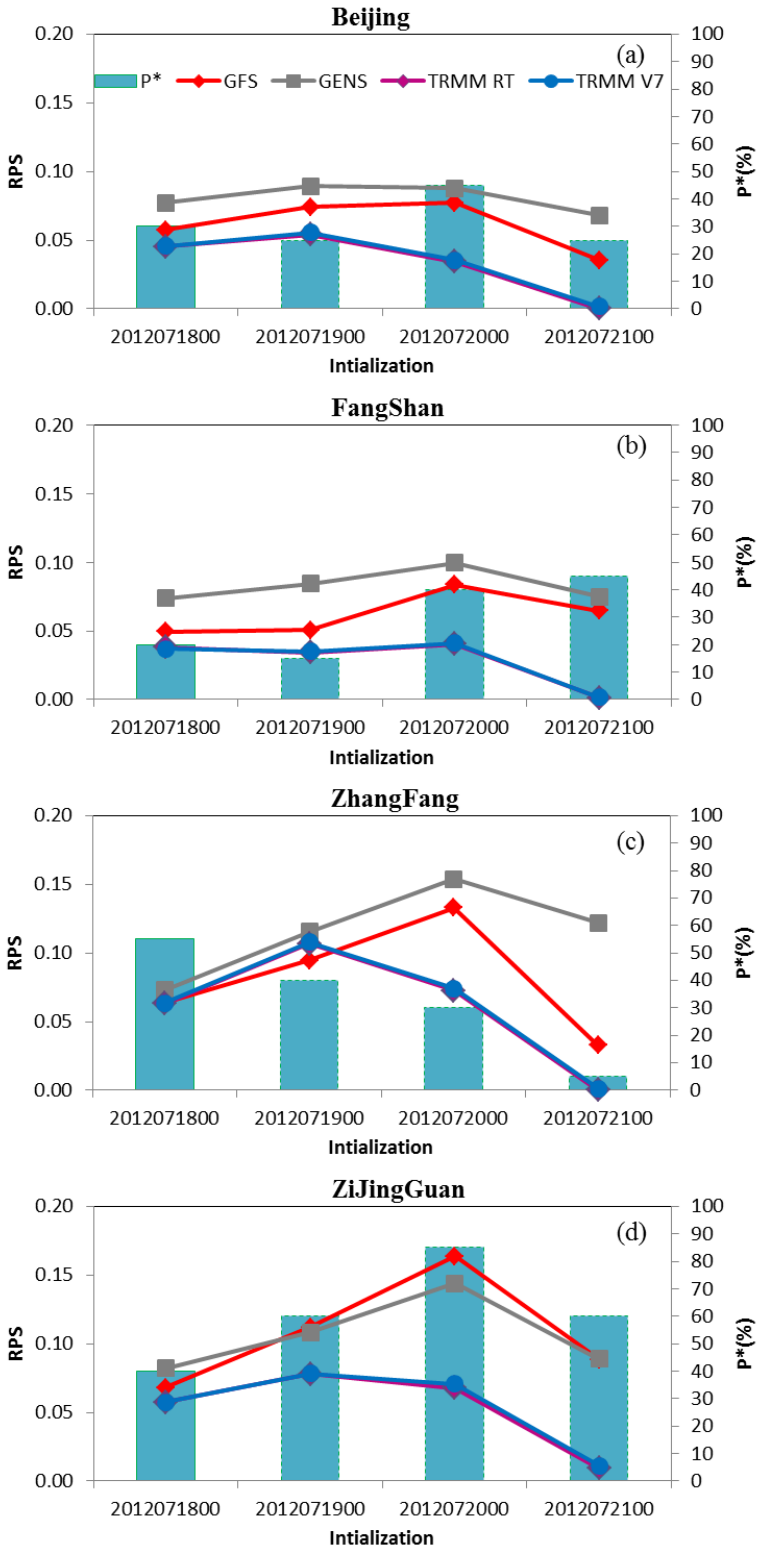

Figure 5.9 RPS of GFS, GENS, TRMM RT, TRMM V7 and the predictive efficiency of GENS in terms of RPS relative to GFS

Similarly to the ensemble predictive efficiencies in term of RPS, the ensemble predictive efficiency in term of peak volume $P^{\#}(PV)$, peak timing $P^{\#}(PT)$, both peak volume and timing $P^{\#}(PVT)$ are defined as shown by equation (4), (5) and (6).

$$P^{\#}(PV) = \frac{n(PV)^{\#}}{n} \tag{4}$$

$$P^{\#}(PT) = \frac{n(PT)^{\#}}{n} \tag{5}$$

$$P^{\#}(PVT) = \frac{n(PVT)^{\#}}{n} \tag{6}$$

$n(PV)^{\#}, n(PT)^{\#}, n(PVT)^{\#}$ are the total number of ensemble streamflow that have more accurate steamflow forecast in terms of peak volume, peak timing, and both peak volume and timing relative to the deterministic forecast. Likewise P^{*} , $n(PV)^{\#}, n(PT)^{\#}, n(PVT)^{\#}$ also demonstrate the possibility that ensemble forecasts can deliver more accurate and reliable early warning information regarding on the peak volume and timing of a rare event (Figure 5.10).

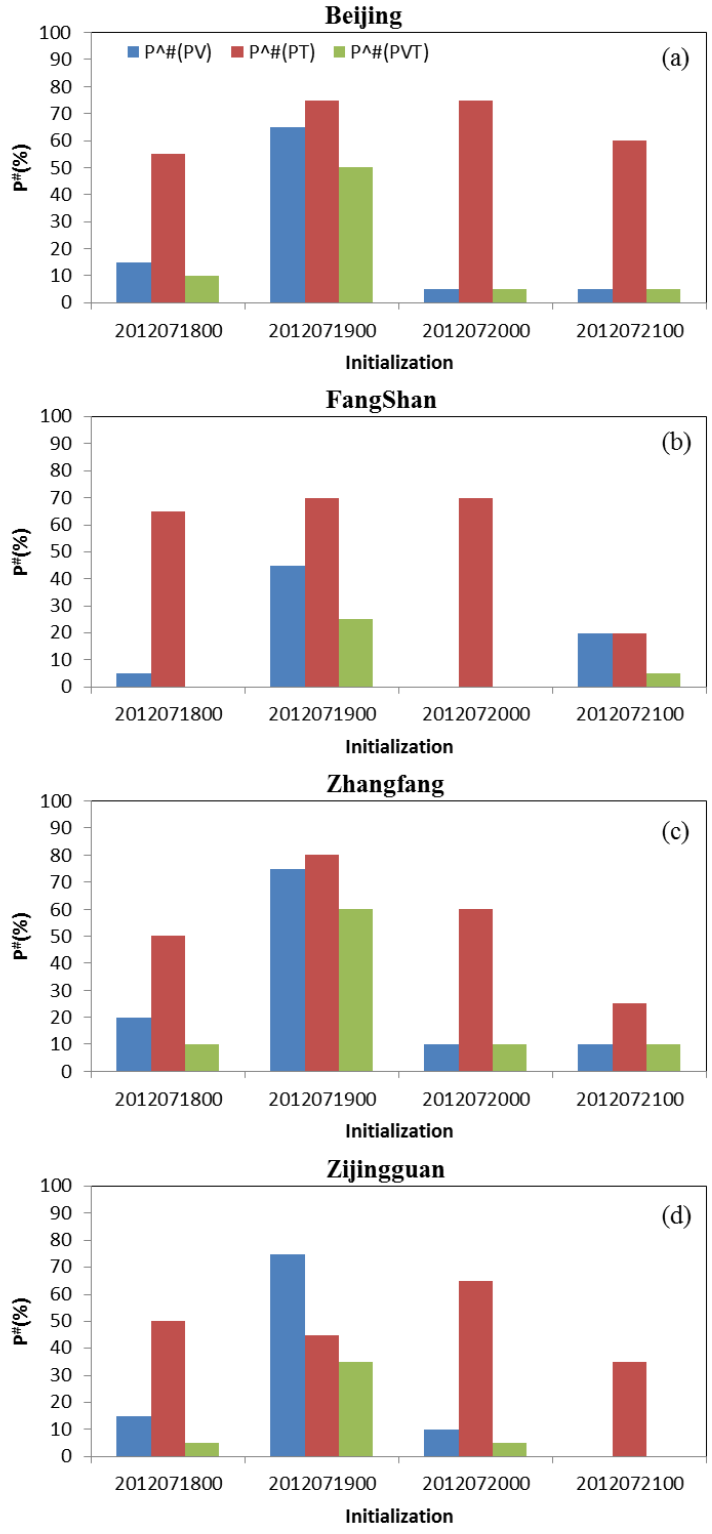

Figure 5.10 The predictive efficiency of GENS in terms of Peak Volume (PV), Peal Timing (PT) and both Peak Volume and Timing (PVT) relative to GFS

The above predictive efficiencies of the GENS demonstrate the usefulness of the NCEP ensemble forced streamflow prediction relative to that of the deterministic forecast. As (Bartholmes; Todini 2005) mentioned that, "the added benefit of ensemble forecast is not in quantitative flood forecasting (e.g. hydrograph predictions) but in the exceedance of warning levels." In order to further identify the probability of the occurrence of the extreme event, the probabilities of the ensemble forecasts that are exceeding the 50- and 20-year reoccurrence warning levels are calculated at those four locations with different lead time (Figure 5.11). 4-day ahead of the July 21 2012 Beijing extreme event, the deterministic streamlfow forecast at Zhangfang and Zijingguan show substantial underestimation to the reported observations (red asterisks in Figure 5.6(b) and Figure 5.7(b)); even regardless of the reported observations, the deterministic forecasts also bear obvious underestimation compared to the 50- and even 20-year reoccurrence threshold (orange and green dashed lines in Figure 5.6(b) and Figure 5.7(b)), which indicates that purely rely on the deterministic forecast cannot issue an early warning based on the 50- and even 20-year reoccurrence warning levels at Zhangfang and Zijingguan. In contrast, the ensemble forecasts show the probabilities of 20% (Figure 5.11(c)) and 15% (Figure 5.11 (d)) for a 20-year event occurrence, and 5% and 10% possibilities for a 50-year event occurrence at Zhangfang and Zijingguan 4 days ahead of the extreme events. At Beijing (Figure 5.4 (b)) and Fangshan (Figure 5.5 (b)), the deterministic forecast exceed the 50-year reoccurrence warning level at 4 days lead time, which can help issue an 50-year reoccurrence event warning; however, the prediction skill degrade with 3 days lead time at Beijing (Figure 5.4 (d)) and Fangshan (Figure 5.5(d)), the deterministic forecasts do not exceed even the 20-year reoccurrence

warning level, which would make a miss of early warning at this time stage. The occurrence probabilities for 50- and 20-year reoccurrence calculated by ensemble forecast are 10% and 20% at Beijing, 15% and 15% at Fangshan; this provides added information for decision makers to issue an early warning on basis of the deterministic run. Despite the overall poor performance of the occurrence probability (low probabilities under 30%, Figure 5.11) for this particular case, it at least demonstrates the identification of the probability of a rare event, which is considered as the additional value to the deterministic forecast.

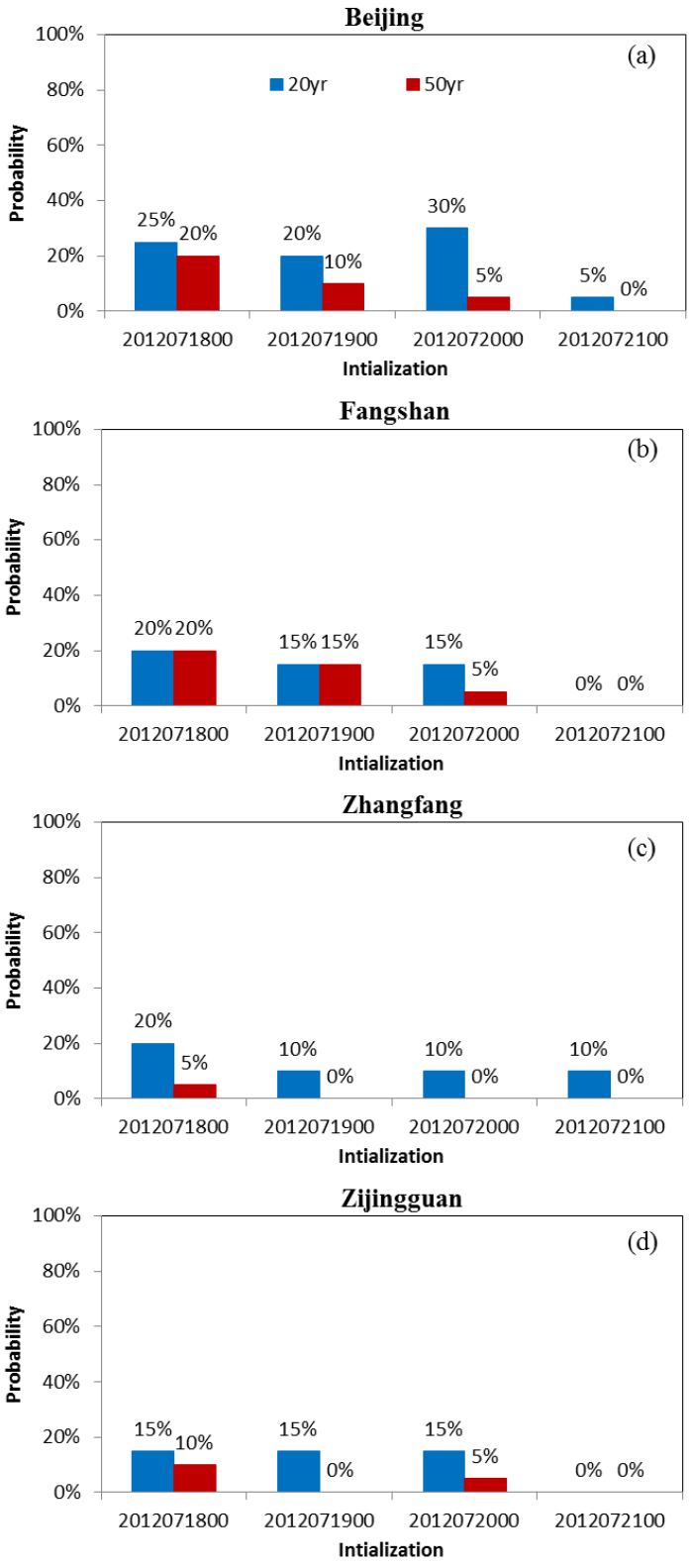

Figure 5.11 The occurrence probability for 50- and 20-year reoccurrence level by ensemble streamflow forecast

5.5 Conclusion and Future Work

The results of this study indicate the disastrous July 21 Beijing hydrometeorological extreme event was detectable by TRMM satellite precipitation estimates and predictable by deterministic GFS rainfall forecasts at least 4 days in advance. These conclusions are based on results from inputting the precipitation estimates and forecasts to the Global Hydrological Prediction System, which has been trained through the use of a decade-long retrospective simulation using TRMM RT rainfall. If the operational hydrological forecast forced by reliable meteorological precipitation forecast products were available and accessible for local stakeholders and integrated into Beijing emergency planning and response decision-making systems, governmental agencies will have adequate time for preparation and thus very likely reducing the impact of flooding, e.g. the loss of human life and property damages. Unfortunately in the real world it is not always effective as this hindcast shown, and the GHPS still needs improvements especially in engaging local stakeholders. In closing, this study examines the detectability and predictability of the current Global Hydrological Prediction System forced by satellite rainfall estimations (i.e., TRMM 3B42 RT and TRMM 3B42V7) and NCEP-produced GFS deterministic precipitation forecast products on the July 21 Beijing extreme event. In addition, this study also explores the additional value of the GFS precipitation ensembles for identifying the occurrence probability of an extreme event in a hydrological forecasting system. Given the global availability of such satellite-based precipitation observing system and GFS precipitation forecasting products, this study demonstrates the opportunities and challenges that exist for an integrated application of GHPS and GFS precipitation for flood prediction, systematically over the globe. The

method of forecasting rare flooding situations by referencing a decade-long retrospective simulation enables the forecasts to be applied in basins without the requirement of rain gauges or stream gauges.

To further improve the Global Hydrological Prediction System for more accurate and reliable early flood warning purpose, some future work are either under conducting or in planning: first, the regionalization of this system with historical GFS precipitation as input for those areas with high occurrence of flooding events is under consideration as it can locally improve the predictive skill with expert local partnerships as well as data availability; second, a much more extensive evaluation with longer period (not only an extreme case study) is planned to be conducted to demonstrate the predictive skill of this system over the globe, we have made efforts and have investigated both the deterministic and ensemble GFS precipitation forecast for the period Jun –Aug 2012 for a more extensive hydrological predictive skill evaluation of the GHPS for the summer season, which is the first step stone towards the envisioned future GHPS forced with the ensemble GFS together with the global parameterization; third, the data assimilation approach, which is increasingly appreciated and supported by the current Aqua/AMSR-E and future SMAP (Soil Moisture Active and Passive, to be launched in 2014) with anticipated better soil moisture data in terms of coverage, accuracy, and resolutions, might be applied to assimilate remote-sensing information for improved hydrological prediction.

References

Adhikari, P., Y. Hong, K. Douglas, D. Kirschbaum, J. Gourley, R. Adler, and G. Robert Brakenridge, 2010: A digitized global flood inventory (1998–2008): compilation and preliminary results. *Natural Hazards*, **55,** 405-422.

Bartholmes, J., and E. Todini, 2005: Coupling meteorological and hydrological models for flood forecasting. *Hydrology and Earth System Sciences Discussions,* **9,** 333-346.

Bradley, A. A., T. Hashino, and S. S. Schwartz, 2003: Distributions-Oriented Verification of Probability Forecasts for Small Data Samples. *Weather and Forecasting*, **18,** 903-917.

Bradley, A. A., S. S. Schwartz, and T. Hashino, 2004: Distributions-oriented verification of ensemble streamflow predictions. *Journal of Hydrometeorology*, **5,** 532-545.

Brakenridge, G. R., S. V. Nghiem, E. Anderson, and R. Mic, 2007: Orbital microwave measurement of river discharge and ice status. *Water Resources Research*, **43,** n/a-n/a.

Brown, J. D., D.-J. Seo, and J. Du, 2012: Verification of Precipitation Forecasts from NCEP's Short-Range Ensemble Forecast (SREF) System with Reference to Ensemble Streamflow Prediction Using Lumped Hydrologic Models. *Journal of Hydrometeorology*, **13,** 808-836.

Brown, J. D., J. Demargne, D.-J. Seo, and Y. Liu, 2010: The Ensemble Verification System (EVS): a software tool for verifying ensemble forecasts of hydrometeorological and hydrologic variables at discrete locations. *Environmental Modelling & Software*, **25,** 854-872.

Buizza, R., 2008: The value of probabilistic prediction. *Atmospheric Science Letters*, **9,** 36-42.

Cloke, H., and F. Pappenberger, 2009: Ensemble flood forecasting: a review. *Journal of Hydrology*, **375,** 613-626.

Demargne, Julie, Mary Mullusky, Kevin Werner, Thomas Adams, Scott Lindsey, Noreen Schwein, William Marosi, and Edwin Welles, 2009: Application of Forecast Verification Science to Operational River Forecasting in the U.S. National Weather Service. *Bulletin of the American Meteorological Society*, **90,** 779-784.

Demargne, Julie, Limin Wu, Satish Regonda, James Brown, Haksu Lee, Minxue He, Dong-Jun Seo et al, 2013: The Science of NOAA's Operational Hydrologic Ensemble Forecast Service. *Bulletin of the American Meteorological Society*.

Gneiting, T., F. Balabdaoui, and A. E. Raftery, 2007: Probabilistic forecasts, calibration and sharpness. *Journal of the Royal Statistical Society: Series B (Statistical Methodology)*, **69,** 243-268.

Gouweleeuw, B., J. Thielen, G. Franchello, A. D. Roo, and R. Buizza, 2005: Flood forecasting using medium-range probabilistic weather prediction. *Hydrology and Earth System Sciences*, **9,** 365-380.

Han, J., and H. L. Pan, 2011: Revision of convection and vertical diffusion schemes in the NCEP global forecast system. *Weather and Forecasting*, **26,** 520-533.

Hlavcova, K., J. Szolgay, R. Kubes, S. Kohnova, and M. ZvolenskÝ, 2006: ROUTING OF NUMERICAL WEATHER PREDICTIONS THROUGH A RAINFALL-RUNOFF MODEL. *Transboundary Floods: Reducing Risks Through Flood Management*, J. Marsalek, G. Stancalie, and G. Balint, Eds., Springer Netherlands, 79-90.

Hong, Y., R. F. Adler, F. Hossain, S. Curtis, and G. J. Huffman, 2007: A first approach to global runoff simulation using satellite rainfall estimation. *Water Resources Research*, **43,** W08502.

Hopson, T. M., and P. J. Webster, 2010: A 1-10-Day Ensemble Forecasting Scheme for the Major River Basins of Bangladesh: Forecasting Severe Floods of 2003-07*. *Journal of Hydrometeorology*, **11,** 618-641.

Huffman, G. J., D. T. Bolvin, E. J. Nelkin, D. B. Wolff, R. F. Adler, G. Gu, Y. Hong, K. P. Bowman, and E. F. Stocker (2007), The TRMM Multisatellite Precipitation Analysis (TMPA): Quasi-Global, Multiyear, Combined-Sensor Precipitation Estimates at Fine Scales, *Journal of Hydrometeorology*, *8*(1), 38-55.

Jolliffe, I. T., and D. B. Stephenson, 2012: *Forecast verification: a practitioner's guide in atmospheric science.* John Wiley & Sons.

Kanamitsu, M., and Coauthors, 1991: Recent changes implemented into the global forecast system at NMC. *Weather and Forecasting*, **6,** 425-435.

Khan, S. I., P. Adhikari, Y. Hong, H. Vergara, R. F Adler, F. Policelli, D. Irwin, T. Korme, and L. Okello, 2011a: Hydroclimatology of Lake Victoria region using hydrologic model and satellite remote sensing data. *Hydrology and Earth System Sciences*, **15,** 107-117.

Khan, Sadiq I., Yang Hong, Jiahu Wang, Koray K. Yilmaz, Jonathan J. Gourley, Robert F. Adler, G. Robert Brakenridge, Fritz Policelli, Shahid Habib, and Daniel Irwin, 2011b: Satellite Remote Sensing and Hydrologic Modeling for Flood Inundation Mapping in Lake Victoria Basin: Implications for Hydrologic Prediction in Ungauged Basins. *Geoscience and Remote Sensing, IEEE Transactions on*, **49,** 85-95.

Liang, X., D. P. Lettenmaier, E. F. Wood, and S. J. Burges, 1994: A Simple Hydrologically Based Model of Land-Surface Water and Energy Fluxes for General-Circulation Models. *Journal of Geophyicals Research Atmospheres*, **99,** 14415-14428.

Nijssen, B., D. P. Lettenmaier, X. Liang, S. W. Wetzel, and E. F. Wood, 1997: Streamflow simulation for continental-scale river basins. *Water Resoucesr Research*, **33,** 711-724.

Pappenberger, F., K. Scipal, and R. Buizza, 2008: Hydrological aspects of meteorological verification. *Atmospheric Science Letters*, **9,** 43-52.

Schaake, J. C., T. M. Hamill, R. Buizza, and M. Clark, 2007: HEPEX: The Hydrological Ensemble Prediction Experiment. *Bulletin of the American Meteorological Society*, **88,** 1541-1547.

Seo, D. J., H. D. Herr, and J. C. Schaake, 2006: A statistical post-processor for accounting of hydrologic uncertainty in short-range ensemble streamflow prediction. *Hydrology and Earth System Sciences Discussions*, **3,** 1987-2035.

Smith, K., and R. Ward, 1998: *Floods: physical processes and human impacts.* Vol. 408, Wiley Chichester.

Wang, J., Y. Hong, L. Li, J.J. Gourley, S.I. Khan, K.K. Yilmaz, R.F. Adler, F. S. Policelli, S. Habib, D. Irwn, A. S. Limaye, T. Korme and L. Okello. 2011: The coupled routing and excess storage (CREST) distributed hydrological model. *Hydrological Sciences Journal*, **56,** 84-98.

Wang, X., 2010: Incorporating ensemble covariance in the gridpoint statistical interpolation variational minimization: A mathematical framework. *Monthly Weather Review*, **138,** 2990-2995.

Wang, X., D. Parrish, D. Kleist, and J. Whitaker, 2013: GSI 3DVar-based Ensemble-Variational Hybrid Data Assimilation for NCEP Global Forecast System: Single Resolution Experiments. *Monthly Weather Review*.

Westerhoff, R. S., M. P. H. Kleuskens, H. C. Winsemius, H. J. Huizinga, G. R. Brakenridge, and C. Bishop, 2013: Automated global water mapping based on wide-swath orbital synthetic-aperture radar. *Hydrology and Earth System Sciences*, **17,** 651-663.

Wu, H., R. F. Adler, Y. Hong, Y. Tian, and F. Policelli, 2012: Evaluation of Global Flood Detection Using Satellite-Based Rainfall and a Hydrologic Model. *Journal of Hydrometeorology*, **13,** 1268-1284.

Yang, F., H. L. Pan, S. K. Krueger, S. Moorthi, and S. J. Lord, 2006: Evaluation of the NCEP Global Forecast System at the ARM SGP site. *Monthly Weather Review*, **134,** 3668-3690.

Yilmaz, K. K., R. F. Adler, Y. Tian, Y. Hong, and H. F. Pierce, 2010: Evaluation of a satellite-based global flood monitoring system. *International Journal of Remote Sensing*, **31,** 3763-3782.

Zappa, M., F. Fundel, and S. Jaun, 2013: A 'Peak-Box'approach for supporting interpretation and verification of operational ensemble peak-flow forecasts. *Hydrological Processes*, **27,** 117-131.

Chapter 6. Overall Conclusion

Accurate and reliable flood prediction, especially in cases of catastrophic flooding events that lead to huge fatalities and economic losses, is of significant importance for issuing early warning and producing enough time for "preparedness" in advance. The impact of human activities and possible climate change is anticipated to cause more frequent and severe flooding events. Therefore, further efforts need to be made in the real time operational flood monitoring and flood forecasting in order to mitigate the huge potential loss from such extreme flooding events. The remote sensing technique, which provides a mean of observing hydrological variables at large scales, endeavors to further improve flood prediction, especially for those regions with sparse gauge observations or even no gauge observations. In addition, compared to the point based gauge observations, remote sensing observations can better represent the spatial variability of the hydrological components such as precipitation and soil moisture. While remote sensing technique improves the understanding and the detection of flooding, the recently developed Numerical Weather Prediction (NWP) system which provides precipitation forecasts several days in advance to drive the hydrological model, has the potential to further improve the hydrological predictions by extending its forecasting horizon (lead time). Together, the increasingly accurate precipitation forecast products from the NWP and remote sensing precipitation estimation into the hydrological model, are expected to improve the accuracy and reliability of hydrological monitoring and forecasting at fine spatial resolution and with longer lead time.

6.1 Remote sensing products for flood monitoring

The development of remote sensing technique explores the possibility of hydrological predictions for ungauged regions as well as for large-scale or even global scale predictions by utilizing the remote sensing data for model set-up, parameterization, and forcing, etc.

The topography data such as the Digital Elevation Model (DEM) can be observed from the freely available Advanced Spaceborne Thermal Emission and Reflection Radometer (ASTER) with 83° N to 83° S coverage and around 30m spatial resolution, and the Shuttle Radar Topography Mission (SRTM) with 60° N to 56° S coverage and around 90m spatial resolution from NASA can be applied to calculate the slope and extract the river net for both global and regional hydrological model set-up.

At global scale, both the Advanced Very High-Resolution Radiometer (AVHRR) and the MODerate resolution Imaging Spectroradiometer (MODIS) provide global land cover information which estimates the hydrological physical parameters, such as the saturated hydraulic conductivity and the maximum soil water capacity in the CREST model.

Besides contributing to the hydrological model set-up and parameterization, remote sensing data also provides information for specific hydrological components to be used either as the forcing data (e.g. precipitation) or observation (e.g. soil moisture and streamflow) to be assimilated into the hydrological system in order to improve its predictive skills. The global-wide precipitation can be estimated from multiple satellite missions and sensors such as TRMM - Tropical Rainfall Measuring Mission from

NASA, CMORPH – CPC Morphing technique from the Climate Prediction Center at NOAA, PERSIANN - Precipitation Estimation from Remotely Sensed Information using Artificial Neural Networks that is operational at the University of Arizona, etc. Soil moisture, another major hydrological component that controls how much of the excess rainfall is infiltrated into the soil and how much of the excess rainfall is generated as the overland flow, can be retrieved from both active and passive microwave sensors. The global remote sensing soil moisture missions and sensors include the passive AMSR-E - the Advanced Microwave Scanning Radiometer - Earth Observing System from NASA, the passive SMOS - The Soil Moisture and Ocean Salinity from European Space Agency (ESA), the active ASCAT - the Advanced Scatterometer from NOAA, and the future mission SMAP – Soil Moisture Active and Passive from NASA which estimates the soil moisture by combing both active radar observation and passive radiometer observation and will be launched in the year 2014. In addition to the remote sensing precipitation and soil moisture estimation, the AMSR-E and MODIS were recently used to estimate the streamflow at ungauged basins as mentioned in Chapter 2 and 3; this can be either directly applied to estimate the streamflow for flood detection or be utilized as the data assimilation source to update the internal states of the hydrological model, thus improving the hydrological predictive efficiency.

In this study, Chapter 2 and 3 are two proof-of-concept studies that explore and demonstrate the applicability of utilizing TRMM precipitation as forcing and assimilating spaceborne AMSR-E streamflow signals in both actual domain and frequency domain to improve the steamflow prediction in a sparsely gauged basin –

Cubango which is located in Africa. However, TRMM has the key limitation in underestimation of the precipitation in higher latitude and in the regions of intense convection over land. The application of AMSR-E streamflow signals for hydrologic perspective, which are impacted by factors including width of the river, channel geometry, water temperature relative to land, and measurement pixel resolution, can be obtained from Global Flood Detection System (http://www.gdacs.org/flooddetection/) at near real time.

Chapter 2 shows that opportunities and challenges exist for an integrated application of a suite of satellite data to flood prediction by careful fusion of remote sensing and in-situ observations and further effective assimilation of the information into a hydrological model. The approach developed and benchmarked in Chapter 3 has great potential for probabilistic flood prediction for the vast number of river basins throughout the world that are poorly gauged or even ungauged. Chapter 4, which conducts the evaluation of the hydrological performance of two TMPA 3B42 products - the real time and the post real time rainfall estimation with CREST model, demonstrates the potential of utilizing the remote sensing precipitation for real time flood detection over the globe.

6.2 NWP products for flood forecasting

While the remote sensing satellite data facilitates global flood monitoring, the Numerical Weather Prediction (NWP) products (e.g. the precipitation forecasts and the temperature forecasts) bring the potential to extend the hydrological prediction horizons thus benefit the early warning system. In addition to the deterministic precipitation forecasts from the NWP, ensemble precipitation forecasts address the uncertainty in hydrological forecast for flood risk management. And the ensemble streamflow forecasts are expected to have much more added value in longer lead time hydrological forecast.

The currently available NWP systems include the National Centers for Environmental Prediction (NCEP) Global Forecasting System (GFS) at NOAA, U.S., and the European Centre for Medium-Range Weather Forecasts (ECMWF) at U.K., etc.

Chapter 5 demonstrates the prototype of a Real Time Global Hydrological Prediction System (GHPS), which is forced by NOAA's Global Forecast System (GFS) deterministic and ensemble precipitation forecasts, and then evaluates the performance of this system for an extremely rare event – the July 21, 2012 Beijing event—in both deterministic domain and probabilistic domain. Given the global availability the GFS precipitation forecasting products, this study shows the potential of an integrated application of GHPS and GFS precipitation for flood prediction, systematically over the globe. The method of forecasting rare flooding situations by referencing a decade-long retrospective simulation driven by TRMM precipitation, enables the forecasts to be applied in basins without the requirement of rain gauges or stream gauges.

6.3 Challenges

The use of remote sensing data and NWP products for hydrological detections and predictions is becoming a widespread activity. The Chapters 2 to 5 in this study have demonstrated its effectiveness. But challenges still exist in the following aspects:

- Improving the current satellite remote sensing products in terms of higher spatial, temporal resolution and better accuracy

- Improving the current NWP system in terms of higher spatial, temporal resolution, better accuracy and longer lead time

- Global hydrological model parameterization and data assimilation

6.4 Future research directions

At both regional and global scales, the real time operational hydrological prediction can be increasingly appreciated and supported by the current TRMM, future GPM (Global Precipitation Mission), and the precipitation forecasts from the NWP system, together with the future SMAP. The new satellite missions are anticipated to provide better precipitation and soil moisture data in terms of coverage, accuracy, and resolutions. Those stated improved perspectives of the soil moisture mission SMAP, are expected to significantly benefit the hydrological data assimilation thus improving the predictive skills. To further extend the forecast horizons of the Global Hydrological Prediction System for more accurate and reliable early warnings: first, the regionalization of the Global Hydrological Prediction System with historical GFS precipitation as input for those areas with high occurrence of flooding events is under consideration as it can locally improve the predictive skill with expert local partnerships as well as data availability; second, the finer spatial resolution of the GFS precipitation forecasts, or the reliable dynamic downscaling technique is expected to better represent the spatial variability of the precipitation and facilitate the hydrological predictions; third, a much more extensive evaluation over a longer time period (in addition to an extreme case study as in Chapter 5) is planned to be conducted to demonstrate the predictive skill of this system worldwide. We have made efforts and have investigated both the deterministic and ensemble GFS precipitation forecast for the period June - August 2012 for a more extensive hydrological predictive skill evaluation of the GHPS for the summer season, which is the first stepping-stone towards the envisioned future GHPS forced with the ensemble GFS together with the global parameterization.